PREDICTIVE THEORETICAL AND COMPUTATIONAL APPROACHES FOR CHARACTERIZING ENGINEERED BIOSWALE SYSTEMS PERFORMANCE

A DISSERTATION SUBMITTED TO THE GRADUATE DIVISION OF THE UNIVERSITY OF HAWAIʻI AT MĀNOA IN PARTIAL FULFILLMENT OF THE REQUIREMENTS FOR THE DEGREE OF

DOCTOR OF PHILOSOPHY

IN

CIVIL AND ENVIRONMENTAL ENGINEERING

MAY 2019

By

Joshua Lelemia Irvine

Dissertation Committee:

Albert S. Kim, Chairperson
Roger W. Babcock Jr.
Sayed M. Bateni
Robert H. Richmond
Kirsten L.L. Oleson

Keywords: Bioswale Systems, Low Impact Development (LID), Best Management Practice (BMP), Stormwater Management, Computational Fluid Dynamics (CFD)

Dedication

He lei kaananiau no ke ao nei.

A lei of “managing the rolling beauty of time” for this world.

ACKNOWLEDGMENTS

akua lako. (God provides). All blessings come from akua.

Kūpuna lako. (Ancestors provide). Mahalo/Gracias to our ancestors' ingenuity, mana, and knowledge that they have passed down to us, their descendants.

Mahalo ā piha i ka ʻohana. (Gratitude to my family members). I am a product of a "kolohe" summer love between my parents who met canoe paddling. Foremost, this dissertation work would not have been possible for my mother, Jamie, and father, Alford. I am equally grateful to Paul Akiu for his unstinting support. I am deeply grateful to Elaine Miles for standing in the gap in caregiving for my ailing father and your unconditional aloha to our ohana. My aloha/cariño wells up with the utmost appreciation goes to the genealogists of both branches of my family for meticulously documenting our familial stories and connections so I know who I am today. *Mil gracias* and *mahalo* to Marcella Gonzales, Stella Ordaz, Sweetheart "Ipo" Irvine, Florence Waikahe Lono Kalawa Tabag, Kalani Kahulamu Wilson, Noeleen Calderia, Sherry Kaku, Kiʻilei Balaz-Oblero, Angie Merola, Ronette Obrey, and countless others. I am equally grateful to my Aunties and Uncles for their support throughout my life and the writing process, including Jimmy Myrick, Jeff Myrick, Junior Irvine, the late Huli Irvine, Cyrus Irvine, Ellory Irvine, Daryl Flores, Kalā Bernard, Mahealani Pai, Alika Silva, and Glen Kila. Thank you kindly to all my cousins, Lynnie Kauhane, Elaine Lena Brown, the late Joe Boy Irvine, Pua Irvine, Patty Irvine, Ilona Irvine, Alexander Bulla Irvine, Noe Irvine, Ola Irvine, Pohai Irvine, Leihulu Irvine, Sabrina Haaheo "Brina" "Haʻa", Hulali Pai, Dorian Kalikolehuaolokelani Cabanting, Pokiʻi Balaz, Temehani Bernard-Garcia, Anthony "Tony" Provencio, Rinda, Mary Soliz, Marissa Soliz, Zachariah Rel, and countless others for the many concerts, outings, talk-story sessions, and encouraging support. I am immensely grateful to the descendants of Francis "Hudie" Kekaualua for their generous support. To my Mauiākakalana brothers, nui mahalo! I am most indebted to my sister, Aliah, for her big heart to support me and for always having my back. Aliah, you are the epitome of *kaikaina*. I dedicate this achievement to my ʻohana/familia.

Mahalo ā nui i nā kumu aʻo. (Gratitude and appreciation to my teachers). At a young age, I knew that science has a healing power to help my ʻohana, our lāhui, and the world. In Waiʻanae intermediate, I took a strong affinity to grow my knowledge in maths and sciences which led me to participate in science fair. I asked Mr. Thomas, my 8th-grade science teacher, "I like math and biology. What should I take in college?" "Biological engineering" was Mr. Thomas' reply. That was the first time I had ever heard of the word "engineer". I remembered this thought and planned from then on what classes I needed to take in high school so as to matriculate into a Biological Engineering program in college. My intellectual lineage in science, technology, engineering, and mathematics (STEM) stretches back to playing outside, watching cartoons, Mr. Thomas, Mr. Kim (sophomore honors chemistry teacher), Mr. Grach (honors physics), Ms. Murakami (Algebra II

teacher) and then to UH Mānoa's Biological Engineering Department where I worked for a half-decade with Dr. Ping-Yi Yang in waste, wastewater, and water treatment. I am indebted to all these kumu for teaching me the fundamentals of physics, biology, chemistry, and mathematics. My special thanks goes to Dr. Rosie Catherine who helped me become an intern abroad at Universidad EARTH, Costa Rica which was the spark that launched me into engineering research. In particular, my special thanks are due to Dr. Chittaranjan Ray who encouraged me to apply to the Civil Engineering Ph.D. program at Mānoa and sowed the seed in me that I can become an academic in STEM.

Mahalo ā nui i nā kumu. (Gratitude and appreciation to my mentors). Countless others have shaped me as a Hawaiian engineer, indigenous scholar, and practitioner. This includes living treasures, and others proceeding me that have gone to the realm of the ancestors. Kuʻumeaaloha Gomes has been an unfailing source of encouragement, advice, and reassurance for instilling in me the value of giving back to our lāhui through mālama ʻāina. I am immensely grateful to Kumu Hula ʻuniki Dr. Kalani Akana for further opening my ʻōiwi optics and to demonstrate to me how to touch, hear, feel, taste and see like our ancestors. I am immensely grateful to K.H. Dr. Akana's hālau papa kūkui for their continuous reassurance, which includes Aulii Aweau, Anuhea Borengasser, Kanani Pharr Cadaoas, Kumu Hula ʻuniki Gail Lehua Gaison-Tyler, Brian Keoki Faria, Makalauna Feliciano, Kanaʻi Gomes, Ronnie Inagaki, Malia Haumschild, Kumu Hula ʻuniki Inger Hojfeldt, Nuuanu Lenchanko, Kū Souza, Kumu Hula ʻuniki Mark Tang, and Kumu Hula ʻuniki Ipolani Vaughan. I owe many thanks to academics and kumu outside of my discipline who provided additional mentoring, academic and personal support on my intellectual journey as a Hawaiian scholar, including Dr. Noelani Arista, Dr. Marie Alohalani Brown, Kumu Hula ʻuniki Mehanaokala Hind, Dr. Kuʻualoha Hoʻomanawanui, Dr. Kaiwipunikauikawēkiu "Punihei" Lipe, and Kumu Kalei Nuʻuhiwa.

Mahalo ā nui i nā mea kakoʻo. (Gratitude and appreciation to my supporters). It takes a village to raise an academic. I cannot thank enough those behind the scenes at the University that make the backbone of academe. My heartfelt thanks are due to the office staff at the Department of Civil and Environmental Engineering, Janis Kusatsu and Jean Zheng, who has always made the time to help and support me. For valuable feedback on my writing style, I thank Karyl Garland and Dr. Sue Haglund. I cannot thank enough UH faculty and staff outside my disciplines for their continuous guidance, patience, and encouragement in wayfinding my way through the academy, including Dr. Myhraliza Aala, Dr. Lucia Aranda, Teresa Bill, Dr. Healani Chang, Kinohi Gomes, Dr. Maile Goo, Dr. Daniel "Bubba" Lipe, and Dr. Julieene K Maeda.

Mahalo ā nui i nā mea waihona kālā kūmau. (Gratitude and appreciation to my funders). My gratitude is also extended to the generous support by The Kohala Center of Hawaiian Scholars Doctoral Fellowship Program, The Deviants from the Norm Fund and Dr. Paul and Elizabeth Nakayama. I would not have continued on and completed my Ph.D. journey without their financial support. I am also grateful to the staff of Kuaʻana Native Hawaiian Student Services, Nā Pua Noeʻau,

the College of Engineering Student Ambassadors Program, and the Native Hawaiian Science and Engineering Mentorship for their support throughout the years.

Mahalo ā nui i nā hoa aloha. (Gratitude and appreciation to my friends). I want to express my gratitude to my good friends whom I have shared many late night talks, ʻawa sessions, and laughter on constellating our respective life passions. There were a multitude of individuals who helped me to arrive at this point, and my warmest thanks go to Dr. Patricia Fifita, Dr. Lea Lani Kauvaka, Dr. Sue Haglund, Dr. Kamuela "Wela" Yong, Dr. Ann M. Cross, Rodney Lui, Chablis Paris Mathai, Samson Aeloa Souza, Elizabeth Kaiʻulani Takamori, Leʻa Kimura, Shannon McCandless, Kalei Akaka, Erin Akaka, Kelani Feliciano Cummings, Mark Guerin, Mrs. Nancy Guerin, Dr. Richard Guerin, the late Richard Guerin Jr., Robert Guerin, Meiko Guerin, Queena Tahi, Hoʻoheno Haumea, Ecaterina Apostoiu, Donna "Sweetie" Kuehu, Jordan "Koa" Melcher, Mitch "Kapena" McLean, Haunani Kane, John Ewalt, Keano Pavlosky, Dr. Kealoha Fox, Dr. Kiana Frank, Alana Wilson, Deann Nishimura-Thornton, and countless others. A very special thanks go to my friends from the Civil Engineering department, including Dr. Eulyn Pagaling, Joe McVey, Alex Ferrufino, Shelby Fillinger, Manuela Melo, Angel Herrera Jr., and Sabrina Diemert. I would like to thank all personnel in the Computational Environmental Physics Lab including Tyler Tsuchida, Myung Jin Koh, Noelle Chen, and Siu Fung Tang for wonderful memories. *E kala nui mai iʻau, lo lamento mucho*, my humblest apologies if I overlook anyone in the above acknowledgements, as it is not my intention. You all have been there to uplift me in so many ways.

Mahalo nui loa i mau lālā o kaʻu kōmike. (Gratitude and appreciation to my committee members). My heartfelt appreciation to my committee member's time, attention, and support. I gratefully acknowledge Dr. Robert H. Richmond for his valuable discussion to push me to think critically about the broader impacts of my research. I am grateful to Dr. Babcock for his advice throughout the years. I wish to thank Dr. Sayed Bateni for his continued interest. I want to express my sincere gratitude to Dr. Oleson for her encouragement and serving on my committee.

Mahalo palena ʻole i kuʻu meʻe. (Gratitude and appreciation beyond measure to my dissertation chair). Last but certainly not the least, no words can express and articulate my appreciation to my mentor, Dr. Albert S. Kim, for taking me in as his pupil and shaping me to become an academic. Thank you for providing laboratory space and equipment required during this investigation. Dr. Kim has taught me the value of self-study, the challenging skills of technical writing, and opened my intellect to connect the dots. I am also grateful to Dr. Kim for his valuable counsel not only during this research and dissertation preparation, but throughout my entire academic tenure within graduate school. I admire and hope to emulate your unstoppable enthusiasm for discovery. I owe a great deal to Dr. Kim's family including Mrs. Kim, Ben, and Steve for their sacrifices and lending him to me for conference travels, extended study, and intensive research.

ABSTRACT

Runoff phenomena from urbanization exist as a leading cause of non-point source (NPS) pollution in receiving water bodies. Within island communities such as the archipelago of Hawai‘i, discharging runoffs into the ocean severely affect hydrological, ecological, and anthropogenic environments. Low-impact development (LID) technologies provide environmentally friendly methods to treat polluted runoff flows with a reduced flow rate. Among the plethora of contemporary LID strategies, bioswales are considered as engineered, natural porous media used for the on-site retention of stormwater runoff and treatment of NPS pollution. Despite the global widespread use of bioswales since the early 1990s, current design guidances provide mostly empirical estimates of removal capabilities as opposed to scientific predictions based on underlying transport mechanisms. Thus, design optimization of bioswales at a fundamentally scientific level has prompted the current investigation to deal with the ubiquitous problem of stormwater management.

In this dissertation, Chapter 1 provides the overview and underlying purpose of the research, which explores methods for understanding engineered bioswale phenomena. To achieve this goal, both theoretical and computational investigations were conducted in Chapter 2 through Chapter 4. Chapter 2 presents an original conceptual framework to quantify bioswale performance, which treats a bioswale as an engineering unit consisting of several conventional physico-chemical processes used in a water and wastewater treatment plant (WWWTP) with basic physical and chemical principles. A detailed conceptual model was created which described a bioswale as analogous to a conventional WWWTP process. This comprehensive conceptual model includes applicable fundamental equations to characterize transport phenomena and evaluate bioswale performance. Chapter 2 suggests innovative and original perspectives regarding computational fluid dynamics (CFD) as promising tools to compensate for existing deficiencies within conventional design approaches.

In Chapter 3, CFD simulations were conducted so as to fundamentally investigate hydraulic and chemical transport phenomena within a bioswale system, as introduced in Chapter 2. In particular, coupled transport phenomena within a bioswale were studied using the open-source CFD software, OpenFOAM (`www.openfoam.org`), which was unprecedented in the theoretical bioswale literature. The unsteady behavior of momentum and mass transfer was investigated in a double-layered bioswale by seamlessly linking overland and infiltration flows at various time scales. To study the diffusive transport of a model pollutant, a new solver named interPhaseDiffusionFoam (available at `https://github.com/enphysoft/interPhaseDiffusionFoam`) was developed, which better mimics interfacial transport phenomena of dissolved non-volatile species at a water-air boundary. This investigation identified that heterogeneous infiltration patterns are originated in a strongly coupled manner by stormwater runoff velocity, reverse air flow, and the presence of the drain pipe. Overall, the 2D CFD simulations, used for multi-phase (water, air, and soil) transport phenomena, can be further applied to the structural designs of bioswales with specific geometric and hydraulic

conditions throughout communities all around the world.

Chapter 4 provides theoretical hydraulic-design perspectives regarding the characterization of the bioswale vegetation layer (BVL). The Chapter 4 study employed a meta-research approach ("research on research") consisting of an original meta-theoretical development based on an in-depth literature review of well-accepted theories. The newly described design equation within this chapter links stormwater hydraulic properties (represented by Reynolds number Re) and bioswale geometry (characterized by a geometrical ratio, denoted as η) to predict the minimal bioswale length for effective performance within an emergent case. An innovative graphical method is developed so as to estimate the optimized length-to-width ratio of a respective bioswale. Moreover, this study found that a critical Reynolds number ($\mathrm{Re}_{\mathrm{p,cr}} = 10^{1.5} = 31.623$) exists as being universal and, hence, independent of a geometrical parameter ab. If the Reynolds number is higher than $\mathrm{Re}_{\mathrm{p,cr}}$, then the bioswale geometry solely determines η without being influenced by stormwater hydraulics. Cross-validation of the new meta-theory is conducted indirectly using experimental data available within the scientific literature. Thus, it is recommended based on chapter 4 findings that a safety factor of 3–5 be multiplied by the theoretical η (obtained using the graphical method) to ensure that the BVL zone provides effective hydraulic resistance to sufficiently decelerate incoming runoff flows within a surface BVL zone. This design theory, with the graphical method, is, to the best of my knowledge, the first approach that links the hydraulic characteristics of stormwater runoff and the geometric properties of a bioswale.

Chapter 5 presents the final conclusions and suggestions for the future development of bioswale systems. The results of this dissertation revealed, for the first time, the relevant underlying physics of stormwater dispersal within a bioswale as an unsaturated porous media. The present bioswale study ultimately represents a further step towards designing ubiquitously robust stormwater treatment facilities so as to protect our precious land and natural waterways.

TABLE OF CONTENTS

LIST OF TABLES

LIST OF FIGURES

CHAPTER 1
INTRODUCTION

1.1 Overview of problem

A bioswale is a landscape structure for reducing stormwater runoff and removing non-point source pollutants using the chemical, biological and physical properties of plants and soil grains [2]. The bioswale exist as a sustainable and renewable technology for efficient low-impact development (LID) and best management practice (BMP) [3]. Over the last three decades, bioswales have been widely implemented to manage on-site stormwater at several urban locations such as parking lots, roadways, and highways [4–6]. The bioswale hydraulics require in-depth analyses of transport phenomena through the surface and interior soil zones.

In bioswale design practice, current guidelines and standards do not guarantee site-specific optimal performances for regular storm events. At present, five bioswale design methods [7] meet regulatory goals in extremum (or to the extremum given current objectives) for stormwater management. These (sizing) methods include (1) Darcy's law [4], (2) the rational method [8–10], (3) Manning's equation [11], (4) the curve number method [12], and (5) the first-flush sizing method [13–16]. For more reliable and sustainable designs, computational approaches are of great necessity to improve the LID/BMP designs so as to deal with both quantity and quality issues regarding stormwater runoff.

Computational fluid dynamics (CFD) has attracted growing attention within various engineering disciplines, including civil and environmental engineering. CFD can be used to predict the hydraulic and transport phenomena at the conceptual design stage [17], providing the following specific advantages. First, CFD can provide a cost-effective means to predict the complex transport phenomena of momentum, energy, and mass (of chemical species) within the multi-phase environment [18]. Second, CFD can calculate flow velocity and pressure profiles of specific hydrologic scenarios [19], especially when experimental design is restricted due to the environmental conditions [20]. Third, CFD can generate numerical data sets for scientific visualization while analytical and experimental approaches have limits to investigate transport processes, especially for coupled cases [21]. Applications of CFD are, however, limited by the model incompleteness, unknown boundary conditions, and numerical errors that make verification difficult.

Modeling is critical for design improvement, cost-effectiveness, and (long-term) maintenance of bioswale systems. In the LID/BMP literature, software programs that can model subcatchment-scale systems include the Guelph All-Weather Sequential-Events Runoff (GAWSER) model [22], the Model for Urban Stormwater Improvement Conceptualization (MUSIC) [23–25], the Soil Conservation Services (SCS) model using the curve number [26], the Smart Growth Water Assessment Tool for Estimating Runoff (SG WATER) [27], the Storm Water Management Model (SWMM) [28, 29], the Storm Water Management Model and Best Management Practice Decision Support

System (SWMM-BMPDSS) [30, 31], and the System for Urban Stormwater Treatment and Analysis Integration (SUSTAIN) [32]. To date, these modeling investigations of bioswales are primarily concerned with routine analyses of experimental data through the examination of macroscale water balances. Throughout the extent of my inquiry, I have found that the current bioswale modeling research related to hydrology and hydrodynamics provides large-scale investigation of runoff and infiltration [7, 33, 34], urban water management employing fuzzy logic [35], water reuse [36], runoff volume reduction at a watershed level [37, 38], and urban runoff control with the SUSTAIN model [31]. These macroscopic modeling methodologies incorporate only approximate overall mass balances, and therefore do not precisely describe the underlying fundamental transport mechanisms at a microscopic scale or pinpoint where ineffective operations of LID/BMP devices may occur.

For the ideal practice of bioswale design, CFD can be an accurate tool to assess various design configurations for pollutant removal and stormwater runoff reduction. Afrin et al.'s [39] CFD work investigated the microscopic flow-field through a perforated drainage pipe. However, their investigation did not include coupled flow-mass transport occurring on the top surfaces and in the internal spaces of the bioswale. Improperly designed units may cause unexpected hydrodynamic problems and subsequently make stormwater management more complicated. Well-researched initial design is essential for long-term sustainability and proper LID/BMP functionality. More specific and reliable design tools are, therefore, of necessity for the optimized bioswale practices. This work, for these reasons, aims to develop specific computational theories, numerical algorithms, and, finally, a CFD solver to predict the performance of bioswale systems based on physical and chemical sub-processes within bioswale soil-zones.

1.2 Objectives

The objectives of this dissertation, including principal tasks to be accomplished, are formulated as follows:

1. A survey on the literature regarding bioswale systems (Chapter 2) so as to develop a conceptual framework to quantify the performance of a bioswale treated as a combination of conventional physico-chemical processes

2. A study of the unsteady flow behavior of a double-layered bioswale in 2D spaces (Chapter 3) so as to simulate the diffusive transport of a model pollutant by developing a new solver named interPhaseDiffusionFoam and to determine the influence of a drain pipe on stormwater infiltration patterns

3. An investigation of the conventional theories of canopy flow (Chapter 4) so as to develop a design equation for an emergent bioswale vegetation layer (BVL), which suggests the proper length-to-width ratio of a bioswale as a function of a runoff's respective hydraulic characteristics.

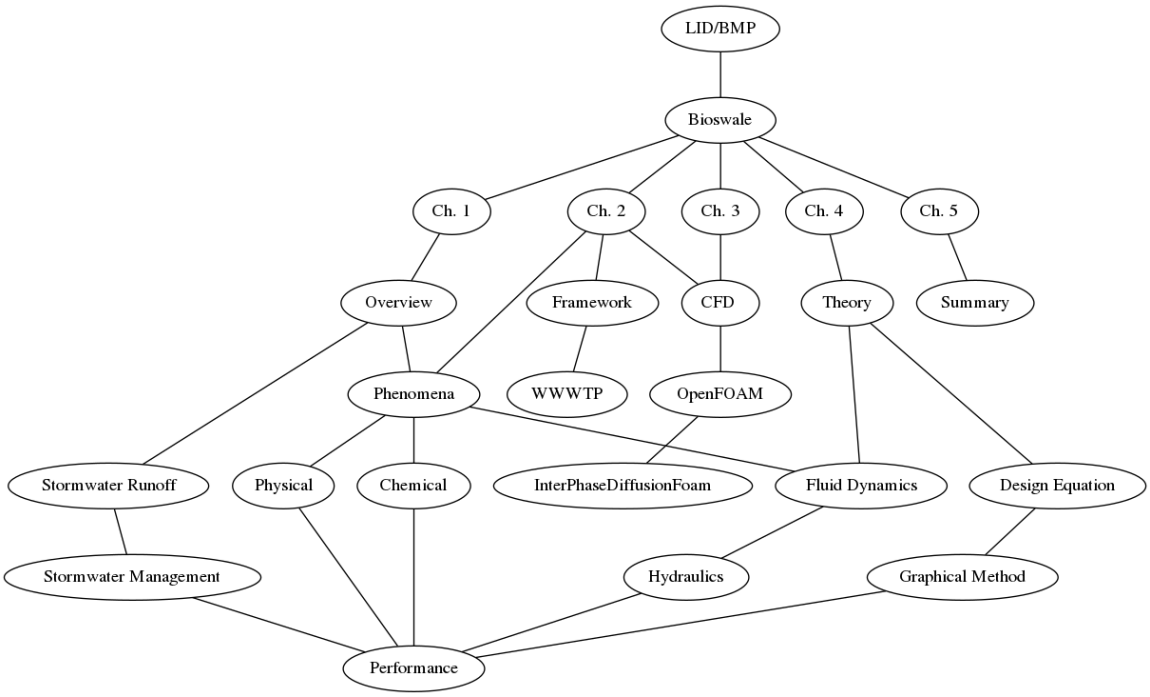

Figure 1.1: Organizational structure of the dissertation.

1.3 Thesis organization

Fig. 1.1 presents an overview of the thesis organization. What stands out in this figure is that the first two nodes, LID/BMP, and Bioswale are the central focus of this scientific inquiry. The Bioswale node is further divided into five categories, which represent the five chapters of this dissertation. The predominant thesis within each chapter investigates specific aspects of respective engineered bioswale systems.

Chapter 1 investigates the promising potential of bioswale systems and includes a brief overview of stormwater runoff and management. This initial chapter succinctly describes the relevancy, urgency, and overall objectives regarding bioswale system research. In Chapter 2, an extensive review of bioswale systems literature is presented. As show in Fig. 1.1, the Ch. 2 node sub-divides into Phenomena, Framework, and CFD, which exist as the three primary themes addressed in Chapter 2. This chapter also investigates the current state-of-the-art technological developments and practical applications and discusses the origins and usages of specific LID/BMP terminologies. A universal research framework is proposed regarding how to analyze bioswale systems as a miniature version of a combined water and wastewater treatment plant (WWWTP). Dominant transport phenomena are reviewed with basic governing equations so as to quantify bioswale performance. Since LID/BMP devices are installed underground, transport phenomena are difficult to measure continuously in real-time. Thus, Chapter 2 presents perspectives regarding how CFD can be used to investigate the mass and momentum transport phenomena within the subsurface bioswale zone.

In Chapter 3, as shown in Fig. 1.1, the Ch. 3 node proceeds to discuss CFD for LID. The CFD platform employed is OpenFOAM [40–42], an open-source software used for multi-physics simulations. To the best of my knowledge, chapter 3 is the first CFD study on LID devices in the OpenFOAM literature. Due to computational limitations, a pseudo-2D configuration of a bioswale was investigated, which provides valuable insights of coupled transport between runoff momentum and pollutant mass transport phenomena. In this chapter, a new solver, named interPhaseDiffusionFoam (available at [1]) was developed to study the diffusive transport of a model pollutant. The interPhaseDiffusionFoam solver better mimics (than conventional OpenFoam solver, interFoam) transport phenomena of non-volatile species at a phase boundary between water and air. Results in chapter 3 have significant potential implication in the design and analysis of bioswales for better efficiency and stable maintenance. Findings of this study formed the problem identification of further study in our next chapter. The newly developed CFD solver is discussed and applied to characterize a bioswale as a runoff-storing and pollutant-filtering media.

Chapter 4 identifies the design problem that originated from the research detailed in Chapter 3. From Fig. 1.1, the Ch. 4 node connects to the subcategory of Theory, which further breaks down into Fluid Dynamics and the Design Equation. In this chapter, a meta-research, meaning "research of research," approach is applied, consisting of an in-depth literature review of conventional theories of canopy flows followed by original theoretical development. A design equation and supplementary graphical method are presented as efficient tools to determine bioswale length in order to enhance performance. Fig. 1.1 illustrates that all nodes descending from the initial LID/BMP node lead to the better understanding of an engineered bioswale's respective Performance. Finally, Chapter 5 summarizes the conducted research on bioswale systems included within this dissertation.

[1] `https://github.com/enphysoft/interPhaseDiffusionFoam`

CHAPTER 2
UNDERSTANDING BIOSWALE AS A SMALL WATER AND WASTEWATER TREATMENT PLANT: A THEORETICAL REVIEW

This part of the dissertation is a manuscript submitted on June 15, 2018, and accepted for publication on September 12, 2018, to Desalination and Water Treatment.

Stormwater threats can be mitigated with the application of sustainable and renewable technologies such as low-impact development (LID) and best management practice (BMP). This paper aims to fill the present gap in practical applications and engineering science regarding modeling bioswales, a type of LID/BMP devices. Included is a new theoretical framework that treats bioswales as combined physico-chemical processes. A discussion of a coherent analogy between the bioswale and a conventional water and wastewater treatment plant (WWWTP) is presented without including biological processes. Finally, we provide new perspectives regarding computational fluid dynamics (CFD) for widespread use as a promising tool to optimize LID/BMP design for stormwater management.

2.1 Introduction

Low-impact development (LID) and best management practice (BMP) are important components within the praxis of stormwater management. These management practices have evolved considerably in the last five decades. In 1972, the United States (US) created the National Pollution Discharge Elimination Systems (NPDES) program through the legalization of Section 402 of the federal Clean Water Act. This action further led to the US Congress amending the Water Quality Act in 1987, which established a framework for regulating the quality of stormwater discharges. The NPDES permit, which is issued by the US Environmental Agency (EPA) or an authorized State [43], has been functional since the 1990s. Subsequently, the term BMP entered mainstream usage with the intention to control stormwater quality and treat storm flows within urban areas by emulating pre-development flow regimes [44].

Structural BMPs include the application of artificial units such as infiltration, filtration, detention/retention systems, wetlands, vegetated systems, and water quality treatment systems. Nonstructural BMPs consist of system maintenance, land-use planning, and outreach programs [45]. A bioretention system (represented by a bioswale) has received close attention in the past thirty years, as it can effectively provide in-situ stormwater quality and quantity control. A bioswale comprises small areas excavated and backfilled with a mixture of high-permeability soil and (optional)

organic matter. The systems are often covered with native terrestrial vegetation to provide natural landscaping and maximum infiltration.

The creation of a bioswale, first practiced in Prince George's County, Maryland, USA [46], depends on ecological interactions within a natural system for the stormwater and pollutant removal. Interactions between human-made bioswales and the natural environment rely on various physico-chemical factors, such as precipitation patterns, solute-soil interactions, and size of sediment particles and soil grains. The infiltration occurs after the runoff process starts until the bioswale is fully saturated, but the transport phenomenon has a wide span of timescales within this context. Stormwater infiltration and pollutant convection occur within the order of a few hours, which depends on the size and porosity of the bioswale [47]. The evapotranspiration requires a considerably longer time span—an order of a few days—based on the characteristics of the vegetation and topsoil layers [47, 48].

Bioswale modeling is critical for optimal designs, cost-effective building, and long-term maintenance. To date, most simulation investigations on bioswales are limited to the analysis of experimental data and modeling macroscale (e.g., watershed) water balances. Specifically, bioswale modeling research related to hydrology and hydrodynamics include runoff and infiltration [33, 34, 49], urban water management employing fuzzy logic [35], water reuse [36], runoff volume reduction at a watershed level [37, 38], urban runoff control with the System for Urban Stormwater and the Analysis Integration (SUSTAIN) model [31] and DRAINMOD [49]. Palla and Gnecco [50] simulated the hydrologic responses of an urban catchment for various rainfall scenarios using the EPA Storm Water Management Model (SWMM) with LID control modules for a large land area of 5.5 ha. Their results confirmed that land use should be minimized for effective LID operation, and hydrologic performance improves as the size of the effective impervious area decreases. Xu et al. asserted that SWMMM provides the highest level of accuracy in design tools [51]. In particular, Xu et al. investigated optimal ratios of land-use/land-cover for the development of urban catchments, however, this approach did not consider localized phenomena to optimize the performance of a single LID device. Similarly, Bloorchian et al. used the personal computer stormwater management model (PCSWMM) which is a GIS version of EPA SWMM. This method is an idealized subcatchment approach to simulate runoff reduction within a bioswale, vegetated filter strip, and infiltration trench using the Manning's equation [52]. Other modeling studies directly related to bioswale have investigated the removal of suspended solids and metal ions from the urban runoff flows [53–55]. For bioretention systems, Brown et al. predicted the continuous, long-term hydrologic response of the technology to influent runoff using DRAINMOD [49]. The calibrated and validated model predicted runoff volume for contributing area runoff of varying imperviousness. Similarly, Hathaway et al. studied bioretention function under possible climate change scenarios in North Carolina, USA, utilizing calibrated DRAINMOD models to establish hydrologic regimes under present day and projected future climate scenarios [56]. Their study focused primarily on water balances

to cope with increased rainfall magnitude instead of dealing with specific chemical, physical, and biological transport phenomena. However, these modeling studies were limited to the analysis of experimentally observed data and did not consider a range variation of bioswale configurations.

Green roof systems, a type of LID device, perform similar primary functions as a bioswale with regards to runoff reduction and pollutant removal. Stovin et al. developed a conceptual hydrological flux model and used 30-year hourly climate projections in multiple United Kingdom locations to simulate the long-term runoff and drought risk associated with the application of green-roof systems [57]. Their modeling methodology was based on solving governing equations of large scales from hydrological and agricultural science literature. A comprehensive review study concerning green roof's hydrologic performance can be found elsewhere in the literature [58]. A similar technique can be employed to estimate a long-term performance of unit bioswale systems based on fundamental governing equations in fluid mechanics. We believe that computational fluid dynamics (CFD) modeling is a more accurate simulation approach, which can also predict the momentum and mass transport across the bioswale. The coupling of surface and porous-media flows with non-volatile solute transport in an aqueous phase, however, presents a difficult task in the achievement of rigorous modeling of bioswale systems. Afrin et al.'s most recent CFD work investigated the flow field through a perforated drainage pipe [59], but their work did not include coupling of the overland and infiltration flows on the top bioswale surface. For accurate prediction and design optimization of bioswales, a holistic modeling framework is of great necessity, which can consist of dominant transport mechanisms and governing equations for each subzone within the bioswale.

This review paper proposes that a bioswale, on a theoretical level, can be considered as a combined unit process of hydraulic, chemical, and biological treatments. Therefore, the paper describes a coherent analogy between the bioswale and a conventional water and wastewater treatment plant (WWWTP). The theoretical framework includes dominant transport mechanisms and governing equations for accurate prediction and design optimization. Finally, our work provides new perspectives of using CFD as a universal modeling platform to specifically investigate coupled transport phenomena in bioswale systems.

2.2 Theoretical review of basic transport phenomena

This section includes the fundamentals of transport phenomena in direct relation to those that take place in a bioswale. The momentum transfer phenomena include overland surface flow, outgoing overflow, infiltration, and drainage; and the mass transfer phenomena comprises sedimentation, granular media filtration (GMF), and granular activated carbon (GAC) adsorption. Our technical review focuses on specific models of each subprocess with governing equations, which can further enhance a holistic understanding of the bioswale transport phenomena.

2.2.1 Overview of specific processes

A bioswale contains numerous external and internal components. An inlet structure is created in a bioswale as a slanted surface to direct urban runoff from the surrounding areas. The top area

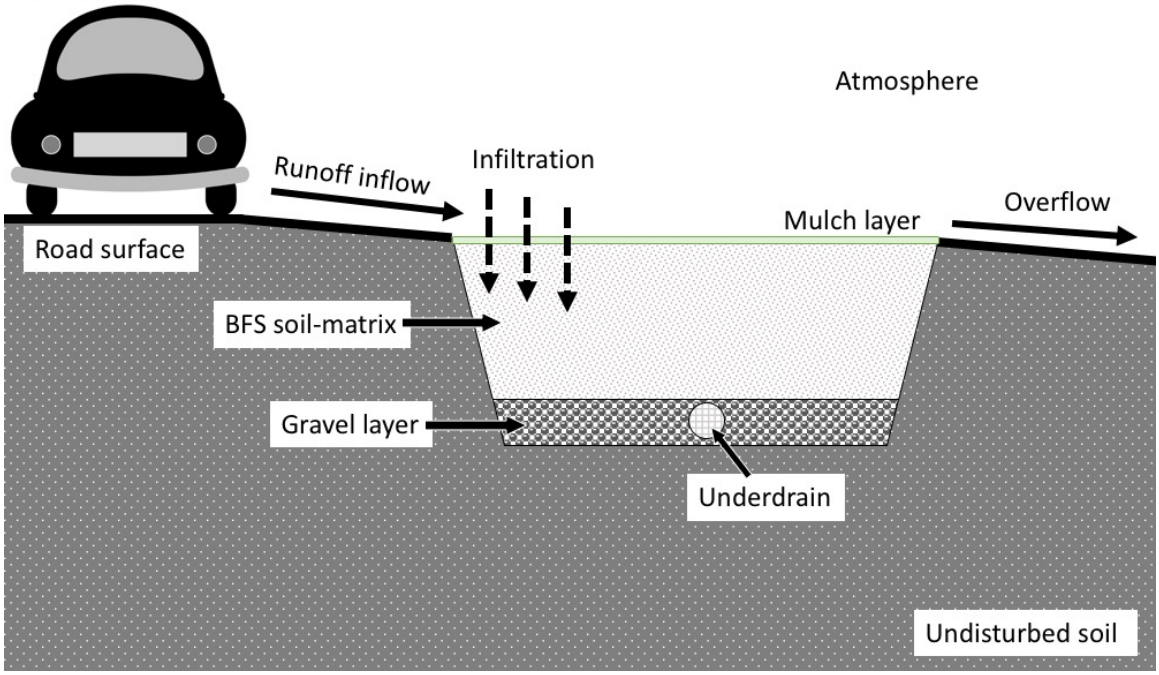

Figure 2.1: Schematic of a typical bioswale system.

of a bioswale is designed to store ponded water. An overflow bypass diverts accumulated water that exceeds the respective unit's ponding capacity. An underdrain structure, or pipe, can be optionally installed at the bottom of the unit to prevent unnecessary water stagnation over a prolonged period. Filtration media is an amended soil that contains considerably higher permeability compared to those of the natural ambient soil materials. Considering the previously mentioned structural aspects, a bioswale can be perceived to form a miniature WWWTP.

Figure 2.1 offers a schematic diagram of a typical bioswale system. In this study, we analyze transport phenomena in a bioswale, considered as a complex system containing numerous unit processes as described as follows. First, the inlet structure and the top surface of a bioswale usually contain vegetation layers, consisting of grasses, low-growing plants and ground cover, which are known as short plants. These vertically embedded natural objects offer hydraulic resistances to runoff water and capture large debris on or within the vegetation layers. One of the functions of the vegetation layer is analogous to the performance of bar racks in WWWTP. The top surface of a bioswale is often located slightly below the overflow structure in order to generate a necessary ponding capacity. Runoff water flows in a lateral direction from the inlet to the outlet sides. As the vegetation in this potential ponding zone offers significant hydraulic resistance, flow deceleration can enhance the sedimentation rate of large particulate materials on orders of 10 microns or above. Second, a mulch layer may cover the root zone of the plants, which can provide organic environments for small living organisms [7, 60]. This mulch layer is installed to conserve soil moisture and prevent weed growth. Conversely, a dry mulch layer absorbs initial rainwater and contributes to the removal of specific chemicals in runoff water. Third, the granular soil media has high permeability and is often mixed with organic matter to enable the adsorptive removal of organic pollutants. The combined media, consisting of the top mulch layer and the internal mixed-soil zone, can play similar roles of GMF of particulate materials, GAC adsorption of organic matter, and biological degradation of inorganic pollutants in the WWWTP.

Fourth, the porous zone covering the underdrain pipe comprises of gravel or stones, which possess considerable hydraulic conductivity. This underground drainage mimics the distributing unit of WWWTPs, because discharged water may not contain a higher pollutant concentration than that within the runoff. Primarily, a bioswale can significantly reduce stormwater volumes through real-time infiltration and post-storm evapotranspiration. The bottom drain zone of a bioswale can be specifically designed to retain previously infiltrated water until the occurrence of the next storm event. As the hydraulic permeability of the bioswale soil is usually considerably higher as compared to that of the ambient soil, the permeability at underground boundaries between the bioswale and ambient soil zones may not serve as a significant factor so as to estimate the bioswale performance. Fifth, the water volume, initially reduced by a dry bioswale, is equal to the internal void volume of the bioswale (i.e., the overall volume multiplied by the average porosity of the composting soil media). When a dry bioswale becomes fully saturated with infiltrated water, various pollutants

from non-point sources can be captured and removed by the bioswale at the point sink. Prediction of the pollutant removal by the bioswale is a difficult task because the chemical and biological characteristics of the bioswale are only partially known. In this section, we specifically characterize a bioswale in terms of overland and infiltration flows, vegetation layer of high hydraulic resistance, sedimentation of suspended solid in the vegetation layer, GMF of fine particles by soil grains, GAC process for the adsorption of organic matter, and underground drainage. Pollutant removal using microorganisms living in the bioswale is another important topic, which is, however, out of our research scope, as the fluid flow and chemical transport significantly influence biological activities in engineered systems. Conventional and contemporary theories are introduced to investigate the complex transport phenomena in the bioswale.

Overland flow on the bioswale surface consists of inflow and overflow of the bioswale, and the fractional difference between these two flow types is equivalent to the infiltration flow. Darcy's law and the principle of continuity of flow through a porous media dictate the form of equations prescribed to describe the infiltrating motion of water through a particular kind of soil. As water is an incompressible fluid, flow rates of the inflow, overflow, and infiltration flow are strongly coupled by the constant density and viscosity of water. The rigorous numerical solution that completely couples groundwater to surface water through a non-homogeneous soil is represented by the Richards equation

$$\frac{\partial \theta}{\partial t} = \frac{\partial}{\partial z}\left[K\left(\theta\right)\left(\frac{\partial h}{\partial t} + 1\right)\right] \tag{2.1}$$

where K represents the hydraulic conductivity, h implies the matrix head induced by capillary action as a function of x and y in three-dimensional space, z refers to the elevation above the vertical datum, θ is the volumetric water content, and t is the time. The Richards equation, in reality, comprises of several models and numerical techniques for a better approximation of infiltration, and the multidimensional Richards equation can be applied to simulate the solute transport for various cases but barely used to investigate LID/BMP systems [61].

2.2.2 Flows in free and porous spaces

If the solid matrix possesses uniform porosity and a constant saturation ratio initially, then some theoretical approximation are available to solve the infiltration flux for a single rainfall event [62–65]. Green and Ampt assumed that the soil surface is covered by a thin water layer with negligible thickness [62], which implies that its infiltration capacity f_p is a linear function of S/L

$$f_p = K_s \frac{L + S}{L} \tag{2.2}$$

where S represents the capillary suction at the wetting front, L forms the distance from the soil surface to the wetting front, and K_s represents the hydraulic conductivity of a saturated zone. However, Mein and Larson [63] re-defined

$$f_p = \frac{\mathrm{d}F}{\mathrm{d}t} = K_S \left(1 + \frac{S\Delta\theta}{F}\right) \tag{2.3}$$

where F is the cumulative depth of infiltration, equivalent to $S\Delta\theta$, and $\Delta\theta$ represents the initial moisture deficit. The Green-Ampt Mein-Larson approach presumes the slope of the energy line as identical to the slope of the flow plane. These basic mass balance equations implicitly assume that the overland flow of a finite water-depth does not affect the infiltration rate.

For a shallow overland flow, a kinematic wave equation is expressed as

$$\frac{\partial A}{\partial t} + \frac{\partial Q}{\partial x} = j_e b \tag{2.4}$$

where A represents the wetted cross-sectional area of the plane flow, Q the discharge rate, j_e the rainfall excess (velocity), and b stands for the lateral extent of the flow. Eq. (2.4) indicates that the precipitation flow rate equals the difference between the inflow plus the discharge rates per length along the direction of the surface flow. The velocity and pressure gradients, nevertheless, are still assumed to be negligible in this case.

In CFD, a free-surface can be modeled to track and locate the phase interface using the Volume of Fluid (VOF) method [66, 67]. A two-phase flow of incompressible and immiscible fluids of air and water with a specific surface tension can be examined in a full domain consisting of an open space and a porous medium. Instead of dealing with transport in each phase separately, a phase-averaging method was employed in the VOF method. For a mixture of water (denoted as 1) and air (denoted as 2) in a fluid cell, their fractions (α) should satisfy a sum rule: $\overset{[}{i}= 1]2\sum\alpha_i = \alpha_1 + \alpha_2 = 1$, indicating that the volume of the fluids is invariant. The evolution of α_i is governed by the following transport equation

$$\frac{\partial \alpha_i}{\partial t} + \boldsymbol{U} \cdot \nabla \alpha_i = 0 \tag{2.5}$$

where $\boldsymbol{U}$ represents the mean velocity of the fluid because all the fluid is assumed to be incompressible in the VOF method. The incompressible form of the governing equation includes the zero divergence of ($\nabla \cdot \boldsymbol{U} = 0$). The Navier-Stokes (N-S) equation for this case is

$$\frac{\partial \boldsymbol{U}}{\partial t} + \nabla \cdot (\boldsymbol{U}\boldsymbol{U}) - \nabla \cdot (\nu \nabla \boldsymbol{U}) = -\nabla p \tag{2.6}$$

where ν represents the kinematic viscosity and p forms the pressure. The basic balance equations (2.5)-(2.6) of the VOF method can be employed to accurately simulate the overland flows on various types of surfaces. To the best of our knowledge, CFD applications for the initial design stages of bioswales or LID/BMP are very limited within the literature.

Fluid dynamic simulations in interstitial spaces between soil grains continue to pose a formidable task for researchers. Instead, the soil media can be treated as a uniform porous media characterized by the use of constant porosity and hydraulic conductivity or permeability. In isotropic porous

media, the volumetric flux density $\boldsymbol{q}$, i.e., flow rate per unit cross section, can be expressed using Darcy's law

$$\boldsymbol{q} = -\frac{\kappa}{\mu}\nabla p \tag{2.7}$$

where κ and μ represent the soil permeability and the water viscosity, respectively. When an inertial effect of the porous media flow is important, the pressure gradient exerts non-linear effects on $\boldsymbol{q}$, expressed as Darcy-Forchheimer law

$$\nabla p = -\frac{\mu}{\kappa}\boldsymbol{q} - \frac{\rho}{\kappa_I}|\boldsymbol{q}|\,\boldsymbol{q} \tag{2.8}$$

where κ_I represents the inertial permeability. Note that $\boldsymbol{q}$ implies an average flow rate of fluid through a porous media per unit cross section, equal to the incoming or exiting velocity of the porous medium. In this case, we have $\boldsymbol{q} = \boldsymbol{U}$ on the boundary between the free and soil spaces. The microscopic fluid speed between adjacent soil grains must exceed $\boldsymbol{q}$ and be approximately equal to q divided by the average porosity.

In a 2017 study, García-Serrana et al. discussed significant issues on bioswale modeling research [68]. These are summarized as follows: (1) seamless integration of the overland flow and infiltration models, as the overland flow is influenced by slopes and lateral surface properties; (2) the accuracy of the side-slope model, which is currently limited to Manning's equation adopting the slope and roughness parameters; (3) optimal relationship between the lateral slope and surface characteristics of a bioswale; and (4) effects of hydraulic properties on runoff volume reduction. To the best of our knowledge, VOF and Darcy's law, also known as the Darcy-Forchheimer law, have not been combined and applied to investigate the fluid dynamic characteristics of the bioswale at a fundamental level. In our opinion, the theoretical combination constitutes a fundamental approach for the simultaneous modeling of overland and infiltration flows in bioswale. The effect of water depth and speed on the infiltration rate can be systematically examined by considering specific scenarios such as the relative magnitude of rainfall rate, saturated conductivity, and infiltration capacity. The VOF is believed to constitute a reasonably accurate model. This approach can be applied to resolve the runoff flows for impervious rough surfaces. One can examine the optimal conditions for the geometric configuration of the side-slopes and the hydraulic properties of the bioswale soils, which can be employed to optimize the bioswale performance. The bioswale design can be enhanced for specific sites through the consideration of regional patterns of precipitation rates and runoff flows. This fundamental fluid-dynamics approach does not require the calibration of specific parameters utilizing observation or simulation data sets. Bioswale designs will be less sensitive to empirical correlations of transport phenomena, of which universal applications are fundamentally questionable.

2.2.3 Vegetation layers

The use of asphalt and concrete surfaces has altered environmental hydrodynamics and surface

erosion on natural ground since it was first used to pave streets throughout the US in the 1870s [69]. In practice, the retrofitting of paved surfaces to natural vegetated systems can allow the re-saturation in the first few inches of topsoil, thus reducing stormwater runoff [70, 71]. The vegetation layer in a bioswale offers specific hydraulic resistance and modifies the overland flow [72]. The damping capability of the vegetation layer decelerates the plane flow over the bioswale surface and dissipates the hydrodynamic energy carried by the runoff water. Non-vegetated bioswale surfaces are often subjected to soil erosion, due to low-quality landscaping. The essential plant characteristics for creating a flexible vegetation layer comprise volume-fraction, size, shape, and thickness. Native species plantings are preferred for overall bioswale sustainability, but they do not always provide optimum solutions for hands-free maintenance. The structure of vegetation layers, therefore, require careful design to ensure the optimal, consistent operation of a bioswale. The calculation of the hydraulic resistance of the vegetation layer is a complex task due to the intrinsically flexible features of the plants. Depending on the runoff depth, the vegetation layer can be described as submerged or emerged.

The following review includes further research work on fluid flows over or through rigid and flexible vegetation layers. Vargas-Luna et al. [73] stated that there are limited modeling studies that investigate vegetation effects on morphodynamics, performance, and applicability ranges. In CFD modeling, the vegetation layer can be represented by cylindrical rods if the plants have enough rigidity. Zhang et al. [74] examined the transverse distribution of open-channel velocity through an artificial emergent vegetation layer. In their, pairs of large and small buoyant spheres form a chain-like flexible structure, which resembles buoyant-positive emergent plants. They modified Shiono and Knight's work [75] (hereafter referred to as SK) concerning depth-averaged N-S equations and supplemented the vegetation drag force F_d expressed below

$$\rho g H S - \frac{1}{8} f U_d^2 + \frac{1}{2}\left(\frac{f}{8}\right)^{1/2} \rho \zeta H^2 \frac{\partial^2 U_d^2}{\partial y^2} - \sum F_d = \frac{\partial \left[H \left(UV\right)_d\right]}{\partial y} \tag{2.9}$$

where ρ represents the fluid (water) density, g constitutes the gravitational acceleration, f the drag coefficient, ζ the transverse eddy viscosity coefficient, H the water depth, S the bed slope, and U and V represent the flow velocity components in $x-$ and $y-$directions respectively. The subscript d (of U_d and $(UV)_d$) indicates the depth averaging of a respective quantity. A central approximation employed within the Zhang et al.'s approach is $(UV)_d = \overline{k} U_d^2$, where the empirical proportionality $\bar{K}$ is determined by fitting suitable experimental data. An asymptotic solution was developed as follows: $U_d^2 = C_0 + C_1 e^{(\beta_1 y)} + C_2 e^{(\beta_2 y)}$, where coefficients C_i and β_i are determined using boundary conditions. Calculated depth-averaged velocities demonstrate reasonable agreement with measured data for various water depths. Differences between measured and simulation results were observed primarily along the interface between the vegetated and non-vegetated domains. This consistent discrepancy must be caused by the strong 3D turbulence flow at the interface. Note that the depth-

averaged NS equation is fundamentally limited to the depth of maximum 0.2 m. In a 2013 study, Liu et al. modified the SK method for both emergent and submerged vegetation and derived the depth-averaged velocity and bed shear stress of an open channel flow [76]. The Liu et al. research group discovered that the sign of the secondary flow parameter is determined by the rotational direction of the secondary current cells and is dependent on the flow depth. Thus, it is implied that overlooking secondary flow seems to cause a noticeable computational error.

Since real-world flows are transient, the large-eddy simulation (LES) approach is a standard method for many turbulence investigations. To study the flow, scour, and transport processes, Kim et al. [77] applied the LES approach with a ghost-cell immersed-boundary method proposed by Nabi et al. [78] and computed the flow and bed morphodynamics through model vegetation consisting of emergent rigid cylinders. This approach provided a robust framework of combined hydrodynamic modeling, sediment transport, and a morphodynamic approach. In principle, the LES method resolves the computational issue of the large eddies first and then computes smaller ones with a turbulence closure. The subgrid-scale (SGS) stress deals with the effect of small scales on the resolved turbulence [79]. The morphodynamic model created by Kim et al. mimics the temporal elevation of the bed due to the growth of deposited particles and offers a reasonable agreement between the computation and actual experiments [77]. LES applied with the ghost-cell method, however, does not accurately account for the fluid velocity of the free surface, which is treated as a rigid surface for local acceleration. Gao et al. employed a 3D LES approach with the finite volume method (FVM) so as to simulate the flow field and buoyant jet dilution through emergent vegetation [80]. The presence of vegetation diminished the channel velocity but promoted strong flow spreading and effluent dilution. Lu and Dai employed various CFD methods (LES, Reynolds-averaged Navier-Stokes, laser Doppler anemometer, and particle image velocimetry) to model 3D flow fields and scalar transport in an open channel consisting of submerged and emergent vegetation layers [81]. Lu and Dai obtained a reasonable agreement between the simulation results and data measurements. In the case of understanding bioswale performance, the LES approach can be applied to simulate flow patterns in the vegetative layer.

Wang et al. examined the interplay between emergent vegetation density and rainfall intensity [82]. They represented the dimensionless drag term, C_d, by modifying the Saint-Vanent equations as a function of bed slope, pressure, advection, and rainfall rate. However, to analyze this correlation, a few parameters should be determined through empirical data fitting. Therefore, the model predictability is limited to available experimental data of a specific bioswale. Bioswale research tends to neglect the heat transfer between runoff water and bioswale soil layers. Larmaei and Mahdi applied the double-decomposed depth-averaged continuity and momentum equations to simulate 2D heat flux, and fluid flows in various vegetation layers [83]. In their work, case studies compared the effects of different plant configurations for emergent and submerged vegetation. It was shown that the vegetation structure primarily influences the flow field followed by the heat flux. For long-term

operations, evapotranspiration of the bioswale must depend upon humidity and temperature profiles. This review shows that little research has investigated systematically coupled heat and mass transfer in a bioswale.

Our current understanding of vegetation effects on fluid flow and sediment transport is limited to the use of simple models, which are primarily based on experimental approaches. In the past decade, advances in computational resources have been made to simulate flow fields within vegetation layers, as described previously. However, less explored topics in CFD research include how the vegetation layer controls the particle sedimentation by exerting effective hydrodynamic drag forces and torques. In particular, limited research has been conducted to estimate the apparent coefficient of vegetation drag in terms of plant species, biological characteristics, geometric configurations, and the Reynolds number. Since these flow behaviors in bioswales are very complex, the derivation of analytic solutions through mathematical calculations is a challenging task. Therefore, we suggest CFD simulation as a reliable, complementary tool for the precise prediction of coupled phenomena not only for vegetation fluid dynamics but also for gaining an in-depth understanding of basic transport phenomena of the respective bioswale.

2.2.4 Sedimentation

Sedimentation plays a significant role in solid-liquid separation. In the initial stages of a precipitation event, stormwater enters the mulch and vegetation layers, where surface clogging occurs initially due to the deposition of organic matter and particulate sediments. Fine particles (less than 6 μm in diameter) are primarily responsible for surface clogging, which progressively reduces the infiltration rate [84]. A few micron-sized particles are subjected to both the Brownian motion and the shear rate so that the dynamic behavior of the particles is generally hard to predict. The reduced infiltration rate is ascribed to the reduction of soil porosity and, hence, hydraulic conductivity. In practice, it is recommended to replace the bioswale soil mixture every 15 years due to the long-term accumulation of particles and pollutants, which leads to clogging and exhaustion of the bioswale, respectively [85]. Conversely, whether 15 years constitutes a reasonable life expectancy remains contestable. Effective maintenance strategies include the replenishment of the mulch layer, removal of weeds and dead plants, and stabilization of eroded soils [86, 87]. Filter strips and grass swales are widely used as a pretreatment for other LID/BMP approaches to prevent premature clogging. When the pollutant removal is less important than the runoff mitigation, swales and filter strips do not contain an engineered filter media or soil matrixes [12, 88, 89]. Restoring the bioswale capacity after each storm event must be a more significant issue in the maintenance strategy instead of replacing the engineered soil matrix periodically. Lu and Dai specifically investigated scalar transport in a flow through a vegetated channel by combining momentum and diffusion equations [81]. Incompressible continuity and N-S equations were employed to attain the momentum transfer. The convection-diffusion-reaction equation was applied for the solute transport in the following manner

$$\frac{\partial C}{\partial t} + \nabla \cdot (\boldsymbol{u}C) = \nabla \cdot (D_t \nabla C) + S_c \tag{2.10}$$

where C and D_t are the concentration and effective diffusivity of particles, and S_C represent a source term. Furthermore, the random walk equation was employed to track the diffusing particles, originally studied by [90] as depicted below

$$x_p\left(t+\delta t\right) = x_p\left(t\right) + \left(\bar{u}_p + \frac{\partial D_t}{\partial x}\right)\delta t + \xi_p\sqrt{2D_t\delta t} \tag{2.11}$$

where x_p and $\bar{u}_p$represent the position and mean velocity of a particle, and ξ_p represents a random number following the normal distribution of zero mean and unit variance. The last term in Eq. (2.11) represents the Wiener process that considers the average length of the random displacement as proportional to $\sqrt{\delta t}$. Note that, in Eq. (2.11), the convective displacement increases linearly with δt. Furthermore, the diffusivity D_t superimposes molecular, turbulent, and mechanical diffusivities. The simulation results of this study are consistent with experimental observations, but mass diffusion phenomena appear to be double-counted in Eulerian Eq. (2.10) and Lagrangian Eq. (2.11).

Bergman et al. applied a mass balance to model clogging in an infiltration trench (for a single trench) [91]. The performance of two stormwater events was compared using the operation data of the initial three years and periods between years 12 to 15. They simulated the clogging phenomena and applied Warnaars et al.'s semi-conceptual infiltration model to verify their predictions [92]. Further, Mikkelsen et al. introduced the clogging trend of a trench and described infiltration rate, Q_f [93] as follows

$$Q_{\mathrm{f}} = K_{\mathrm{fs,bottom}} \cdot l \cdot w \; + K_{\mathrm{fs,sides}} \cdot 2h \cdot (l + w) \tag{2.12}$$

where K_{fs} comprises the field-saturated hydraulic conductivity, estimated using simple flow theory, and l, w, and h represent the trench dimensions. The formation of a clogging layer of fine particles between the soil and trench was modeled with the assumption that the clogging layer thickness increases linearly with respect to time. An effective value of $K_{\mathrm{fs,bottom}}$ was formulated as a function of time

$$K_{\mathrm{effective,\,bottom}}(t) = \frac{b_{\mathrm{total}}}{\sum_{i=1}^{N}\frac{b_i}{K_i}} \approx \frac{b_1}{\frac{b_1}{K_1} + \frac{b_2(t)}{K_2}} = \frac{b_1}{\frac{b_1}{K_1} + \frac{a\cdot t}{K_2}} = \frac{1}{\frac{1}{K_1} + c\cdot t} \tag{2.13}$$

where the parameter b_i denotes layer thickness, and indexes 1 and 2 denote the initial soil layer below the trench (thickness unknown) and the clogging layer, respectively. For simplicity, the soil-layer thickness was assumed to be equivalent to the total thickness of sedimentation. The parameter c varies with the soil layer thickness (b_1), growth rate of the clogging layer (a), and its hydraulic conductivity (K_2). Bergman et al. observed that clogging in the infiltration trench

reduced infiltration rates by a factor of 2 to 4 after the 15th year of operation.

Achleitner et al. used a mass balance to describe the contaminant removal capacity of local infiltration devices, installed within six parking lots [85]. The motivation behind this study revolved around questions regarding whether this considered life expectancy value was feasible. The majority of Cu concentrations were found to be retained in the first 30 cm of soil, which did not exceed the limit of 100 mg/kg. This assessment was conducted using mass balance equations for the total accumulation of Cu after 15 years. Only one site out of six was found to exceed the regulatory limit values.

Furthermore, Le Coustumer et al. examined the clogging phenomena of stormwater biofilters in temperate climates, using the results of a long-term (72 weeks) laboratory experiment [94]. They observed that smaller systems, in relation to their catchment loads, demonstrate greater susceptibility to clogging as the hydraulic and sediment loading increases. Specifically, they reported that infiltration systems clog over the 72-week testing period by a decreasing factor of 3.6. In biofilters' design, the careful selection of appropriate vegetation and structural sizing is recommended to maintain low clogging phases. The particle deposition layer, however, can serve as a dynamic pretreatment step for long-term media filtration.

In the design of permeable pavements, a clogging factor is computed [95] as follows

$$\text{Clogging Factor} = \text{Y}_{\text{clog}} \cdot \text{Pa} \cdot \text{CR} \cdot (1 + \text{VR}) \cdot \frac{(1 - \text{ISF})}{\text{T} \cdot \text{VR}} \tag{2.14}$$

where Y_{clog} constitutes the estimated number of years required for a complete clogging, Pa represents the annual rainfall amount over the site, CR denotes the pavement's capture ratio (defined as the area that contributes runoff to the paved area), VR represents the system's void ratio, ISF constitutes the impervious surface fraction, and T stands for the thickness of pavement layer.

In a 2014 study, Kachchu Mohamed et al. investigated the utility of swales as a pre-treatment for clogging before stormwater enters the permeable pavement systems [96]. They observed that short swales shorter than 10 m achieved 50-75 % removal of total suspended solids (TSS) and swales longer than 10 m only provided a marginal 20% reduction in TSS. Their study does not provide an analytical formulation (validated by experimental observations) to predict optimal swale length depending on various overland flow velocities. These results, however, suggest that excessively long swales may not present a cost-effective solution to treat stormwater runoff.

Sun and Davis investigated the fate of heavy metals (Zn, Cu, Pb, and, Cd) with two mass loadings in laboratory pots for modeling bioretention systems [97]. The treatment of stormwater runoff showed that the removal ratio of the influent metals is higher than 90% within 25 cm of the bioretention depth. The removal efficiencies for Zn, Cu, Pb, and Cd are proportional to the contaminant loadings. Based on the laboratory study, soil replacement took place within a depth of 25 cm, but the roles of mulch and vegetation layers were not specifically studied.

The current understanding of clogging phenomena was limited to the physical modeling studies

used for permeable pavements [98], river morphology [99], and riverbank filtration [100]. Locatelli et al., for example, overlooked clogging in the determination of the static performance parameters of inflow and outflow rates for infiltration trenches, despite the existence of extensive experimental research showing that the build-up increases over runoff time [101]. Thus, additional research is required so as to model clogging reduction when LID/BMP takes place in a treatment train in series. Existing literature does not include a universal modeling technique for LID/BMP systems and specifically does not distinguish between surface and subsurface clogging mechanisms. To the best of our knowledge, there are no studies that have investigated the effects on surface clogging of bioswales from wind erosion and dust particles. We believe that multi-phase and multi-scale CFD may provide a fundamental framework for elucidating the surface and subsurface clogging near top bioswale surfaces.

2.2.5 Granular media filtration

The basic model for the granular media filtration was first developed by Yao et al. [102]. Without the inclusion of chemical or biological reactions of particles, a filter equation was derived as

$$\ln \frac{C}{C_0} = -\frac{3(1-\epsilon)\eta\alpha L}{2d_c} \tag{2.15}$$

where C_0 and C represent influent and effluent concentrations of suspended particles, respectively, ϵ and L form the porosity and length (or depth) of the filter media, respectively, d_c represents the filter grain diameter, and η and α constitute the transport and attachment efficiencies, respectively. The transport efficiency η includes three representative mechanisms: the interception (η_I) of particles moving along streamlines, sedimentation (η_G) of particles due to gravitational forces, and Brownian diffusion (η_D) based on random displacements. A superposition approach, i.e., $\eta = \eta_I + \eta_G + \eta_D$, is widely applied to combine the three major transport mechanisms [103–105]. To accommodate the effect of dense granular packing, Nelson and Ginn employed Happel's sphere-in-cell porous media model to calculate the effective flow field near grains and capturing efficiency [106]. Various applications of Happel's cell [106] model can be found elsewhere [107–110]. In addition to these basic filtration mechanisms, gradual changes in infiltration capacity based on filter ripening and surface clogging form important practical concerns for long-term stable operation and maintenance of GMF.

The soil matrix of a bioswale is similar to the GMF used in WWWTP, in which suspended solids are removed by the passage of water through a porous media. Unlike that in WWWTP, intermittent wet and dry periods represent unique natural occurrences in the bioswales and, in general, stormwater treatment systems. These conditions may affect the removal of pollutants. The direct application of the GMF theory within a bioswale system requires a restriction that the interstitial spaces between soil grains are completely saturated. A further fundamental investigation is specifically required for particle filtration within the saturating bioswale during coupled runoff-generated infiltration [111–114].

LID type	Soil	Pollutant	Removal	Scale
Bioretention [47]	Sand, soil, and mulch	P	67.0-98.0%	Laboratory
Bioswale [116]	Engineered soil (75% lava rock and 25% loam soil)	Minerals Metals Carbon Solids	95.3% 86.7% 95.5% 95.5%	Field
Rain garden [117]	Sand	Cu Pb Zn	56.4-93.3% 81.6-97.3% 73.5-94.5%	Laboratory
	Sand/topsoil	Cu Pb Zn	53.0-77.4% 89.1-96.9% 81.2-87.9%	
	Topsoil	Cu Pb Zn	0.3-69.0% 89.5-98.6% 60.5-71.4%	
General LID [118]	Biochar	Metals & metalloids Organics Nutrients	0.0-75.0% 45.0-100% 29.2–100%	Laboratory and field
Bioretention [119]	Sand/compost, sand, pea, stone, and gravel layers without sorbtive media	TSS N P	89.0-97.0% 38.0-.57.0% 86.0-94.0%	Laboratory and field

Table 2.1: Studies examining granular carbon adsorption by LID

The gain and loss of transported particles on a porous surface are controlled by wind-influenced evapotranspiration intensity in dry weather and rainfall intensity in wet weather [55]. During a storm period, the suspended particles in the runoff stream accumulate upon the bioswale surface and reach a steady state that balances sedimentation, filtration, and overland flow. Delleur reviewed fundamental approaches regarding sewer sediment movement in 2D, which includes roles of bedload movement, suspended load, total load, near-bed solids for both steady and unsteady flows; and emphasized the significance of the particle size distribution [115]. As of 2018, models that can provide analytic equations for the particle transport in unsaturated media are still in a developing stage given current literature and have not been used for bioswale applications.

2.2.6 Organic and inorganic pollutant removal

Organic materials can be mixed with engineered soil grains to enhance the removal of organic pollutants in runoff water. In the granular activated carbon (GAC) process of WWWTPs, an adsorption isotherm quantifies the affinity of the adsorbate (i.e., organic pollutant) for an adsorbent

(i.e., GAC). The isotherm is used to describe the ratio of the adsorbate amount adsorbed onto an adsorbent surface at equilibrium condition. If the aqueous-phase concentration of the adsorbate is in a steady state, the adsorption equilibrium capacity can be estimated using the following mass balance

$$q_e = \frac{C_0 - C_e}{M/V} \tag{2.16}$$

where q_e represents the equilibrium adsorbent-phase concentration of adsorbate [mg-adsorbate/ g-adsorbent], C_0 and C_e represent the adsorbate concentrations in the initial and equilibrium phase, respectively, while M/V indicates the adsorbent mass M per unit volume V. Typically, three types of isotherms are widely used: linear, Langmuir [120], and Freundlich [121]. The Langmuir isotherm assumes a reversible adsorption of an adsorbate, forming a monolayer upon adsorbent surfaces in equilibrium. Then, the rates of adsorption and desorption are assumed to be equal. In the isotherm, a mass loading q_e is derived as

$$q_e = Q_{max}\frac{bC_e}{1+bC_e} \qquad \text{or} \qquad \frac{Q_e}{q_e} = 1 + \frac{1}{bC_e} \tag{2.17}$$

where b represents the Langmuir adsorption constant of adsorbate and Q_{max} is the maximum limit of q_e. Next, the Freundlich isotherm was originally proposed as an empirical equation to fit non-linear trends of $q_e$with respect to the equilibrium concentration C_e, which is due to the heterogeneity of adsorbent surfaces:

$$q_a = K_a C_a^{1/n} \qquad \text{or} \qquad \ln q_a = \ln K_a + \frac{1}{n}\ln C_a \tag{2.18}$$

where K_a is the adsorption capacity parameter, n is the dimensionless adsorption intensity parameter. In this isotherm, a unit of K_a depends on the value of n. Finally, the linear isotherm represents a special case of Langmuir and Freundlich isotherms known to be valid in solutions of low adsorbate concentrations.

For adsorption of a single component adsorbate, the constant influent concentration, C_{inf}, in the mass balance along the depth z is given by

$$\frac{C(z)}{C_{inf}} = \frac{q(z)}{q_e(C_{inf})} \tag{2.19}$$

Table 1 summarizes studies that examined the effects of soil type on the performance of various LID/BMP in terms of the organic and inorganic removal. The results of these studies cannot be cross-compared as they measured different performance indicators. Among them, Xiao and McPherson performed field experiments and observed the performance of engineered soil and trees in a bioswale built next to a parking lot [116]. During the testing period from Feb. 2007 to Oct. 2008, a total precipitation of 563.8 mm was reported by 50 storm events. The bioswale had a

length of 10.4 m, a width of 2.4 m, and depth of 0.9 m. The engineered soil media, composed of a mixture of 75% lava rock and 25% loam fractions, had a total volume of 28.3 cubic meters and was surrounded by a fine graded non-woven geotextile. A pollutant removal study was conducted for minerals, metals organic carbon, and solids, as shown in Table 1. Their average pollutant loading reduction was reported as 95.4% in addition to the 86% iron removal and 97% nitrogen removal. As these solutes are directly from storm runoff, their specific chemical forms were not reported. Hsieh et al. studied phosphorus removal from urban stormwater runoff using repetitive (lab-scale) bioretention columns. In their study, two types of columns are used called RP1 and RP2 [47]. They examined dual-layer RP1/RP2 configuration where the media of low/high hydraulic conductivity are overlapped with high/low hydraulic conductivity. The column having the length of 40 cm and the inner diameter of 6.4 cm was designed to have sufficient organic matter to serve as a plant growth media. During the three months of experiments, they conclude that RP2, consisting of more conventional media, is more efficient in total removal of phosphorus, dissolved from sodium phosphate dibasic (Na_2HPO_4). The input phosphorous concentration is 3 mg/L and the effluent concentration varies from 0.55 to 1.2 mg/L, which is equivalent to the total phosphorus removal ratio shown in Table 1. Good et al. built lab-scale rain garden systems for stormwater treatment, consisting of topsoil-only, topsoil/sand mixture, and sand-only compositions [117]. The rain garden is of the mesocosm-scale having a cylindrical configuration with 180 L internal volume and 0.17 m^2 surface area. The thickness of the top mulch layer above the topsoil was 20 mm in order to mimic the diffusive motion of stormwater across the column of the vegetation layer. An organic topsoil was investigated for the removal of heavy metals (such as Zn, Cu, and Pb) and nitrate. The well-graded coarse sand layer was prepared to provide hydraulic throughput under given rain events. Based on their experimental data shown in Table 1, they concluded that the topsoil is not the optimal substrate to enhance metal or nutrient removal in bioinfiltrative systems, which can be attributed to the inability of topsoil to buffer the pH of incoming stormwater. Mohanty et al. discussed biochar, a carbonaceous porous adsorbent, application as a soil media in general LID systems for stormwater treatment [118]. The pollutant removal and runoff reduction by biochar are determined by various factors, such as particle size, roughness, porosity, hydrophobic surfaces, redox active sites, ash/mineral content, surface function groups, and biological activities.

Shrestha et al. studied nutrient and sediment removal in roadside bioretention systems using various soil media, vegetation, and hydrologic treatments [119]. A total of 121 storms were evaluated for the removal of total suspended solids, nitrate/nitrite-nitrogen, ortho-phosphorus, total nitrogen, and total phosphorus. Ranges of removal efficiencies of total suspended solids, total nitrogen, and total phosphorus are summarized in Table 1. Negative removal values were often listed in their work, which must be attributed to the adsorbed fractions of solutes from the previous storm events. Due to the high organic nitrogen portion, the aerobic condition is required in the soil media to drive mineralization consisting of ammonification and nitrification. On the other hand, the phosphorus

removal is deteriorated due to the saturation of the soil media due to the desorption of soluble phosphorus. They concluded that the nitrogen removal is closely linked to the microbial processes (i.e., nitrification and denitrification), but phosphorus removal heavily relies on soil chemical parameters of the timescale. Although Table 1 implies that a LID type can be classified by it nutrient removal characteristics, representative LID structures such as bioretention, bioswale, and rain garden are originally classified by their geometrical and hydrological aspects. (See the next section for details.) Charlesworth et al. analyzed the application of green and food-based compost to enhance water quality in SUDS/LID devices including swales [122]. They observed that both green compost (GC) and food/green-mixed compost (MC) demonstrated improved performance compared to topsoil in pollutant removal; however, pollutant removal efficiencies were not specifically reported. Trowsdale and Simcock monitored the performance of bioretention consisting of topsoil, subsoil, and sand layers [123] and observed high removal efficiencies of TSS, Pb, and Zn due to the heterogeneous profile of soil permeabilities. The measured data set was only partially reported. Davis et al. [124] summarized the current knowledge on the removal capability of bioretention units for suspended solids, nutrients, hydrocarbons, and heavy metals using, in principle, filtration, adsorption and possibly biological treatment. They indicated the necessity of systematic research on composition and configuration of filling media, drainage configuration, basin geometry, ponding depth, vegetation types, and cost analysis for maintenance and various designs [124]. Moreover, Hunt et al. considered a bioretention as one of the most commonly used stormwater control measures (SCMs) and researched on how to design the bioretention systems to meet the regulatory needs. Specific guidelines are reviewed for geometric sub-zones (called components), fluid dynamic (peak-flow mitigation, hydrology and infiltration), chemical (sequestration of total dissolved solid, pathogen-indicator species, metals and hydrocarbon, phosphorous removal, and thermal pollutant abatement) and biological (nitrogen removal) aspects [125]. It is difficult to make a quantitative conclusion for bioswales' removal capabilities of various solute species due to the lack of fundamental theories and systematically prepared data sets.

2.2.7 Underground drainage

If the bioswale soil is partially saturated or unsaturated, the infiltration of incompressible water into the porous soils pushes pre-existing (compressible) air in the interstitial void spaces between soil grains. Therefore, the surface flow above the bioswale does not move uniformly so as to quickly reach a steady state. This fluid behavior may be a result of micro-scale heterogeneity of the soil packing and the air compressibility. On the other hand, installation of the drainpipe is an optional commitment. Perforated pipe systems can be employed to improve water drainage, reduce subgrade moisture, and convey stormwater offsite promptly. These drainpipes are extensively applied in various LID/BMP strategies including bioretention ponds [123], bioswales [70], exfiltration trenches [128], French drains [129], infiltration trenches [130], permeable pavements [131], and rain gardens [132]. Table 2 shows the original definitions or descriptions of three LID structures, i.e., bioretention

LID/BMP Device	Definition
Bioretention [124]	"General features of a bioretention system include 0.7-1 m of sand/soil/organic media for treating infiltrating storm-water runoff, a surface mulch layer, various forms of vegetation, orientation to allow 15-30 cm of runoff pooling and associated appurtenances for inlet, outlet, and overflow."
Rain garden [126]	"Rain gardens are shallow depressions in the landscape that are planted with trees and/or shrubs, and covered with a bark mulch layer or ground cover. They allow stormwater to infiltrate, recharge aquifers, and reduce peak flows. In addition, they are expected to provide pollutant treatment, which has been attributed to several processes including adsorption, decomposition, ion exchange, and volatilization."
Bioswales [127]	"Bioswales are generally at least 30 m (100 ft) long, 0.6 m (2 ft) wide, range in longitudinal slope from 0.5% to 6%, and located in series with detention ponds, which store runoff and reduce peak discharges. Although they are designed to convey runoff from the 100-year 24-h storm event, they are only intended to treat runoff effectively from much smaller and more frequent storms, typically up to the 2-year 24-h storm event."

Table 2.2: Original definitions of key LID structures.

[124], rain gardens [126], and bioswales [127] in terms of geometrical and hydrologic aspects. This is because, in our opinion, pollutant transport and removal processes are not significantly influenced by the LID dimensions and structures. Standard pipe materials include corrugated steel, corrugated aluminum, and polyvinyl chloride. Small holes or slits are periodically formed along the drainpipe. The mean distance between two consecutive holes ranges from 3 to 6 inches [133]. These holes are usually downward facing in order to prevent gravitational clogging [134]. The collected water in the drainpipe is conveyed to the discharging system or to the natural environment.

The hydraulic behavior of perforated pipes has been examined since the early 20th century [135, 136]. The pipe geometry is often complex, and, therefore, analytic solutions for the fluid flow are challenging to obtain. Instead, fundamental CFD modeling can provide accurate solutions for coupled mass, momentum, and heat transfer, in principle, but it often requires high-performance computing. To the best of our knowledge, CFD tools have been employed only in the past decade to understand the discharge characteristics of the perforated pipes for LID and BMP [59]. As stated above, Afrin et al.'s work focused on the flow patterns and streamlines porous bioswales [59], and the perforated void portion of the pipe surface is exploited as an exit boundary. Their 3D model was validated using experimental results of fluid flows but did not include overland and infiltrating flows on the topsoil of the bioswale. The infiltration direction is usually oblique in the unsaturated aggregate zone but remained in their study primarily vertical in the saturated soil zone. This result implies that considering a porous pipe as an orifice is not a valid assumption for the momentum transport in bioswale systems. Infiltrating water occupies the void space in the unsaturated zone

and consequently pushes air blobs downward. Buoyant forces offer balance to the hydrodynamic drag on the air blobs. Therefore, the channeling of air occurs in the dynamic saturated zone during the process of infiltration, which is due to the local heterogeneity of micro-packing structure soil grains and the initial distribution of the blobs. This exchanging phenomena of water and air fluids in the porous bioswale is currently not found in the related literature and will be studied in our next CFD paper.

The types of drainpipe structures employed in bioswale systems can be classified into three categories: no drain, a linear drain, and elevated drain. The drainpipe is not a mandatory element of a bioswale, but it may determine the available amounts of drainage and retention of a bioswale. After an exhaustive saturation of the bioswale due to precipitation events, evapotranspiration can form the only physical mechanism to remove the infiltrated water inside the soil grain surfaces. Unless biological degradation is consistent, convected pollutants may continuously accumulate on soil grain surfaces depending on the adsorption capability of the engineered soil. Consequently, the capacities of granular media and activated carbon will reach their maximum limits. The long-term accumulation of organic/inorganic/particulate pollutants in bioswales can cause further leaching problems which cause unscheduled replacements of soil matrixes. Disposal of the contaminated soil grains generates another challenge within the bioswale maintenance. In our opinion, the optimal usage of the bioswale should include a periodic dilution of the pollutant level by artificially flushing the bioswale using low-cost water [137–141].

A linear drain installation includes a typical cylindrical pipe with periodic perforation, installed horizontally near the bottom of the bioswale. Neighboring zones around the linear pipe are often prepared using coarse grains to allow the fast discharge of infiltrated water and, more importantly, to prevent pipe clogging due to fine grains. The drainpipe is usually installed in the longitudinal direction of a bioswale, but the main pipe can be connected to transverse pipes for faster discharge appearing at regular intervals. This transverse configuration treats a long bioswale as a series of small independent bioswale units, which give evenly distributed draining performance. The transverse pipe outlet can be elevated to maintain a specific depth of saturated zone above the drainpipe. Consequently, this configuration prevents soil compaction and pipe clogging, which are caused by the complete dryness of the soil layer. The elevated pipe configuration requires the periodic dilution process to maintain a low pollutant level inside the bioswale. More significantly, microbial activities can be maintained in the semi-permanently/permanently saturated zone, depending on flow patterns in the subsurface. Chemical equilibrium can be attained for a short span of time immediately after the end of a storm event. Residual pollutant concentration from the previous storm event may primarily contribute to the discharge concentration of the subsequent storm event [111, 142]. The drainpipe not only discharges infiltrate water but also controls hydrodynamic and chemical reactions in the bioswale. For example, one can often observe mass-balance violation due to the initial conditions of a bioswale. If infiltration of the last storm even (of high runoff pollutant

concentration) ended at the final stage of the storm, the residual pollutants must remain within the bioswale in either the dissolved or absorbed phase. If the next rain event contains low runoff concentrations, then the first effluent from the bioswale must have a (much) higher concentration than that of the new influent. The prediction of the first influent concentration requires very detailed local information within the soil zone of the bioswale which seems to be challenging.

2.3 CFD as a universal modeling platform

Sustainable and renewable strategies can strategically mitigate stormwater threats, but present-day design methodologies emphasize only minimal, required criteria [9, 143]. More specific and reliable design tools are, therefore, urgently needed for optimized LID/BMP practices. In our opinion, LID/BMP structures without regional optimizations can cause unexpected hydrologic events unless the plane runoff patterns are holistically well-understood. In this light, we propose CFD as a universal modeling tool for design and optimization of LID/BMP systems [144, 145]. In this section we discuss the future direction of bioswale CFD modeling so as to systematically elucidate upon the coupled transport phenomena.

Within most engineering processes, a fluid flow often provides a platform for mass and heat transfer. For complex systems, interfaces and boundaries play critical roles in transferring physical quantities from one phase to the other. Dominant transport phenomena of a bioswale can be considered within various sub-zones as follows. First, on the topsoil surface of the bioswale, the entering overland flow is separated into infiltration and discharge, and flow pattern within the vegetated layer depends on the overall plant configuration. Therefore, the coupling of the open-channel and porous-media flows should be carefully merged for the topsoil boundary surface of the bioswale. Second, the infiltration within the vegetation layer enhances the sedimentation of suspended solids, which initiates the surface clogging. The hydrodynamic resistance will gradually increase and reduce the infiltration rate. The feedback effect of cake layer formation caused by deposited particles should be included in the long-term simulation of the bioswale performance while a constant thickness of the clogging layer can be assumed for short-term studies. Third, the infiltrating flow carries fine particles, a fraction of which will be filtered by soil grains. A phenomenon similar to the standard GMF occurs in the bulk phase of the porous bioswale. A unique difference between the bioswale system and conventional GMF for particle filtering is the heterogeneous, unsteady distribution of unsaturated zones and the dynamic migration of the zone boundary. Fundamental mechanisms regarding the particle transport near the zone boundary continues to be an area of active research. Fourth, organic and inorganic reactions primarily depend on concentrations of solute species in the infiltrated runoff water because the timescale for the chemical equilibrium is much shorter than the respective particle relaxation time. The solute species can be assumed to be in equilibrium to those adsorbed on the soil grain surfaces. In this case, the interstitial flow brings solutes to the vicinity of the soil grains but do not noticeably affect the pollutant removal efficiency due to the instantaneously reached equilibrium state. The validity of this local equilibrium approach depends

on the grain size distribution, which mainly determines the hydraulic conductivity or permeability. Finally, the interstitial flow reaches the drainpipe and exits the porous media into an open space, such as a receiving water body. This exit water-flow is balanced by the reversely entering air flow from the drainpipe to the porous region near the pipe. This volume exchanging phenomenon between water and air flows is also significant during the initial infiltration stage. To the best of our knowledge, this phase-exchange phenomena has not been reported in the bioswale literature and will be addressed in our next research.

Overall, the transport phenomena of the bioswale can be summarized as the changes of flow regimes from free space to the porous media and from the porous media to the drainpipe. The dominant factors that alter the interstitial flow pattern include the heterogeneity of soil structures followed by the initial distribution of air blobs in the unsaturated bioswale. Assuming solutes are not volatile, physical and chemical removal of suspended particles and chemical species depends upon the local infiltration patterns. In this case, the mass transport mechanisms, such as convection, diffusion, and reaction, can be treated as perturbative transport phenomena occurring on top of ambient, interstitial fluid flows. The mass removal processes do not provide noticeable feedback effects to fluid flows. Treating the soil grain packings as a continuous, homogeneous porous media, two-phase CFD can accurately predict the flow of water and air. The mass transport phenomena can be independently studied using the simulation results of fluid motion afterward. Based on our current review, we observed that the flow coupling at the topsoil surface is the most critical sub-process that determines the bioswale performance. Analytic solutions for the two-phase flow having multiple interfaces is theoretically a difficult task. CFD simulations with specific solute transport mechanism can therefore give more fundamental and accurate prediction of the bioswale performance.

2.4 Concluding remarks

In this study, we reviewed dominant transport mechanisms inside the bioretention system by treating a bioswale as a miniature water and wastewater treatment plant. Fluid dynamic aspects consist of runoff, overland, infiltration and discharge flows. The mass transfer phenomena reviewed include sedimentation of suspended particles, conventional filtration of fine particles, and removal of organic and inorganic pollutants because unsteady variations of (micro)biological processes are theoretically challenging and more importantly chemical, physical and fluid dynamic conditions provide basic conditions to the biological process. We restrict ourselves to physical, chemical, and fluidic processes, excluding biological reactions. Within each sub-topic of fluid dynamic and mass transfer phenomena, key theories were selected and examined in detail to construct a universal model as a seamless combination of well-defined unit processes. Due to the intrinsic challenges involved with data acquisition, the current bioswale research is limited to empirical studies and data fitting based on simple flow models or mass balance equations. CFD is proposed as a universal modeling platform in the application of bioswale research because it can predict various mass transfer

mechanisms as passive transport phenomena in the pre-determined, multi-zone flow fields. The size of LID/BMP systems is significant because these devices are almost permanently installed. Considerably more work will be needed to include detailed optimization tests using CFD for various hydrologic and physico-chemical scenarios, which will be discussed in the next chapter.

CHAPTER 3
COUPLED TRANSPORT PHENOMENA OF A BIOSWALE PROCESS DURING STORM RUNOFF EVENTS: A CFD STUDY USING OPENFOAM

This part of the dissertation is a manuscript submitted on June 15, 2018 and accepted for publication on November 9, 2018, to *Desalination and Water Treatment*.

Coupled transport phenomena within a bioswale are studied using the open-source computational fluid dynamics (CFD) software OpenFOAM. We investigated the unsteady behavior of momentum and mass transfer in a double-layered bioswale. To study the diffusive transport of a model pollutant, we developed a new solver, that we named interPhaseDiffusionFoam (`https://github.com/enphysoft/interPhaseDiffusionFoam`), which better mimics transport phenomena of non-volatile species at a phase boundary. We observed that heterogeneous infiltration patterns are strongly dependent upon stormwater runoff velocity, reverse air flow, and the presence of the drain pipe. The performance estimation and optimal design of a bioswale were thoroughly examined using 2D CFD simulations for a holistic understanding of coupled mass and momentum transport phenomena.

3.1 Introduction

Modern urban development has resulted in noticeable hydrological alterations, especially near the boundaries between urban surfaces and natural ground [146]. Impervious surfaces consisting of stone, pavement, and roofing structures change hydrological and hydraulic flow patterns at a macroscopic scale. Stormwater runoff on impervious areas often causes urban flooding and, hence, leads to a deterioration in the respective ecosystem's functions [147, 148]. Conventional structures for runoff management include roof gutters, storm sewers, and detention basins that are aimed to convey promptly stormwater runoff to off-site drain discharge locations. The continued increase in impervious areas will reduce natural porous surfaces to infiltrate rainfall and enhance the frequency and intensity of urban flooding [28, 54, 149, 150].

Since the 1970s, onsite stormwater management approaches have been described by various technological terms, which include best management practices (BMPs) [151], green infrastructure (GI) [152], integrated urban water management (IUWM) [153, 154], low-impact development (LID) [155–158], low-impact urban design and development (LIUDD) [159], source control (SC) [160, 161], stormwater control measures (SCMs) [87, 162], sustainable urban drainage systems (SuDS) [96, 122] sustainable drainage systems (SUDS) [163, 164], and water sensitive urban design (WSUD) [3, 165–168]. Thorough reviews of these terms can be found in work by Fletcher et al. [169] and Eckart

et al. [170]. These management methods aim to retain the stormwater runoff with devices that emulate the natural hydrology before urbanization. One significant task when researching urban flooding mitigation is, per our investigation, the enhancement of onsite infiltration capability by increasing permeable catchment areas. Thereby, this paradigm shift from impervious to hybrid permeable surfaces has the potential to increase the threshold precipitation rate under which urban flooding begins within a certain lag time after a precipitation event starts. The hydraulic benefits of LID/BMP devices, however, cannot be fully attained without detailed analysis of the individual transport components at various scales.

Computational fluid dynamics (CFD) receives growing attention in the civil and environmental engineering field. This method can be used to enhance stormwater management design and optimize LID/BMP devices, especially at the conceptual stage of design development. CFD for LID/BMP applications possesses the following advantages. First, CFD provides an alternative cost-effective means to predict the complex transport phenomena of mass, momentum, energy, and especially chemical species in multi-phase LID/BMP devices. Second, CFD can model flow conditions when experimental tests are not easily reproducible because of limited environmental conditions for physical observations. In the case of LID/BMP, the various scenarios regarding stormwater runoff and pollutant transports are too immense and arduous to study experimentally. Finally, CFD provides much more detailed visualization as compared to analytical and experimental approaches. In analytical approaches, it is difficult to solve flow profiles in complex geometrical domains. Physical experimentation requires substantial resources, as well as cost and time to observe fluid flows and pollutant transport. In addition the quantitative description of fluid dynamic experiments does not provide complete data sets within available operating conditions. Using CFD, however, can evaluate and visualize the flow behavior over a range of parameters such as the flow speed and the hydraulic pressure. If CFD is well conducted within the design process, then LID/BMP systems can be optimized in terms of dimensions and cost. As a result, the unexpected effects of structural change could be identified and removed in early stages.

Limitations of CFD include inaccuracy of physical models, selection of appropriate boundary conditions, and unstable algorithms due to numerical errors. In the LID/BMP literature, software programs that model site-specific, sub-catchment scale systems are not CFD-based, which include Guelph All-Weather Sequential Events Runoff (GAWSER)[22], Model for Urban Stormwater Improvement Conceptualization (MUSIC) [23–25], Soil Conservation Services (SCS) model using the curve number [26], Smart Growth Water Assessment Tool for Estimating Runoff (SG WATER) [27], Storm Water Management Model (SWMM) [28, 29], Storm Water Management Model and Best Management Practice Decision Support System (SWMM-BMPDSS) [30, 31], System for Urban Stormwater Treatment and Analysis Integration (SUSTAIN) [32], and MIKE SHE [171]. These macroscale fluid dynamics approaches do not originate from fundamental, microscopic transport mechanisms, but employ approximate mass balances that often rely on experimental data. Thus,

these approaches cannot identify local areas where ineffective operations of LID/BMP devices may occur.

In the practice of bioswale designs, guidelines and standards do not exist so as to provide optimal performance calculations during storm events. These design guides are not necessarily clear regarding proper specifications and bioswale hydraulic performance. For example, the *Low Impact Development: A Practitioner's Guide for Hawaii* [143] specifies the minimum requirements to design swales for various annual rainfall ranges. However, no detailed specifications exist regarding the proper sizing of underdrain pipes for swales Similarly, guidelines for the states of Alaska [16] and Arizona [172], and the city of Las Vegas Valley, Nevada [15] offer qualitative descriptions for swale and bioretention systems, but these guidelines do not include methods to analyze pre-built LID/BMP structures. The BMP manual of Hawaii [9], as well as, the technical guides of New Mexico [8], and Utah [10] adopted the rational method for peak runoff to design swale and bioretention systems, which was initially proposed by Prince George's County in 1993 [173]. Furthermore, the state of Washington requires the use of Manning's equation as a first approximation to obtain swale geometry [11]. The State of Oregon Manual [12], however, prescribes the bioswale sizing method based on the SCS quantification approach to treat a 24-hour storm event. Whereas, the state of California determines filter bed sizing using Darcy's Law [4], which was first developed by the city of Austin, Texas in 1996 [174]. Finally, the Idaho Department of Environmental Quality recommends swale geometry to cover a percentage of the total impervious drainage area [13]. In summary, our review of stormwater guidelines from the Western United States reveals that there are five approaches for the sizing of bioswales [4, 9, 8, 10–13, 15, 16, 143, 172, 174]. In engineering praxis, these guidelines provide no rigorous quantitative guidance or sizing formula to address site-specific applications for bioswale designs. Thus, the design approaches based on general specifications may not meet regulatory goals for stormwater quality and quantity. Therefore, universal and reliable computational methods are of great necessity to ensure optimal and sustainable LID/BMP designs.

In theories regarding porous media flow, Darcy's law is limited to the saturated flow. Richards equation is a nonlinear partial differential equation without a general closure, which extends the Darcy law to represent the water flow within unsaturated soils. The Richards equation includes the capillary force, converted to a form of the hydraulic head as a function of locations in a porous media. The capillary forces are usually over-emphasized, and solution methods for the Richards equation often do not converge. The CFD algorithm employed in our study is the volume of fluid (VOF) approximation, which considers averaged phase variables within a computational cell. To the best of our knowledge, the approximation level of phase separation in the Richards equation and CFD are similar regarding the functional variation for the spatial locations. Richards equation is limited to the soil domain and cannot be generally used for interfacial transport at the microscopic soil-water and soil-air boundaries unless certain mathematically particular approximations are employed. The accuracy of the CFD analysis primarily depends on the computational grid structures of VOF

Figure 3.1: Section view of a bioswale in practice along Kualakai Parkway road in Kapolei, Oahu, Hawaii.

methods.

In academic and industrial CFD applications, OpenFOAM has been widely employed for many flow modeling projects [40–42] since its initial release in 2004 [175]. We use OpenFOAM to model transport phenomena of momentum and mass within a bioswale. This paper also discusses the physical domain of the bioswale structure and how to set up an OpenFOAM case: setting up a model bioswale structure, generating bioswale meshes, specifying initial and boundary conditions, and selecting CFD solvers. We also included a brief review of modeling methods because CFD has not been extensively used for LID/BMP designs. In addition, we developed a new algorithm to more accurately investigate the two-phase transport of volatile species. Our focus is to fundamentally investigate the fast discharge of stormwater runoff with a certain pollutant concentration throughout the bioswale system.

3.2 Physical model and numerical solvers

3.2.1 Bioswale structure

Fig. 3.1 depicts a bioswale structure that is practiced by the Hawaii Department of Transportation (HDOT). The bioswale system is 1.8 miles (3.0 km) long and lies along Kualakai Parkway (2.7 miles (4.35 km) long) comprising of a six-lane two-way urban arterial roadway in Kapolei, Oahu, near the University of Hawai‘i–West O‘ahu campus. The primary purpose of bioswale systems is to initially reduce stormwater runoff and partially remove non-point source pollutants, which flow from impervious urban systems such as roadways, highways, and parking lots [5]. Vegetation layers

on the bioswale surface, in general, can decelerate incoming runoff flows and enhance sedimentation of suspended solids. Monitoring infiltration rates and pollutant concentration play a crucial role in the optimization of bioswale performance and also for the prolongation of the soil-matrix replacement period. Bioswales have various geometries, which include trapezoidal, rectangular, squared, and parabolic shapes. During a storm event, stormwater runoff enters the bioswale from one side of the road. Then, the stormwater runoff either infiltrates the bioswale soil zone or overflows to the overland surface. After a long duration, infiltrated water reaches the drain pipe and is discharged with pollutants of typically lower concentration than that of the runoff.

The interior soil region often consists of two layers—that is the topsoil matrix and the bottom layer. The top layer indicates the soil zone from the ground-surface level to the vicinity of the embedded drain pipe. This layer should be more porous than nearby natural ground surface but sufficiently dense to maintain moderate infiltration rate through the porous media for the sake of pollutant removal. The bottom layer consists of gravel and small stones, which has higher permeability than that of the soil matrix. It mechanically supports the drain pipe and accelerates the drawdown of the infiltrated stormwater so as to allow it to discharge into the drain pipe. The drain pipe has perforations at regularly occurring intervals along the pipe length. The interstitial spaces between adjacent gravels should be large enough to allow immediate discharge to the pipe yet small enough to prevent pipe clogging due to downward migration of smaller grains.

3.2.2 Theoretical background

3.2.2.1 Fundamentals

In this section, we briefly introduce the fundamentals regarding the volume of the fluid (VOF) method to perform CFD simulations for bioswale transport phenomena and explain our new solver with a modified algorithm for the transport of non-volatile solutes. The conventional VOF method deals with the two-phase flow by tracing the interfaces where physical quantities are averaged. The mass transport simulation coupled with the VOF method provides noticeable numerical diffusion at the phase-interface, especially for non-volatile solutes.

Phase averaging A two-phase flow of incompressible and immiscible fluids of air and water with specific surface tension is examined in an open atmosphere and a porous bioswale. Under the influence of gravity, the VOF method is used to investigate phase-averaging transport phenomena of fluids. The phase average of an arbitrary quantity, q, is defined as follows

$$q = q_1\alpha_1 + q_2\alpha_2 \tag{3.1}$$

where α_i and q_i are fractions and a value of q in phase i (1 for water and 2 for air). Because of mass conservation, the phase fractions should satisfy the sum $\alpha_1 + \alpha_2 = 1$.

Phase-averaged governing equations Due to the incompressible characteristics of water and

air, the fluid velocity u satisfies the continuity equation,

$$\nabla \cdot \boldsymbol{u} = 0 \tag{3.2}$$

and the Navier-Stokes equation for momentum transport is represented using the continuum surface force model [67, 176] as

$$\rho \left(\frac{\partial \boldsymbol{u}}{\partial t} + \boldsymbol{u} \cdot \nabla \boldsymbol{u} \right) = -\nabla p + \nabla \cdot \boldsymbol{T} + \boldsymbol{F}_s \tag{3.3}$$

where ρ $(\rho_1 \alpha_1 + \rho_2 \alpha_2)$ represents the phase-averaged fluid density, p $(= P - \rho g z)$ presents the net hydrostatic pressure, which exists as the difference between the absolute pressure and the liquid-phase pressure depending on depth, and $\boldsymbol{F}_s$ represents the interfacial force due to the surface tension. In Eq. (3.3), the viscous tensor $\boldsymbol{T}$ is given as

$$\boldsymbol{T} = \mu \nabla \left(\boldsymbol{u} + \boldsymbol{u}^t \right) \tag{3.4}$$

where $\mu (= \mu_1 \alpha_1 + \mu_2 \alpha_2)$ represents the phase-averaged viscosity, and superscript t indicates transpose. The interfacial force is crucial where the boundary shape strongly depends on the capillary force, which is often solved using the standard continuum surface force (CSF) model [176]:

$$\boldsymbol{F}_s = \sigma \nabla \cdot \left(\frac{\nabla \alpha}{\|\nabla \alpha\|} \right) \nabla \alpha \tag{3.5}$$

where σ forms the surface tension at the phase boundary, e.g., $0.072\,\mathrm{N/m}$. In Eq. (3.5), α indicates the water-phase fraction (α_1), and hereafter, the air-phase fraction will be denoted as $1 - \alpha$.

Porous media flow The porous soil zones of the bioswale are modeled using the standard Darcy flow. In this porous region, an extra force term is added on the right-hand side of Eq. (3.3):

$$\boldsymbol{F}_d = -\frac{\rho g}{K} \boldsymbol{u} = -\mu d \boldsymbol{u} \tag{3.6}$$

where K [m/s] represents the hydraulic conductivity, $d (= \rho g / \mu K)$ is the Darcy constant, and g $\left(= 9.81\,\mathrm{m}/s^2\right)$ constitutes the gravitational acceleration. We assume that the density of stormwater is equal to that of pure water. Thus, the density-driven flow is assumed to not be important for our case. The hydraulic conductivity K of a fine soil is of an order of $O\left(10^{-5} - 10^{-6}\right)$ m/s depending on the dryness of the soil zone, which yields the value of d of an order of $O\left(10^{11} - 10^{12}\right)$ m^{-2}. If the fluid inertia is significant in a porous medium, one can apply the Forchheimer approach [177] as an extension of Darcy's law, but it requires the estimation of the secondary proportionality for the extra term proportional to u^2. To avoid the additional complexity due to several parameters, we restricted ourselves to the application of Darcy's flow regime, assuming that the viscous force is dominant and that the capillary force is not significant.

Pollutant transport The unsteady transport equation of the pollutant with phase-averaged

concentration C can be expressed as

$$\frac{\partial C}{\partial t} + \nabla \cdot (\boldsymbol{u}C) = \nabla \cdot D\nabla C \tag{3.7}$$

where $D = D_1\alpha + D_2(1-\alpha)$ constitutes the phase-averaged diffusivity; D_1 and D_2 represent the pollutant diffusivities within the water and air phases, respectively. Typically, a solute diffusivity is considerably higher within a gas phase, when partitioned in both phases $D_2 \gg D_1$. In principle, the governing Eq. (3.7) includes the pollutant diffusion even in a single phase (i.e., either $\alpha = 0$ or 1). If the volatility of the pollutant is negligible, then Eq. (3.7) may provide erroneous results at the phase boundaries, where α value will be of the order of $O(0.1)$. In such a case, the phase-averaged diffusivity D can be considerably higher than D_1, and the diffusive flux from water to air phases is erroneously enhanced. This transport phenomenon is apparent, especially when the pollutant concentration in the air phase is initially zero or D_1 is small enough so that the convective pollutant transport is superior to the diffusive transport. To include interfacial reactive mass transfer, the VOF method [178] was extended as

$$\frac{\partial C}{\partial t} + \nabla \cdot (\boldsymbol{u}C) = \nabla \cdot D\nabla C - \nabla (D\Phi\nabla\alpha) \tag{3.8}$$

where

$$\Phi = \left(\frac{1-H}{\alpha + (1-\alpha)H}\right) C \tag{3.9}$$

contributes to an additional flux. Φ can be used to mimic a concentration jump at the phase boundary. An equilibrium partition of the pollutant in the two phases can be represented using Henry's law:

$$C_2 = HC_1 \tag{3.10}$$

where H is the dimensionless Henry constant, which is typically considerably lower than 1. No mechanism, however, is included to maintain the non-volatile pollutant within the water phase from the initial moment. To the best of our knowledge, the standard VOF method cannot describe the phase boundaries accurately using the extra-diffusion term in Eq. (8). The artificial diffusion from water to air phases can be minimized, however, by using specific parameter settings as follows. In addition to setting $C = 0$ initially in the air phase, one can forcefully set $D_2 \ll D_1$, while the inverse is true in reality. The air-phase concentration can, in principle, be further minimized by setting Henry's constant at a minimal value. By using this lower limit, the governing equation for the pollutant transport is simplified, as to minimize further the artificial diffusion,

$$\frac{\partial C}{\partial t} + \nabla \cdot (\boldsymbol{u}C) = -\nabla \cdot (-\alpha D_1 \nabla C + C D_1 \nabla \alpha) \tag{3.11}$$

On the right-hand side of Eq. (3.11),the first term, $-\alpha D_1 \nabla C$, indicates the diffusive flux of the

pollutant concentration, C, strictly within the water phase with an effective diffusivity αD_1. The second term, most importantly, can be interpreted mathematically as a reverse diffusion of α with an apparent diffusivity CD_1. Note that signs of $D_1\nabla C$ and $\nabla\alpha$ are opposite of each other. An alternative interpretation of the second term exists as the reverse transport of solutes of concentration C with an effective velocity of $D_1\nabla\alpha$. As such, the first and second terms represent solute diffusion within the water phase and the phase-boundary, respectively.

3.2.2.2 Model bioswale structure and mesh generation

OpenFOAM was originally developed to simulate only 3D geometries. To resolve the problem into 2D, a pseudo-3D structure needs to be generated to make pseudo front-and-back surfaces. We constructed the 3D bioswale structure of pseudo thickness of 0.4 m using an open-source mesher, Netgen [179] and exported the netgen mesh to a stereolithographic (STL) file. This STL file was employed so as to generate the OpenFOAM mesh, depicted in Fig. 3.2 (a), using blockMesh and snappyHexMesh commands. The bioswale structure was originally prepared with an arbitrary thickness, but no mesh was generated in the direction normal to 3.2. The bioswale depicted in Fig. 3.2 (a) is 3 m long from the left-most inlet to the right-most outlet and 2 m high from the bioswale bottom to the atmospheric top. Then, we added two dividers to generate refined boundaries between the atmosphere and topsoil and between the top and the bottom soil layers. Finally, all edge boundaries of the bioswale were construed as refined soil-soil interfaces. The number of divisions in the $x-$ and $y-$ were 202 and 135, respectively, which yielded equivalent grid sizes of 1.50 cm in each direction. The generated mesh has 95,498 points, 182,638 faces, and 44,963 cells, and checkMesh command was used to test the mesh's quality. The diameter of the drain pipe, presented in Fig. 3.2,, was 30.48 cm (12 inches), located near the bottom of the bioswale. The left, right, and bottom sides of the bioswale are considered as impermeable walls, which prevent normal fluxes of momentum and mass to the wall surfaces. This assumption is considered reasonable if the soil media has higher permeability than that of the ambient soil, especially for a short-term investigation. The drain pipe contains two small holes located at 4 o'clock and 8 o'clock directions for the discharge of infiltrating water. Runoff water enters the physical domain as shown in Fig. 3.2(a) from the left-hand side corner with a fixed height of 5.0 cm and flows down due to gravity to the bioswale on the 5% downward slope. A stationary water column exists as a boundary condition for a stationary water source and releases water due to gravity. Actual height of the surface flow on the right ground is automatically calculated as a transient result of our CFD simulation. A large fraction of water, not infiltrated into the bioswale, overflows to the right overland surface having the same downward slope.

3.2.2.3 Boundary and initial conditions

Simulations were conducted for two cases: polluting and flushing. The polluting scenario indicates the storm runoff to the ideally fresh bioswale, without having water content and accumulated pollutant masses. A storm runoff containing a pollutant concentration enters the bioswale zone

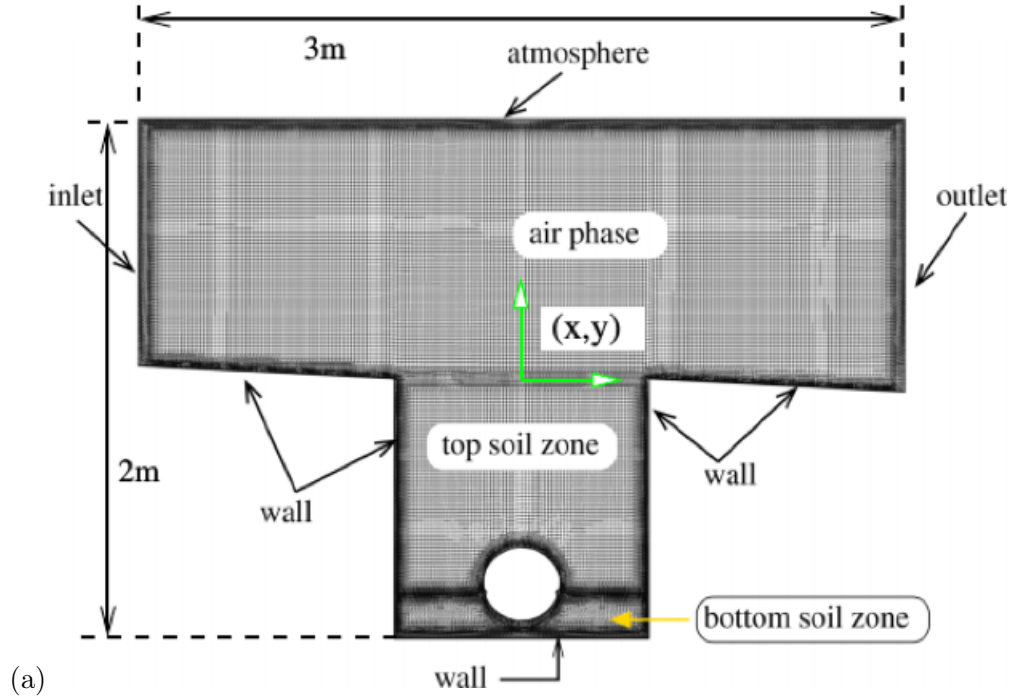

(a)

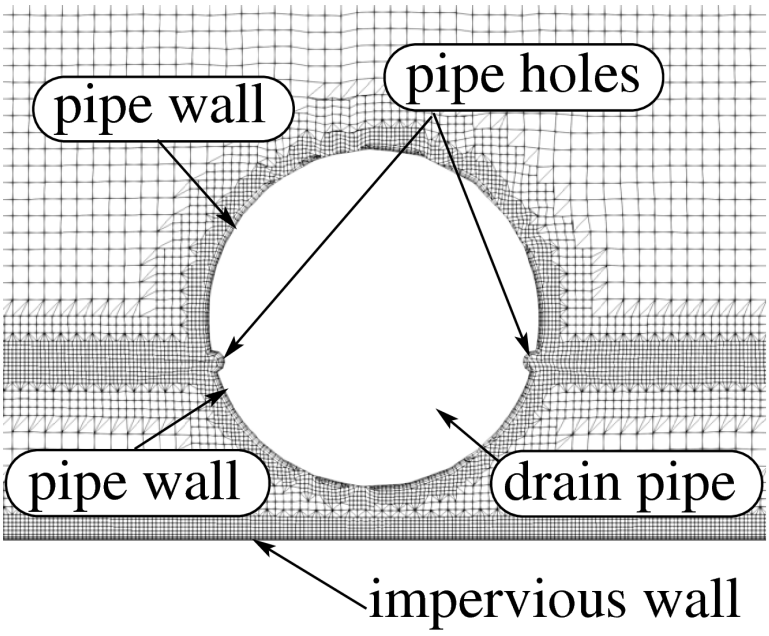

(b)

Figure 3.2: Depiction of (a) pseudo-3D structure of bioswale generated by Netgen and exported to the STL format and (b) drain pipe of 30.48 cm (12 in.) diameter generated mesh using OpenFOAM tools, visualized using ParaView version 5.4 (https://www.paraview.org/). The outer length and height of the bioswale system are 3 m and 2 m, respectively, and left and right ground surfaces have 5% slope.

and infiltrates from the bioswale top into the soil and then to the drain pipe. The flushing is an opposite case, in which the bioswale is pre-contaminated with a specific concentration (assumed to be known) and the entering runoff flow have a negligible pollutant concentration. The hydrodynamic behavior within the bioswale is assumed to be very similar since the pollutant transport is a pass response to the infiltrating flow. Note that chemical and biological reactions are not included in the current study and therefore the convection-diffusion equation 3.7 can be scaled by a reference concentration (of an arbitrary choice). The flushing case was designed to understand the seemingly violating pollutant mass balance. The low-concentration infiltrating flow will sweep the pre-accumulated pollutant in general and as a noticeable consequence the effluent concentration is higher than the influent concentration (of the entering storm runoff). In our fundamental CFD approach, the number of physical parameters is minimized. The inflow rate into the bioswale is not an input parameter or boundary condition on the front cross-section of the bioswale (normal to the entering flow velocity), but calculated during the unsteady CFD simulations. On the bottom-left boundary 5 cm of water is maintained, which flows down on the slanted ground having 5% slope. In this light, we avoid using Manning's equation, which requires to input the hydraulic radius, surface slope, and surface roughness. In 2D geometry, the hydraulic radius can be easily estimated as a ratio of the normal cross-sectional area (to the incoming fluid flow) and the perimeter length wetted by the flowing fluid. Including the roughness at the macroscopic level of Manning's equation can significantly increase the computational runtime, although it is possible. If the roughness is important in a case that the surface is not smooth enough, then the slip velocity can be estimated and used as a boundary condition on the left and right ground surfaces beside the bioswale.

Specific boundary conditions and their physical implications are summarized in Table 3.1 and explained as follows:

Atmosphere The top surface of the computational domain shown in Fig. 3.2(a) indicates the ambient boundary of the stationary atmosphere. The net atmospheric pressure $p-\rho gh$ is set to zero at this boundary as a reference value because only the relative values are important in momentum transfer. U is determined as positive in the $y-$direction on this boundary, and its gradient normal to the atmospheric surface is zero. This is equivalent to the standard out-flow condition for the positive U. If U is determined to be inward to the air phase, then only its normal component is considered as a velocity at the boundary. In OpenFOAM, this boundary condition is implemented as `pressureInletOutletVelocity`. The liquid fraction α and the pollutant concentration C have the similar type of boundary conditions in the following manner. When the flow is exiting the top atmospheric boundary, gradients of α and C are set to be zero; otherwise, no additional flux of α and C are allowed. In OpenFOAM, this specific boundary condition employed for α and C is referred to as `inletOutlet`.

Inlet The left-most side, as shown in Fig. 3.2(a), is assumed to be open to the stationary ambient atmosphere and does not undergo any specific transport except for the surface runoff inflow. The

Boundary	$p - \rho gh$	U	α_1	C [mg/L]
Atmosphere	`totalPressure, 0`	`PressureInletOutletVelocity`	`InletOutlet, 0`	`InletOutlet, 0`
Inlet	`ZeroGradient`	`VarialHeightInlet`	`VarialbeHeight (0,1)`	`InletOutlet, 0`
Outlet	`ZeroGradient`	`InletOutlet, 0`	`InletOutlet, 0`	`InletOutlet, 0`
Drain Left	`HydrostaticPressure`	`InletOutlet, 0`	`InletOutlet, 0`	`InletOutlet, 0`
Drain Right	`HydrostaticPressure`	`InletOutlet, 0`	`InletOutlet, 0`	`InletOutlet, 0`
Walls	`FixedFluxPressure`	`No-Slip`	`ZeroGradient`	`ZeroGradient`

Table 3.1: Boundary conditions used for OpenFOAM (v4.1) simulations. Values next to the specific boundary condition names are used for specific incoming and outgoing flow conditions.

inlet water height is set to 5.08 cm (2 in.), which is geometrically fixed for simplicity. At this boundary, the air velocity is set to zero, and the water velocity is set to be constant $(U_x, 0, 0)$, where U_x alters from 0.1 to 0.3 m/s. Although the height of the water column is fixed as 5.0 cm, the inflow water velocity as an input parameter determines the entering water velocity to bioswale surfaces. Manning's equation is a standard method used to determine the open-channel velocity as a function of slope, water height, and roughness. In contrast, the fixed height of the water column offers more flexibility to control the transient inlet flow as a boundary condition. The pressure gradient is calculated to satisfy the above-determined flow velocity. The α gradient is set to zero, and the solute concentration C is equal to $C_{\max}$ for the polluting and 0 for flushing scenarios; here, $C_{\max}$ represents the maximum pollutant concentration reasonably selected from the current literature. We selected zinc as a model pollutant with the maximum inlet concentration of $1,000.0\mu$g/L and the diffusivity of $D_0 = 7.024 \times 10^{-10}\,\mathrm{m}^2/\mathrm{s}$ [180, 181]. Smolders and Degryse investigated the fate and effect of Zinc from tire debris within soils in which they reported that zinc concentrations in soil layers often reached a few hundred mg/kg [67]. Reported zinc concentrations within 2 m of soil depth are of an order of (100) mg/kg and occasionally exceed 2000 mg/kg [182–186]. Thus, we selected $1,000\,\mathrm{mg/L}$ as an extreme representative value, which does not significantly change the pollutant transport simulation since convection is the only mechanism. In this case, the passage (or rejection) ratio of a pollutant can be used instead of the real concentration, as the convection-diffusion equation 3.7 can be scaled using an arbitrary (but meaningful) representative concentration value.

Outlet The right-most boundary, as shown in Fig. 3.2(a), allows air and water to flow naturally out of the computational domain. Normal gradients of p to this boundary are set to zero. For u, α, and C, their normal gradients are determined as zero for outgoing flow, and the values are fixed at zero for the incoming flow. In this case, the outlet boundary does not allow any incoming transport of momentum and mass.

Ground surfaces and bioswale walls The side walls of the bioswale are considered approximately impervious. At the wall boundary, the water is assumed to be not slipping and fluxes of α and C are zero, i.e., $u = 0$, $\overrightarrow{\nabla}\alpha = 0$ and $\overrightarrow{\nabla}C = 0$. The boundary pressure p is calculated as a proper value to confirm the zero velocity at this boundary. Depending on the regulatory guidelines, the bioswale wall can be prepared as entirely impermeable to prevent any uncontrolled pollutant transfer to the environment.

Air-soil interface No boundary condition is used at the interface between the air phase and on the top bioswale. Instead, the interfacial phenomena are rigorously investigated using finer mesh layers as shown in Fig. 3.2(a) and seamlessly linked governing equations for the two-phase (air and water) flows. The air and heterogeneous soil regions are universally treated as a whole media having spatially-changing porosities and hydraulic conductivities (or permeabilities). In this light, the longitudinal transport normal to the top soil surface does not require a boundary condition.

Pipe surfaces and holes Fig. 3.2(b) shows a detailed mesh structure around the drainage

pipe. The top and bottom surfaces of the circular pipe are considered as impermeable walls in contact with soil grains or water. Semi-circular extrusions on both sides of the pipe indicate fluid volumes made within the pipe holes for discharging. The top half of the drain pipe will always be filled with only air. Extruded semi-circles are used to set up the standard outflow boundary conditions for P, U, α, and C.

3.2.2.4 Cell zone setup

In Fig. 3.2, the air phase is treated as an incompressible gas phase with standard material properties of air. The soil zones of the bioswale are considered as simple porous media, characterized using the Darcy value (i.e., an inversed hydraulic permeability). For an extreme case, a high hydraulic conductivity is employed to treat an aggregate layer as a porous media using $K = 1.2\,\mathrm{m/s}$ [187], which yields the Darcy constant of $d = 8.175 \times 10^6 \mathrm{m}^{-2}$. We are interested in the highly porous soil matrix of this d-value, allowing a fast infiltration within a few minutes. As bioswale can be designed mostly for the swift discharge of initial runoff, the Darcy constant of the order $O(10^6)\,\mathrm{m}^{-2}$ is too low for practical purposes. We made, therefore, that the top and bottom soil zones have Darcy constant $d_\mathrm{t} = 8.175 \times 10^8\,\mathrm{m}^{-2}$ ($K = 0.012\,\mathrm{m/s}$) and $d_\mathrm{b} = 8.175 \times 10^7\,\mathrm{m}^{-2}$($K = 0.12\,\mathrm{m/s}$), respectively. Two pseudo-interfaces of the air-bioswale and top-bottom soil layers were prepared to accurately calculate the boundary phenomena where P, U, α, and C are continuous anywhere within the entire computational domains. Their transports near these interfaces are, however, more complicated than those of bulk phases of air and soil. Therefore, the meshes in these zone-boundaries are prepared more finely in order to accurately capture the interfacial flow patterns. We used, for the pure-phase of air and water, the densities of 1,000 and 1.21 $\mathrm{kg/m}^3$, respectively, and the kinematic viscosities of $1.0 \times 10^{-6}\,\mathrm{m}^2/\mathrm{s}$ and $1.51 \times 10^{-5}\mathrm{m}^2/\mathrm{s}$, respectively.

3.2.2.5 Solvers used and developed

Users of OpenFOAM must select specific solvers that are appropriate for the problem under consideration. OpenFOAM has approximately 80 different solvers for specific applications. When required, users also can modify standard solvers to include specific phenomena. We initially began our simulation work using `interFoam` for an incompressible two-phase flow, which can provide an accurate simulation of coupled runoff and infiltration phenomena. To investigate non-volatile solute species (i.e., zinc in our case), we modified `interFoam` to generate a new solver named `interPhaseDiffusionFoam`, which can simulate solute transport, primarily, in the water phase without providing significant artificial diffusion. Specific algorithms are explained as follows. See the Appendix for details.

interFoam with passive transport (standard) In OpenFOAM, the phase-averaged velocity u in any phase can be calculated for the bioswale by running `interFoam`, and one can use a passive transport solver `scalarTransportFoam` to study the convective-diffusion of the solutes. In this case, the mass transport is primarily controlled by the phase-averaged velocity U. The artificial diffusion occurs because the current version of `scalarTransportFoam` treats the mass flux at the phase

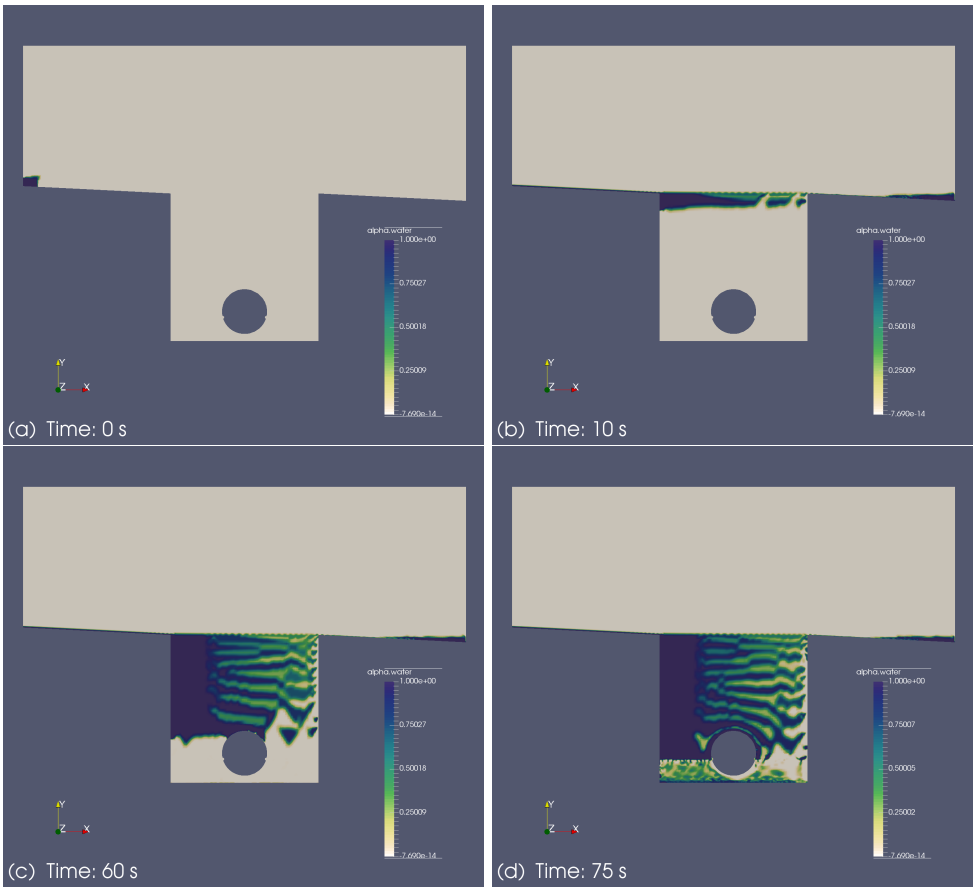

Figure 3.3: Initial infiltration behavior with inflow velocity of 0.1 m/s at time (a) $t = 0$, (b) 10, (c) 60, and (d) 75 s to a bioswale.

boundaries identical to that in a single phase. Transport phenomena of pollutants are passively calculated at each time step using only determined profiles of α and u without distinguishing phases. In summary, `scalarTransportFoam` does not recognize phase boundaries and therefore unnecessarily enhance diffusion from the water to the air phases.

interPhaseDiffusionFoam (developed) Previously, Haroun et al. [178] developed a coupling algorithm of the VOF and solute transport by considering convection, diffusion, and volatilization of solutes. As the VOF method is based on the phase-mixing algorithm, their method requires an extremely fine computational grid for the non-volatile solute transport to eliminate the artificial diffusion. Here, we found specific theoretical approximations for non-volatile solute transfer, coupled with VOF, and described the respective terms in section 2.2.1. Details of the new and original algorithms are mathematically intense, so we include them in the Appendix.

3.3 Results and Discussions

3.3.1 Distribution of infiltrating water

We test the transient flow behavior of a double-layered bioswale with an underdrain pipe in 2D space with high hydraulic conductivities to investigate the short-term transport phenomena for a rapid discharge after a heavy precipitation event. Fig. 3.3 depicts the initial infiltration behavior of a bioswale for the first short duration (75 s) of a precipitation event. The initial height and length of the water body are both 5.08 cm as demonstrated in the left corner of Fig. 3.3(a), and the flow speed is set as 0.1 m/s. After this initial moment of $t(x) = 0$, the water height is automatically adjusted based on and due to the gravity and the surface boundary condition. The top air phase and the bioswale interior are initially set as dry (represented in gray) assuming that the direct flow input from the precipitation is negligible in Fig. 3.3(a). The early infiltration profile is depicted in Fig. 3.3(b) as initiated due to gravity and the high conductivity of the topsoil. The interstitial void spaces in the bioswale soil layers are initially filled with air assumed to be incompressible in the VOF method. The top-left portion of the bioswale receives the running-off water first and then allows the water to pass through with gravitational force. The migration of the infiltrated water in the lateral direction is negligible within the soil layer. Flow inertia is fully damped in the topsoil layer, and the gravity forms the primary driving force for the infiltration at this point. Compressed air in the bioswale, due to the infiltration, generates dynamic channels for the escaping air from the porous soil layer, as depicted in Fig. 3.3(c). As both air and water are assumed to be incompressible, this counter-balanced transport is based on volume exchange between infiltrating water and buoyant air. As time elapses, infiltration flow patterns become uniform along the horizontal direction, but interestingly, striped horizontally. As the air initially in the soil layer is displaced to the right by the entering water from the left, its local density in the bioswale becomes higher in the runoff direction. The presence of the striped distribution of air and water phases, in our opinion, is due to the limited spatial dimension of 2D space. The infiltrating flow at the inlet zone is dispersed within the bioswale. The driving force of the infiltration is gravity, hindered by the presence of soil grains. As noted previously, the downward infiltration is counter-balanced by the upward air flow, exchanging the same amount of volume occupied. In our 2D configuration, pre-existing air is pushed down by the infiltrating water and is effectively forced to move along the runoff direction on the top of bioswale. This lateral migration of air within the bioswale reduces the infiltration of water and induces the water migration in the same direction of the air migration. This distinct striped pattern must be primarily ascribed to the 2D geometry that we employed, which is practically understood by the (mathematically) infinite bioswale length along the normal direction to the cross-sectional area shown in Fig. 3.2–3.6. (See next sections for details.) Fig. 3.3, however, clearly indicates that the distribution of infiltrating water depends on the running-off flow direction, especially when the bioswale has a high hydraulic conductivity. Since the bottom soil layer has 10 times smaller Darcy constant, Fig. 3.3(d) displays higher water content above the top-bottom soil boundary line,

passing through the drain pipe (near pipe holes). The lower water content below the top-bottom soil boundary indicates an accelerated infiltrating flow to the bottom of the bioswale. The bottom soil layer (having a higher hydraulic conductivity than that of the top-soil layer) mechanically supports the less-porous top layer and induces the fast drainage through the pipe holes. The location of the soil boundary can be set above the current boundary by reducing the low-conductivity soil zone. The partitioning the heterogeneous soil zones can be designed based on the rain and runoff patterns to maximize the bioswale performance, which will be the topic of our next study. Partition of the top and bottom soil zones, therefore, can form an important design parameter for both the infiltration rate and for the removal of pollutants.

3.3.2 Effects of inflow velocity on infiltration rate

Fig. 3.4 compares the air-water phase distribution at $t = 60s$ for three inflow velocities, having Darcy values equal to those of Fig. 3.3. For specific comparison, we put Fig. 3.3(a) as identical to Fig. 3.4(a) having an inflow velocity of 0.1 m/s. We observed that the striped pattern disappeared in Fig. 3.4(b) and 3.4(c) for higher inflow velocities of 0.2 and 0.3 m/s, respectively.

Due to the larger amount of running-off water on the topsoil surface, the infiltrating water volume is considerably lesser than that of the laterally migrating water. Water distribution profiles of Fig. 3.4(b) and 3.4(c) appear similar to each other. Thus, this similarity implies that the infiltration velocity is almost independent from runoff velocity (if the runoff velocity is sufficiently fast), but the counter-flow of the air is ubiquitous. This, in practical terms, indicates that the high-conductivity bioswale must have a minimum threshold running-off velocity that generates the spatially uniform infiltration pattern. Below the threshold value, the bioswale must exhibit lesser symmetric infiltration patterns along the central vertical axis. In all cases, the phenomena of volume exchanges between the air and water phases control the distribution of the infiltrating water under the initial runoff effect on a dry bioswale. Now, Fig. 3.5 provides a closer view of the porous topsoil-zone from Fig. 3.4, where the runoff water starts infiltrating due to gravity. The slower infiltration speed is ascribed to a higher Darcy value of the topsoil. The water distribution of the slowest inflow velocity of 0.1 m/s, shown in Fig. 3.5(a), contains a wavy pattern, which is due to the intermediate air back-flow to compensate for the amount of water infiltration. This pattern gradually disappears as the inflow velocity increases to 0.2 and 0.3 m/s, shown in Fig. 3.5(b) and 3.5(c), respectively. Air backflow was observed in two locations, including one near the bioswale inlet and the other at the right outlet. In summary, the three running-off velocities do not change the infiltration depth shortly after the infiltration begins. This supports our previous observation from Fig. 3.4, the infiltration speed and the depth are insensitive to the running-off velocity. Being consistent with the implication from Fig. 3.4, only high conductivity changes the infiltration patterns, regardless of the runoff velocity.

3.3.3 Effects of pipe hole on water-air phase distribution

Unlike conventional approaches that assume the stationary fluid at the porous media interface,

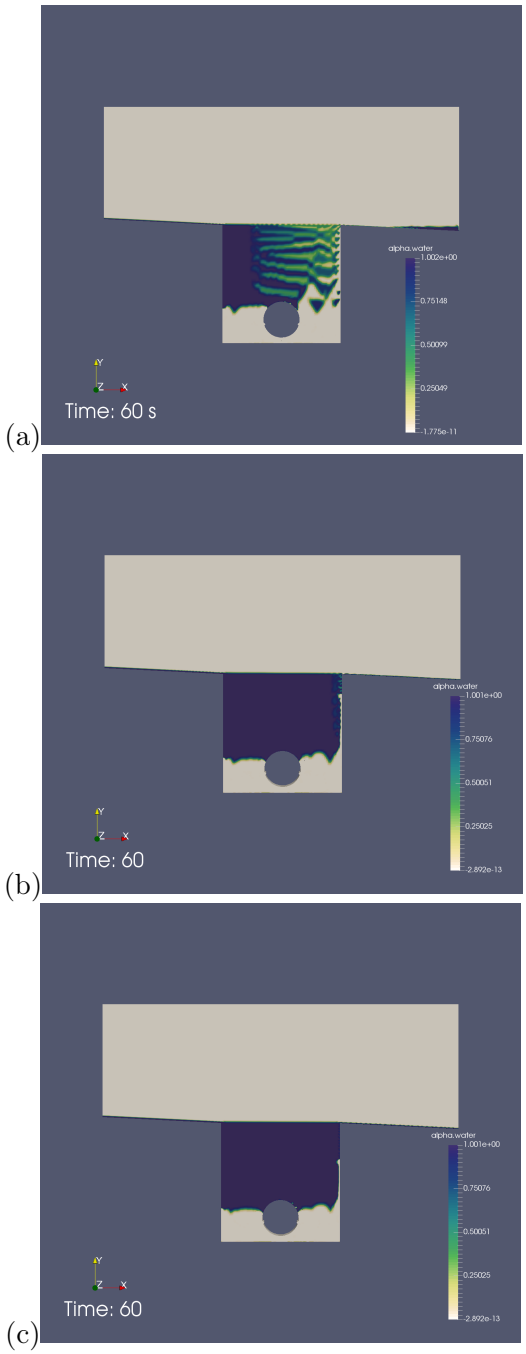

Figure 3.4: Snapshots of infiltrating water distribution at $t = 60$ s to topsoil layer with inflow velocities of (a) 0.1, (b) 0.2, and (c) 0.3 m/s. The two holes of the drain pipe are open.

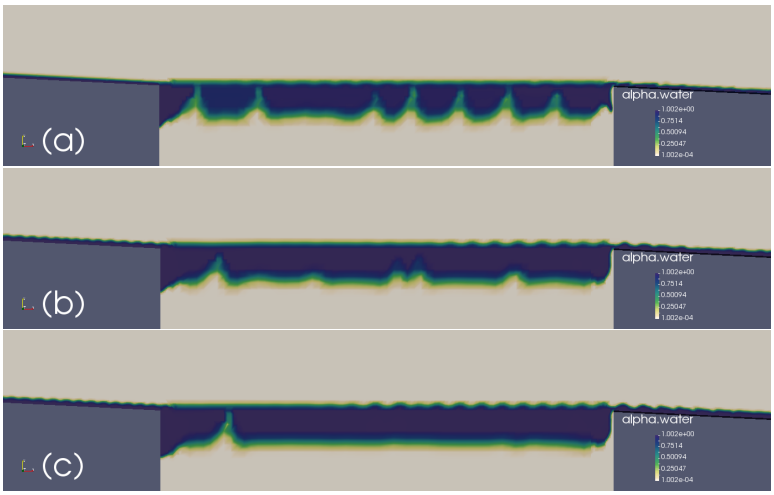

Figure 3.5: Closer visual investigation of infiltrating water distribution at $t = 60\,\mathrm{s}$ to topsoil layer. Runoff velocities of (a), (b), and (c) are equal to those of Fig.3.4.

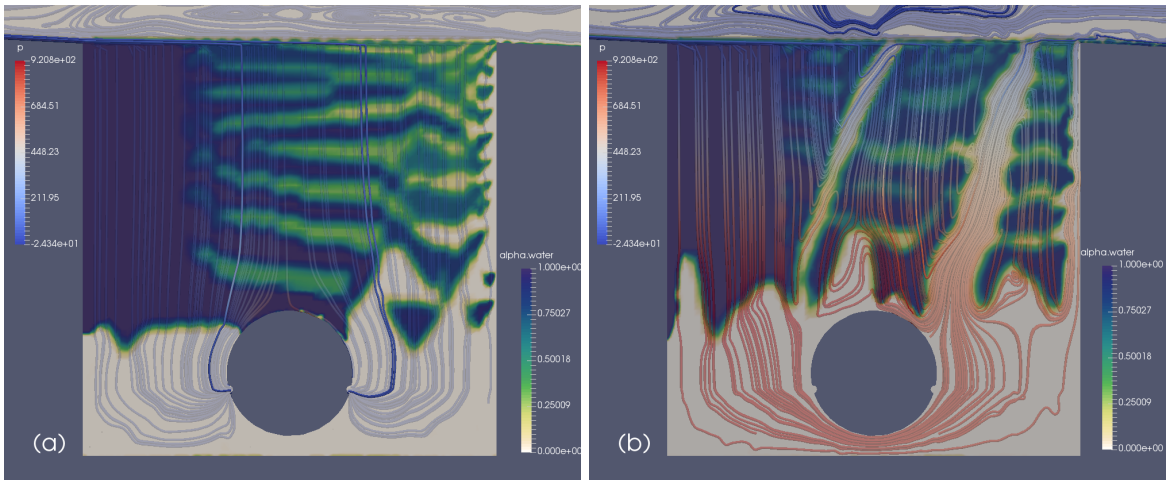

Figure 3.6: Snapshots show the effects of pipe holes on the infiltration patterns, where pipe holes are (a) open and (b) closed. The color of streamlines indicates the intensity of the pressure in the bioswale.

our CFD approach links the fast overland flow and the infiltration flow by introducing small enough time interval of the CFD simulation. Fig. 3.6 depicts the infiltration streamlines of (a) open and (b) closed pipes. For simplicity, we included the infiltration simulation results of Fig. 3.3(a) as Fig. 3.6(a) for open pipe holes, and Fig. 3.6(b) shows streamlines of closed pipe holes. In actuality, the pipe holes are periodically located at every 30 to 60 cm along the pipe. As our simulations are restricted to 2D space for a qualitative analysis with fast computation, the size of pipe holes represents its averaged diameter along the longitudinal direction of the drain pipe. Alternatively, the open and closed pipe hole cases of Fig. 3.6(a) and (b) can be understood as two cross-sections of the bioswale at different locations, one passing through the pipe holes and the other in the middle of the two periodic holes in the longitudinal direction. In the real 3D sub-surfaces of the bioswale, these flow patterns must be periodically mixed depending on the averaged length between two adjacent holes along the drainage direction. Periodically located circular holes will create heterogeneous flow patterns above them since the infiltrating flow will experience the pressure gradient toward the holes from locations above them. If there is no significant driving force to the fluid along the pipe direction, then the flow pattern must also be periodic at the repetitive hole locations. Averaging the flow patterns between two adjacent holes in 3D is equivalent to creating a smaller hole in our 2D configuration, having the same area for water penetration. The equivalent hole size in 2D is calculated as a void area of a real 3D hole divided by the nearest distance between two adjacent holes in 3D. The streamlines in Fig. 3.6(a) demonstrate simple vertical pathways of the mixed phase fluid. The streamlines are shown as smooth and continuous because the bioswale is modeled as a uniform porous media. Note that these streamlines do not individually express the pathway of air and water, but represent phase-averaged flow paths. Because the pipe holes are also pressure outlets, the apparent compression of air phase due to the infiltrating water is less significant than that observed in Fig. 3.6(b). Two vertical columns are observed in Fig. 3.6(b) through which air flows upward to reduce the gas-phase pressure (represented by a reddish color). In OpenFOAM, the pressure of incompressible fluids is calculated as the actual pressure divided by the constant fluid density to take advantage of computational efficiency. The initial air phase of the closed pipe case is either trapped between down-coming water bodies or flowing upward through homogeneous void spaces. Based on our findings, Fig. 3.6 implies that a considerable number of pipe holes may reduce the local compression of air and hence minimize the infiltration resistance due to the counter-balancing air flow. This trend can be limited to the soil matrixes of high permeability, but the air backflow cannot be ignored in mass transport phenomena within the porous bioswale. Finally, we found that a dynamic pattern of air distribution can be partially controlled by the geometrical characteristics of the pipe holes.

3.3.4 Pollutant transport

We simulate the flushing of a partially dry bioswale as a maintenance strategy to washout the pollutant buildup. The mass flux of zinc is calculated as the concentration multiplied by the

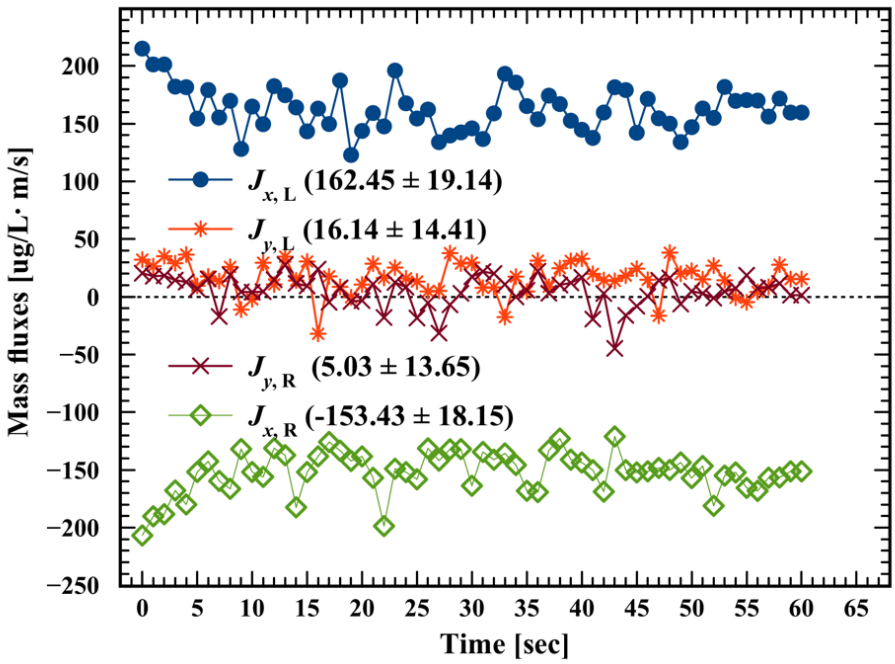

Figure 3.7: Pollutant flux components in $x-$ and $y-$ direction through the left (L) and right (R) pipe holes.

outgoing flow velocity through a pipe hole (i.e., $J = Cu$). It is assumed that a $t = 0$, the bottom soil layer has $\alpha = 1$ and $C = 1,000$ µg/L, and the topsoil layer contains $\alpha = 0.5$ and $C = 500$µg/L. Fig. 3.7 represents the transient mass fluxes in the $x-$ and $y-$ directions at both the left and right holes. The initial discharge flux to the left hole (J_x) decreases rapidly in 10 s due to the gravity-driven flow of water existing in the interstitial spaces. The right J_x shows a symmetric pattern to the left J_x having an opposite direction of the negative sign. The left and right J_x has a mean and standard deviation values of 162.45 ± 19.14 and -152.43 ± 18.15, respectively. A closer investigation shows that the left J_x has a higher magnitude than the right J_x. This result may be explained by the fact that infiltration starts at the left inlet on the top surface of a high conductivity. Furthermore, the difference of J_x in the left and right holes may be attributed to the infiltrating water displaced by the air from the left into the right holes, as confirmed in Fig. 3.3 and Fig. 3.4. The initial infiltration of runoff at the left-top corner of the bioswale surface causes two distinct effects. First, until the bioswale is fully saturated, water content has a decreasing trend along the surface runoff direction. Second, this spatially biased infiltration pushes pre-existing air within the bioswale along the same lateral direction, and, as a feedback, the pressurized air provides hydraulic resistance to the lateral flow. Third, a fraction of pressurized air reaches the right wall and flows up due to the buoyant force. Overall, the infiltration on the left-top surface is balanced with the escaping air-flow

on the right-top surface. The restricted 2D configuration prevents the air and water movements in the normal direction to the runoff (i.e., the pipe-aligned direction). The coupled transport of air and water generates the biased drainage of infiltrated water to the pipe holes. If the bioswale is initially fully saturated, then the magnitude difference of J_x of the opposite-sided holes must be negligible. J_y values for both holes fluctuate near zero but their average values are positive. This is because the holes are positioned at 4 o'clock and 8 o'clock directions and their normal surfaces are slightly directed upward. We observe that when the J_y increases temporarily, J_x decreases. This rather unexpected finding might be a result of the transport across the holes that water discharge and air flows are counter-balanced. This flushing scenario shows that the bioswale can gradually discharge pre-accumulated pollutants. Flushing could be used as a maintenance strategy for the gradual or intermittent release of contaminants below a specific concentration during dry periods.

3.4 Conclusions

CFD simulations have been carried out to investigate coupled transport in a bioswale using OpenFOAM version 4.1. This current study applies a computational approach to simulate the initial infiltration trend with several conditions of the running-off water into a dual-media bioswale with a drain pipe. Our work has several noteworthy features as follows.

First, the current study is, to the best of our knowledge, the first CFD application on bioswale design and performance by the seamless coupling of overland and infiltrating water flows. For the early-stage infiltration of stormwater, a threshold value of the runoff velocity exists, above which the infiltrated water is uniformly distributed and below which the distribution is wavy. For a fast runoff above high conductivity bioswale, the soil zone induces asymmetric water patterns along the runoff direction. Second, a slow runoff velocity yields a wavy profile of the down-coming waterfront, which gradually disappears as the running-off velocity increases. This flow behavior must be partially ascribed to the 2D nature of the simulations, but it emphasizes the reverse flow of air during the initial infiltration to the unsaturated bioswale. Third, the presence of the pipe holes indicates the unique behavior of air dynamics inside the bioswale. When the pipe holes are closed (or clogged), the air-phase pressure increases due to the going-down water volume, and vertical void columns form for air flow channeling. To thoroughly understand the interaction between infiltrating and escaping water flows, 3D CFD modeling is of great necessity, especially in the initial infiltration stage. Fourth, we would like to emphasize that a new solver, interPhaseDiffusionFoam, was successfully developed to simulate the non-volatile pollutant transport in separate phases at different time scales. While the VOF method deals with only the phase-averaged quantities, the new solver employed an algorithmic approximation based on physical interpretation and offered a closer mimicking of the pollutant diffusion in the two-phase flow. Finally, we emphasized a need for universal and reliable computational methods, which can be used to determine the dimensions of bioswales. Note that current bioswale sizing guidelines lack consistency. Our current work is limited to qualitative analyses of short-term and rapid-flow behaviors of highly porous 2D bioswales because

experimental verification is an additional arduous task. These results, however, have significant potential implication in the early-stages conceptual design and analysis of bioswales for better efficiency and stable maintenance.

By having historical runoff data and thorough understanding of precipitation patterns, one can control the time required to fully saturate a bioswale, depending on the periodicity of storm events. Subsequently, CFD analysis can suggest optimal combinations of physical dimensions, hydraulic conductivities, thicknesses of the dual (or even triple) soil layers, as well as the locations and sizes of the drain pipes and perforated holes. Further modeling work is required to develop sizing formulas to ensure optimal hydraulic performance. Long-term transport studies of the bioswale would be beneficial to holistically understand in 3D the physico-chemical/biological reactions of multiple pollutants in unsteady porous-media flow fields.

CHAPTER 4
HYDRAULIC DESIGN PERSPECTIVES OF BIOSWALE VEGETATION LAYERS: A META-RESEARCH THEORY

This part of the dissertation is a manuscript submitted on October 9, 2018 and accepted for publication on November 7, 2018, to *Desalination and Water Treatment*.

Abstract: Optimized bioswale-design requires a fundamental understanding of mass and momentum transfer through a bioswale vegetation layer (BVL) on top of the porous soil zone. Conventional theories of canopy flows are applicable to structuring BVL in a planning phase. Plants in the BVL can be modeled as an embedded collection of cylindrical rods characterized by using (mean) diameter and height. The number density and spatial periodicity of the plants determine the structural and hydraulic characteristics of the BVL. The current paper stands as what we are calling meta-research or "research of research" consisting of an in-depth literature review followed by our own theoretical development. A design equation for an emergent BVL is developed, which suggests the minimum length-to-width ratio of a bioswale as a function of runoff hydraulic characteristics. We calculate a proper bioswale length near which the viscous force fully supersedes the inertial force along the BVL. Moreover, a supplementary graphical method is developed within this study as a simple tool with which to design bioswale dimensions.

4.1 Introduction

A bioswale exists as a nature-based infrastructure, widely used for low impact development (LID) in modern urban environments, which was first practiced in Prince George's County, Maryland, in the early 1990s [2, 46, 173] to reduce stormwater runoff and remove non-point source pollutants [45, 188, 189]. A typical bioswale structure has dual or stratified layers, consisting of overland vegetation and engineered soil zones. The underground soil zone is often pictured as a porous media of varying porosity and hydraulic conductivity. Physico-chemical characteristics of the porous media determine the runoff and pollutant removal capacities [141, 190]. As current bioswale designs depend on empirical guidelines and suggestions, systematic research on bioswale transport phenomena began only recently.

Structural modifications of LID systems are challenging in a practical sense after their initial installation due to their large size and required initial costs. The estimation of the bioswale life-expectancy is, therefore, an important process to ensure long-term operations, possibly with minimum maintenance. Within the existing literature, bioswale research has been focused primarily on experimental observations of runoff infiltration and pollutant removal within the underground soil

media by measuring input and output flow rates and concentrations. The top surface of a bioswale is often covered with a bioswale vegetation layer (BVL) primarily for landscaping purposes. The BVL possesses structural as well as hydraulic aspects, which need to be considered for geometrical designs because the BVL controls the longitudinal flow field and pressure distribution upon the permeable bioswale surface. To the best of our knowledge, engineering roles of the BVL have not been actively studied.

The basic fluid mechanics research on canopy flow can be readily employed to investigate the BVL for the proper management of inland, overland, and infiltrating runoff flows. As the runoff infiltration followed by the pollutant removal depends on the hydraulic drag created in the BVL, a proper design of the BVL is as important as that of the internal porous structure of the bioswale. In this work, we first examine the applicability of canopy-flow theories correspondingly to the BVL analysis. Second, we derive a new design equation for proper bioswale sizing. And, third, we develop a comprehensive graphical method that visually links hydraulic aspects of runoff flows and geometrical aspects of the BVL structures. To explain the coupled role of the BVL, we include a brief research background and a theoretical review in the following sections and propose a practical graphical method as a BVL sizing tool.

4.2 Background

4.2.1 Particle and pollutant removal

A standard bioswale controls pollutant and solid loads from a surrounding catchment area [125]. Bäckström monitored the hydrological performance of a bioswale system over a 12-month period and found that total suspended solids (TSS) removal had been reduced by 99% along a 100m bioswale [191, 192]. Achleitner et al. investigated bioswales ranging from 2 to 10 years of age and reported that regulatory assumptions of 15 years is a reasonable estimation of the replacement time of engineered soil media [85]. Roinas et al. observed that most TSS removal occurs near an inlet bioswale zone [137]. Xiao and McPherson measured inlet and outlet concentration of suspended solids through a bioswale installed in a parking lot and reported 95% of removal by measuring inlet and outlet concentrations [116]. Trowsdale and Simcock also examined the TSS removal capability of a bioretention system, and found that the median concentrations of zinc retained in the bioswale system still exceeded ecosystem health guidelines [123]. Other studies focused on hydraulic and hydrologic aspects of bioswales through field studies [123, 138] and lab-scale experiments [122, 193]. Even though the aforementioned studies provide engineering insights regarding the removal capability of bioswales, these empirical analyses are limited to a small number of detection points, asynchronized measurements with long time intervals, and visual investigation subject to human perspectives. Moreover, coupled effects of surface runoff, the BVL structures, and pollutant/solid removal were not systematically studied.

4.2.2 Design methods

Design methods based on empirical correlations or instructional criteria often indicate the min-

imum regulatory requirements so as to build bioretention systems [14–16, 172]. These guidelines, however, do not provide thorough methods based on scientific rigor in order to address site-specific optimization of a bioswale. Based on our analysis of the stormwater guidelines for the western United States, five approaches exist for sizing bioswales, which include Darcy's law [4, 7], the rational method [8–10], Manning's equation [11], the curve number method [12], and the first-flush sizing method [13]. In reality, bioswales can have various topologies of surrounding ground surfaces, where the runoff flows are conveyed toward bioswale inlets. Although a rigorous computational method such as computational fluid dynamics (CFD) can be used, there still exists a strong need to have improved design equations for the bioswale sizing.

4.2.3 Plant structure

Conventional models for canopy flows have described vegetation structures as rigid or flexible stems. The hydraulic flow with respect to plant height is characterized as in either submerged or emergent conditions, where the physical stem height is lower and higher than flowing water height, respectively. Originally, Petryk [194] experimentally investigated flows passing a group of submerged cylinders in an open channel and developed a model to correlate the mean velocity distribution across the channel, the drag forces upon each cylinder, and the hydraulic resistance among a group of cylinders. This model is, however, limited to uniform laminar flow in a sparse stem configuration for subcritical Reynolds numbers, for which the spacing between the nearest cylinders are at least six stem diameters in the downstream direction. In past decades, various researchers investigated the effect of vegetation configurations on its overall hydraulic resistance to incoming runoff flows [73, 194–199].

4.2.4 Hydraulic/hydrologic aspects

The hydraulic/hydrologic aspects of a canopy layer research can be briefly summarized as follows. For an emergent and flexible vegetation, Fathi-Moghadam and Kouwen developed a mathematical model to estimate Manning's roughness coefficient of flexible, emergent vegetative layers [200]. Finnigan developed a heuristic model, which provides a innovative perspective on turbulence flow passing planted canopies for both the submerged and emergent cases [201]. This model qualitatively describes the three development stages of the mixing boundary layer within vegetation zones of various porosities. The stages include (1) the emergence of the primary Kelvin-Helmholtz instability, (2) the clumping of the vorticity of the Kelvin-Helmholtz waves into vortices, and (3) the kinking and pairing of the vortices. Despite the ecological and engineered significance of hydraulic interactions between vegetation layers and interstitial fluid-flows, there is a paucity of studies that have examined the influences of canopy/bioswale structures on the hydraulic drag to the interstitial flow fields. The direct numerical simulation method (DNS) was used to examine single particle capture by a circular cylinder in vortex-shedding regimes [202–204]. Although the work of Espinosa-Gayosso et al. accurately simulated low-Reynolds number flows, their respective system includes only a pair consisting of a particle and an embedded cylinder so that the many-body hydrodynamics was

not included. King et al. characterized the aquatic vegetation as rigid cylinders fixed upon an impermeable ground surface so as to model flow in the vegetation layer [205]. They conducted physical experiments to validate their turbulence model through emergent and submerged BVL cases. Although the experimental validation was successful within their study, six parameters should be calibrated in addition to the standard $\kappa - \epsilon$ model coefficients: flow depth, vegetative height, drag coefficient, volume fraction, projected plant area per volume, and stem diameter. Existing canopy-flow models are readily applicable to the BVL investigation using the the stem-cylinder analogy [80, 205–207].

As discussed previously, bioswale systems provide an important transition zone from impervious artificial surfaces to porous natural ground. Thus, understanding a bioswale's hydrodynamic response to incoming runoff flow is a critical procedure in order to characterize the respective bioswale structure.

4.3 Theoretical Review

An understanding of flow resistance and conveyance capacity is critical for hydraulic BVL characterization. Vegetation arrays (i.e. geometrical obstacles) can be described as either submerged or emergent conditions, which may dynamically change with time during a precipitation event depending on the runoff height. The obstacles create a specific hydraulic drag that resists the incoming flow to the internal BVL region. The drag coefficient of a canopy medium can be defined as

$$C_{\mathrm{D}} = \frac{F_{\mathrm{D}}/A_c}{\frac{1}{2}\rho V^2} = \frac{\text{disspated energy density}}{\text{kinetic energy density}} \tag{4.1}$$

where F_{D} is the average drag force along the direction of the average flow, A_c is the area of the plant array, ρ is the fluid density, and V is a representative fluid velocity.

Fig. 4.1 shows the geometrical aspect of stems embedded within the bioswale surfaces, in which (a) and (b) indicate the submerged [208–210] and emergent conditions [211–216], respectively, and (c) and (d) show staggered [73, 217] and squared [73, 210] configurations of embedded stems, respectively. The submerged phase indicates that the dynamic water height h_w is higher than the physical plant height h_v, which is equal to the wetted plant height l, i.e., $h_w > h_v$ and $l = h_v$. The emergent phase is characterized using $h_w < h_v$ and $l = h_w$. Mathematically, the wetted length can be expressed as

$$l = \min\left(h_w, h_v\right) \tag{4.2}$$

which means l is the shortest wetted length between h_w and h_v. Runoff flows entering the bioswale generally have an transient water height due to unsteady precipitation patterns. The BVL would, therefore, dynamically experience both emergent and submerged conditions. In particular, if a BVL exists as a short grass layer, then the role of the grasses can be better viewed as a non-smooth surface with a specific roughness providing a slip boundary condition. On the other hand, if the BVL consists of plants of an order of $O\left(10\right)$ cm, the emergent phase is preceded before reaching the

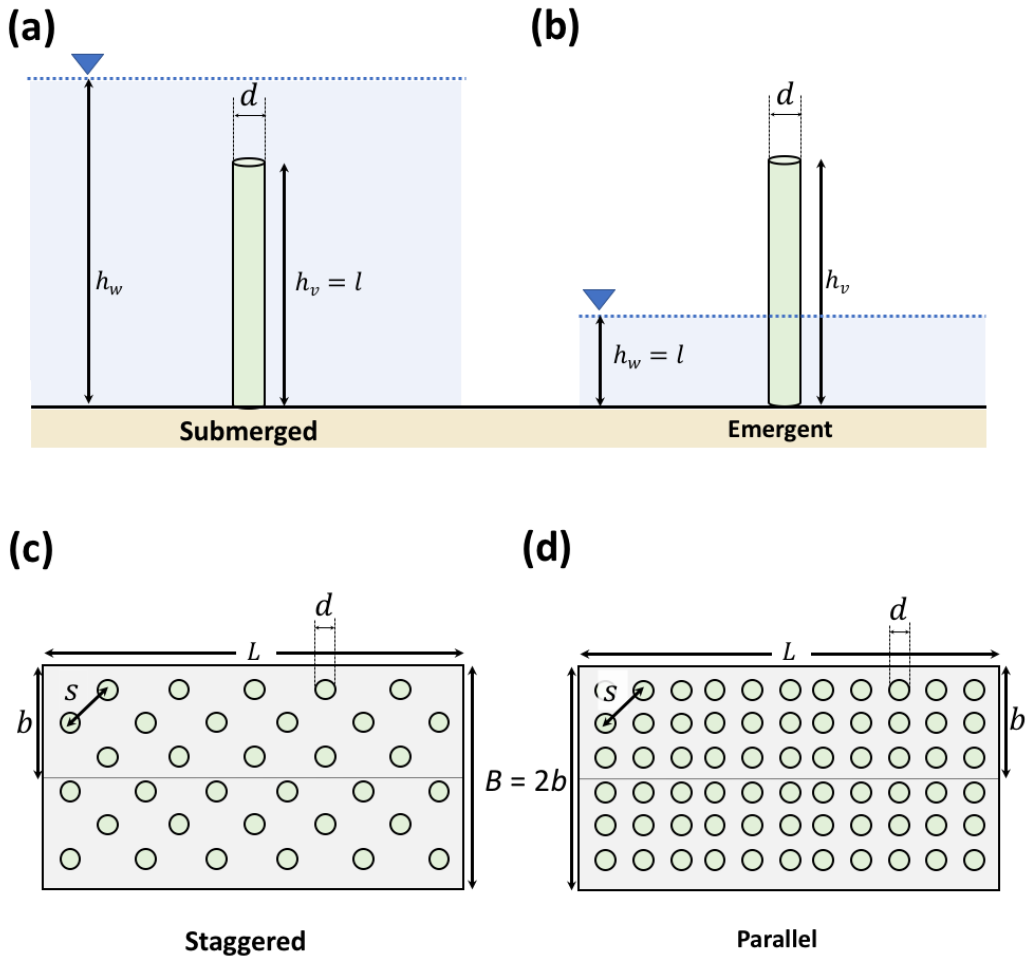

Figure 4.1: Schematic of the geometric properties of an element representing a stem in (a) submerged, (b) emergent conditions, and top view of bioswale dimensions in (c) staggered and (d) parallel vegetation array patterns of length L and width B ($= 2b$).

submerged phase. In this light, we briefly discuss standard theories of canopy flows as applicable to the bioswale sizing.

4.3.1 Submerged canopy theories

Barfield et al.'s work

Barfield et al. [218] developed the general shear stress model for the submerged condition by defining a spacing hydraulic radius

$$r_{\mathrm{BTH}} = h_v \left(\hat{h}_w - 1 + \frac{\hat{s}}{2 + \hat{s}} \right) \tag{4.3}$$

and the ratio between bed and total shear stresses

$$f_{\mathrm{BTH}} = 1 - \left(\hat{h}_w + \frac{1}{2} \hat{s} \hat{h}_w \right)^{-1} \tag{4.4}$$

where $\hat{h}_w = h_w / h_v$ and $\hat{s} = s / h_v$ are normalized lengths of water and stem-spacing by the plant length h_v, respectively, s is the spacing of the elements in the vegetation canopy, and the subscript BTH indicates the three authors of the work [218]. Without losing the generality, Eqs. (4.3) and (4.4) can be applied for an emergent condition by mathematically letting $h_v = h_w$ and $h_v = l$ by considering hydraulic drags generated on the wetted surfaces. For the emergent case, a portion of a stem above the water level is assumed to have negligible contribution to the total hydraulic drag. Therefore, the physical length of the stem can be replaced by the wetted length l.

Stone and Shen's work

Stone and Shen [198] investigated a steady open-channel flow through submerged cylindrical stems of an equal height, distributed uniformly over a bed area. The total stress due to the water flow τ_w was represented

$$\tau_w = \tau_v + \tau_b \tag{4.5}$$

as a superposition of those due to the vegetation layer τ_v and the bed surface τ_b

$$\tau_w = \rho g S h_w \left(1 - \lambda \hat{l} \right) \tag{4.6}$$

$$\tau_v = \tfrac{1}{2} \rho C_D N d_s l V_c^2 \tag{4.7}$$

where g is the gravitational acceleration, S is the channel slope, d_s is the stem diameter, N is the number of plants per unit area, and $\hat{l} = l / h_w$ is the wetted height divided by the physical stem length. In Eq. (4.7), V_c is the maximum velocity within the vegetation layer, which is related to the approaching velocity V_l as

$$V_l = V_c \left(1 - d\sqrt{N} \right) = V_c \left[1 - \sqrt{\frac{4\lambda}{\pi}} \right] \tag{4.8}$$

where the area concentration λ is defined as the fraction of the bed area occupied by cylindrical stems

$$\lambda = \frac{\pi d_s^2}{4} N = \frac{\pi}{4} a d_s \tag{4.9}$$

where $a = N d_s$ is the projected plant area per volume. Then, the bed friction stress is derived as

$$\tau_b = \frac{1}{8} \rho V_l^2 f_b \left(1 - \lambda \right) = \frac{\rho g}{C_b^2} V_l^2 \left(1 - \lambda \right) \tag{4.10}$$

where f_b represents the friction factor, and C_b is the Chézy coefficient of the channel bed [219]. Finally, the flow resistance $R_{\rm SS}$ is represented as

$$R_{\rm SS} = 1.385\left(\frac{1}{\hat{l}} - \sqrt{d_s^2 N}\right)\sqrt{\frac{g}{N d_s h_w}} = 1.385\left(\frac{h_w}{l} - \sqrt{\frac{4\lambda}{\pi}}\right)\sqrt{\frac{\pi g d_s}{4\lambda h_w}} \tag{4.11}$$

of which the coefficient was obtained by a linear regression process using experimental data. In Eq. (4.11), we noticed a condition that $R_{\rm SS}$ is unconditionally a positive definite, which derives an equivalent condition (i.e., $h_w \geq h_{\rm onset}$), where

$$h_{\rm onset} = \sqrt{N\left(d_s l\right)^2} \tag{4.12}$$

is an onset height of the water flow. Our interpretation of $h_{\rm onset}$ is as follows. If $h_w \leq h_{\rm onset}$, then $R_{\rm SS}$ becomes negative, which is unphysical. A possible mathematical treatment is to replace Eq. (4.11) to

$$R_{\rm SS} = \max\left(0, R_{\rm SS}\right) \tag{4.13}$$

to replace a negative value of $R_{\rm SS}$ by 0. This mathematical trick physically implies that the hydraulic drag becomes meaningful if the water level is higher than the critical onset height $h_{\rm onset}$.

Baptist's work

Baptist proposed a resistance coefficient as [220]

$$R_B = \left(\frac{1}{C_b^2} + \frac{C_D a l}{2g}\right)^{-1/2} + \frac{\sqrt{g}}{\kappa}\ln\left(\frac{h_w}{h_v}\right) \tag{4.14}$$

where $\kappa\,(=0.41)$ is the Von Karman's constant [221]. The bed-shear stress is estimated as

$$\tau_{bB} = \frac{\rho g}{C_b'^2}\overline{u}^2 \tag{4.15}$$

using a modified Chézy coefficient C_b':

$$C_b' = C_b + \frac{\sqrt{g}}{\kappa}\ln\left(\frac{h_w}{h_v}\right)\sqrt{1 + \frac{C_D a h_v C_b^2}{2g}} \tag{4.16}$$

which is also applicable to emergent canopies by setting $h_w = h_v$.

Cheng's work

Cheng developed a model to describe an effective resistance above and within the submerged vegetation layer in an open-channel flow [210]. A vegetation-related hydraulic radius was defined in

his work as

$$r_v = \frac{\pi}{4}\frac{\lambda}{1-\lambda}D \tag{4.17}$$

and the global flow resistance is expressed as

$$R_{\mathrm{Ch}} = (1-\lambda)\sqrt{\frac{2gr_v}{lC_D}}\left(\frac{l}{h_w}\right)^{\frac{3}{2}} + 4.54\sqrt{g}\left[\left(\lambda^{-1}-1\right)\left(\frac{1-l/h_w}{d_s/h_w}\right)\right]^{\frac{1}{16}}\left(1-\frac{l}{h_w}\right)^{\frac{3}{2}} \tag{4.18}$$

by calculating the mean flow velocities within and above the vegetation layer. Note that the first and second terms of Eq. (4.18) has dependences on l/h_w and $1-l/h_w$ with the same exponent of $3/2$. In this case, the term of the squared bracket seems to be a pseudo-constant as its exponent is small (i.e., $1/16 = 0.0625$ unless $d_s \ll h_w$).

Ghisalberti's work

Ghisalberti developed a phenomenological model of obstructed flows across vegetation systems and investigated the vertical flow penetration from the top surface of the submerged obstruction layer of $O(0.01-0.1\,\mathrm{cm})$ height [222]. As flow passes downstream through the obstruction zone, the hydraulic drag on the bottom surface initiates an upward flux above the vegetation layer. Ghisalberti introduced a length scale of the vertical flow penetration, denoted as δ_e, and found that $\delta_e C_D a \approx$ constant indicating that the length scale of the drag force is $(C_D a)^{-1}$. A higher drag C_D indicates a lesser penetration depth and lesser up-flow above the penetration zone. This penetration behavior was considered as a cause of vortex generation in the shear zone above the obstruction layer. Ghisalberti's findings can be summarize by $\omega_{\mathrm{rms}} \propto aU_h \propto u_{\mathrm{rms}} \propto u_*$, where ω_{rms} and u_{rms} are the vertical turbulent intensities at the interface and in the streamwise direction, respectively, u_* is the frictional velocity, and U_h is the slip velocity on the top of the obstruction layer.

4.3.2 Emergent canopy theories

Interestingly, the submerged canopy flows are investigated using flow resistance. In this section, emergent canopy theories are reviewed for the drag coefficient C_{D}.

Tanino et al.'s work

Tanino et al. [199] investigated the drag force exerted on randomly distributed, emergent circular cylinders of uniform diameter d, by using the dimensionless ratio of the mean viscous drag per unit cylinder, as originally proposed by Ergun [223] as:

$$\frac{\langle\overline{f_D}\rangle}{\mu\langle\overline{u}\rangle} = \alpha_0 + \alpha_1 \mathrm{Re}_p \tag{4.19}$$

as a function of plant Reynolds number

$$\mathrm{Re}_p = \frac{\langle\overline{u}\rangle d}{\nu} \tag{4.20}$$

where ν is the kinematic viscosity of the fluid, $\langle \overline{u} \rangle$ is the fluid velocity averaged over the void space between stems, $\langle \overline{f_D} \rangle$ is the average drag (in the flow direction) per unit stem length. Eq. (4.19) assumes that α_0 varies with λ, and α_1 is a constant. It has been, however, experimentally shown that α_1 increases monotonically with λ and α_0 is approximately constant if $0.15 \leq \lambda \leq 0.35$. The vegetation layer provides an additional drag, which can be characterized by a drag coefficient (of Eq. (4.1)):

$$C_D \equiv \frac{\langle \overline{f_D} \rangle / \langle \bar{d} \rangle}{\frac{1}{2}\rho \langle \overline{u} \rangle^2} \tag{4.21}$$

using the average over a time interval much longer than representative time scales associated with turbulent fluctuations (denoted by an overbar) and using the space average over a void volume between plants (denoted by angular brackets). Substituting Eq. (4.19) to (4.21) yields a new form of the drag coefficient:

$$C_D = 2\left(\alpha_0 \mathrm{Re}_p^{-1} + 1\right) \tag{4.22}$$

of which the first term represents the viscous contributions, and the second term indicates the inertial contribution occurring due to the pressure loss in the cylinder wake. Previously, Koch and Ladd investigated arrays of $\lambda = 0.05 - 0.4$ and observed that the cylinder drag can be characterized by a linear Re_p dependence similar to Eq. (4.19), but with both α_0 and α_1 varying with ϕ [224]. White also described the C_D of a smooth isolated cylinder for $1 < \mathrm{Re}_p < 10^5$ by an empirical expression [221]:

$$C_D \approx 1 + 10.0\,(\mathrm{Re}_p)^{-2/3} \tag{4.23}$$

or equivalently

$$\frac{\langle \overline{f_D} \rangle}{\mu \langle \overline{u} \rangle} \approx 5.00\,(\mathrm{Re}_p)^{1/3} + \frac{1}{2}\mathrm{Re}_p \tag{4.24}$$

In Eq. (4.24), the second term is dominant relative to the first term based on the exponent of Re_p. It was observed that the inertial term α_1 increases monotonically with λ at a given Re_p, which is attributed in part to the spatial variance of the time-averaged longitudinal velocity which increases with λ. A linear regression of α_1 with λ yielded

$$\alpha_1 = (0.46 \pm 0.11) + (3.8 \pm 0.5)\lambda \tag{4.25}$$

as α_0 is also sensitive to the volume fraction λ [194, 199, 224]. Although Tanino et al. discussed fundamental issues on the drag coefficient [199] as proposed by Ergun's work [223] of Eq. (4.22), the data analysis indicates that α_0 is sensitive to both Re_p and λ.

Rominger and Nepf's work

Rominger and Nepf investigated the interior flow within a rectangular porous zone consisting of embedded cylinders of various blockages, interpreted as an occupied volume fraction by the obstruction [217]. The obstruction layer consists of a collection of uniformly sized rigid cylindrical

plants, as shown in Fig. 4.1(c). The uniform rectangular configuration has a cylinder array in a 2D staggered lattice at half the distance between the nearest neighbor in both the x- and y-directions. Applying the shallow water equations for continuity in the stream-wise and cross-stream directions, the governing equations were set up as

$$\frac{\partial h\left\langle \overline{u}\right\rangle }{\partial x}+\frac{\partial h\left\langle \overline{v}\right\rangle }{\partial y}=0 \tag{4.26}$$

$$\frac{\partial h\left\langle \overline{u}\right\rangle \left\langle \overline{u}\right\rangle }{\partial x}+\frac{\partial h\left\langle \overline{v}\right\rangle \left\langle \overline{u}\right\rangle }{\partial y}=-\frac{1}{\rho}\frac{\partial h\left\langle \overline{p}\right\rangle }{\partial x}+\frac{1}{\rho}\left[\frac{\partial h\left\langle \overline{p}\right\rangle }{\partial x}+\frac{\partial h\left\langle \overline{p}\right\rangle }{\partial y}\right]-hF_{x} \tag{4.27}$$

$$\frac{\partial h\left\langle \overline{u}\right\rangle \left\langle \overline{u}\right\rangle }{\partial x}+\frac{\partial h\left\langle \overline{v}\right\rangle \left\langle \overline{u}\right\rangle }{\partial y}=-\frac{1}{\rho}\frac{\partial h\left\langle \overline{p}\right\rangle }{\partial x}+\frac{1}{\rho}\left[\frac{\partial h\left\langle \overline{p}\right\rangle }{\partial x}+\frac{\partial h\left\langle \overline{p}\right\rangle }{\partial y}\right]-hF_{y} \tag{4.28}$$

where u and v are the fluid velocities in the x- and y-directions, respectively, p is the fluid pressure, and τ is the shear stress. The double average notation is used to denote the flow averaging within the rectangular configuration array within the macro time scale: $\langle\bar{u}\rangle$ indicates an time average of $\bar{u}$ that is the spatial average of u. F_i $(i=x,y)$ is the drag force exerted by the fluid, defined as,

$$F_{x}=\frac{1}{2}\frac{C_{f}}{H}\left\langle \overline{u}\right\rangle \left(\left\langle \overline{u}\right\rangle ^{2}+\left\langle \overline{v}\right\rangle ^{2}\right)^{1/2} \tag{4.29}$$

$$F_{y}=\frac{1}{2}\frac{C_{f}}{H}\left\langle \overline{v}\right\rangle \left(\left\langle \overline{u}\right\rangle ^{2}+\left\langle \overline{v}\right\rangle ^{2}\right)^{1/2} \tag{4.30}$$

in which C_f represents the bed friction coefficient. The vertical length scale, H, is expressed as

$$H=\begin{cases} h_{w} & \text{outside the canopy}\\ \left(1-\phi\right)/a=\frac{1-\phi}{Nd} & \text{inside the canopy}\end{cases} \tag{4.31}$$

where $(1-\phi)/a$ indicates the void volume per projected area of the obstruction. The governing equations (4.27) and (4.28) were scaled using the following characteristic parameters:

$$x\sim L,\quad y\sim b,\quad u\sim U_{\infty},\quad v\sim\frac{bU_{\infty}}{L},\quad \frac{\partial u}{\partial x}\sim\frac{\Delta u}{L},\quad \text{and}\quad \frac{\partial p}{\partial x}\sim\frac{\Delta p}{L} \tag{4.32}$$

to have the following asymptotic relationships without the drag force terms

$$\rho\frac{U_{\infty}\Delta u}{L}\sim-\frac{\Delta p}{L}-\rho\frac{C_{f}}{2h(1-\phi)}U_{\infty}^{2}\left[1+(\frac{b}{L})^{2}\right]^{1/2} \tag{4.33}$$

$$\rho\frac{U_{\infty}\Delta u}{L}\frac{b}{L}\sim-\frac{\Delta p}{b}-\rho\frac{C_{f}}{2h(1-\phi)}U_{\infty}^{2}\frac{b}{L}\left[1+(\frac{b}{L})^{2}\right]^{1/2} \tag{4.34}$$

The pressure and inertial terms must be in a balance unconditionally only if $L\sim b$ for high flow-

blockage. On the one hand, for a zero pressure gradient, the canopy length L is estimated as $(1-\phi)/C_D a$ and further simplified to $L \sim 2/C_D a$ for the low flow-blockage ($\phi \ll 1$) for $L \gg b$ as previously investigated by Belcher [225]. The length scale of the canopy at which the viscous and inertial forces are of the same order of magnitude was suggested as

$$L = (5.5 \pm 0.4)\left[\left(\frac{2}{C_D a}\right)^2 + b^2\right]^{1/2} \tag{4.35}$$

where the coefficient 5.5 ± 0.4 was obtained experimentally. Eq. (4.35) indicates that the representative width b and length L of the canopy are correlated through the drag coefficient, C_D, while the viscous and inertial forces are balanced. To apply Eq. (4.35) to the bioswale design, the drag coefficient C_D needs to be represented using hydraulic parameters of runoff flows.

4.4 Application to bioswale design

4.4.1 Drag Coefficient

Critical theories were closely reviewed in the previous section to determine specific BVL geometries. Within our approach, two conceptual equations are combined:

$$C_D = f\left(\mathrm{Re}_p\right) \tag{4.36}$$

such as Eqs. (4.22) and (4.23) and

$$C_D = f\left(\frac{L}{b}\right) \tag{4.37}$$

such as an inverse form of Eq. (4.35). Eqs. (4.36) and (4.37) can be interpreted as the hydraulic and geometric forms of the drag coefficient, C_D, respectively. For an emergent BVL, we re-write Eq. (4.35) as

$$C_D = \frac{2}{ab}\frac{1}{\sqrt{\eta^2 - 1}} \tag{4.38}$$

where

$$\eta = \frac{L}{5.5b} \tag{4.39}$$

is the dimensionless length scale, defined in this study. As noted above, 5.5 in Eq. (4.39) was empirically obtained in Rominger and Nepf's work [217]. In Eq.(4.38), the denominator ab ($= Ndb$) can be treated as a design parameter. An alternatively meaningful parameter can be a bed volume fraction, defined as

$$\phi = \frac{\frac{\pi}{4} n_p d^2}{2bL} = \frac{\pi}{4} N d^2 \tag{4.40}$$

where n_p is the number of stems within a BVL. Then, parameter ab has a specific expression of

$$ab = Ndb = \frac{4\phi}{\pi}\frac{b}{d} = \frac{2}{\pi}\phi\beta \tag{4.41}$$

where $\beta = 2b/d$ is a dimensionless width (i.e., the bioswale width divided by by the stem diameter). Substitution of Eq. (4.41) into (4.38), gives

$$C_D = \frac{C_D^0}{\sqrt{\eta^2 - 1}} \tag{4.42}$$

where

$$C_D^0 = \frac{\pi}{\phi\beta} = \frac{2}{Nbd} \tag{4.43}$$

The drag coefficient decreases with volume fraction ϕ and the stem diameter d. For a long bioswale ($L \gg b$) of a bed volume fraction ϕ, the asymptotic behavior of the drag coefficient can be approximated as $C_D \propto 1/(L\phi)$. Here, we consider a specific exemplary case such that a stem has a volume fraction of $\phi \sim 0.314$ and diameter 2.0 cm in a BVL of width $2b = 1\,\mathrm{m}$, then we have

$$\beta = 1.0\,\mathrm{m}/0.02\,\mathrm{m} = 50 \tag{4.44}$$

$$ab = \frac{2}{\pi}\phi\beta = \frac{2}{3.14} \times 0.314 \times 50 = 10 \tag{4.45}$$

$$C_D^0 = \frac{\pi}{(0.314) \times 50} = 0.02 \tag{4.46}$$

4.4.2 Graphical Method

To easily estimate an optimized length ratio of a bioswale, we developed a graphical method as shown in Fig. 4.2. The drag coefficient C_D is plotted with respect to $\mathrm{Re_p}$ using Eq. (4.23) and η using Eq. (4.42). For example, if $\mathrm{Re} = 10^{1.4} \simeq 25.10$ (at position a), then C_D is calculated as 2.17 (at position b on the solid line). A horizontal line of $C_D = 2.17$ has nine cross-points with the same number of ab lines (from 0.1 to 20). Among them, we select two cases for $ab = 0.2$ and 2.0 (positions e and c, respectively) for an explanatory purposes. Position d was determined by drawing a vertical line at position c, which gives $\eta = 1.10$ and hence $L/2b = 3.03$. This result indicates that the representative BVL length of 3.03 m (if $2b = 1\,\mathrm{m}$) is required to approximately balance contributions from pressure and viscous forces. In other words, within the BVL of length 3.03 m, the inertial force is dominant over the viscous force. C_D rapidly approaches to 1.0 for $ab = 2$ within the reasonable range of Reynolds number, $10 < \mathrm{Re_p} \leq 100$, of the incoming flows. For $ab = 0.2$, position e provide a specific value of $\eta = 4.72$, which is equivalent to $L/2b\ (= L/B) = 13.0$. This case indicates that for a BVL of width $B = 1\,\mathrm{m}$,the pressure and viscous forces are balanced near the end of the 13 m BVL. In summary, for a specific value of $\mathrm{Re_p} = 25.1$, the two cases of $ab = 2.0$ and 0.2 require the minimum lengths of 3.03 and 13.0 m, respectively, for the width $B = 1.0\,\mathrm{m}$.

A bioswale of low density, narrow width, or smaller stem diameter requires a longer length for the hydraulic balance between the inertial and viscous forces. Position h (i.e., a cross position of $C_D = f(\mathrm{Re_p})$ and that for $ab = 1.0$) gives a special case that $\log \mathrm{Re_p}$ equals to η. A vertical line passing through the position h determines specific values of $\log_{10}(\mathrm{Re_p})$ and η, which are 1.83 for both, and, hence, the length is estimated as $L = 4.40\,\mathrm{m}$ per 1 m width BVL. As C_D is a rapidly decreasing function of $\log \mathrm{Re_p}$ to 1.0, a matching point (like position h) must be located at a very high value of $\mathrm{Re_p}$. In general, specific pair values of Re_p and η fully depend on the two functional representations of Eqs. (4.36) and (4.37). Basic mathematical dependence of C_D on Re_p is obtained by differentiating Eq. (4.23), which qualitatively gives

$$\frac{\partial C_D}{\partial \mathrm{Re}} < 0 \quad \text{and} \quad \frac{\partial C_D}{\partial \eta} < 0 \tag{4.47}$$

As Fig. 4.2 indicates, C_D unconditionally decreases with respect to $\mathrm{Re_p}$ and eventually converges to $C_D \to 1$ in the limit of $\mathrm{Re}_p \to \infty$. Variations of C_D with respect to L or η with a specific ab require significant elongation of the bioswale length at a high Reynolds number to decelerate the inter-stem flow enough. As we suggest this BVL length as the minimum, the designed BVL length can be a few factors longer than the minimum length estimated using the graphical method of Fig. 4.2. Differentiation of C_D with respect to the length L gives

$$\frac{\partial C_D}{\partial L} = -\frac{2}{abL}\frac{\eta^2}{[\eta^2 - 1]^{3/2}} \to -\frac{11}{aL} \tag{4.48}$$

which physically implies that for a long BVL (i.e., $\eta \gtrsim 3$ at least), the variation rate of C_D with L is insensitive to the half-width b.

4.4.3 Structure linked to hydraulics

Fig. 4.3 shows the geometrical ratio η plotted as a function of of Re_p, through Eqs. (4.23) and (4.38), by eliminating evaluation of C_D. Note that this design relationship is applicable only for emergent conditions within specific ranges of $0.1 \le ab \le 20$ and $10^0 \le \mathrm{Re_p} \le 10^5$. Here, we select a slightly different value of $\mathrm{Re_p} = 10^{1.5} = 31.623$ (at position j) for a particular site; then, a vertical line is drawn that intersects with several crossing points of specific ab values. An exemplary case of $ab = 0.2$ is selected at position k from j. Then, position l was determined by drawing a horizontal line from b, which gives $\eta = 4.899$ and hence $L/B = 13.472$. For the BVL to be affective in decelerating flow, the length of the bioswale should be, in our opinion, three or more times the estimated L to ensure that the inertial force is dominant only near the inlet zone. Moreover, Fig. 4.3 shows interesting trends as follows. η rapidly increase with Re_p approximately for $ab \le 1$. For cases of $ab \gtrsim 1$, η shows a very gradual increase in Re_p. In principle, one can eliminate C_D by

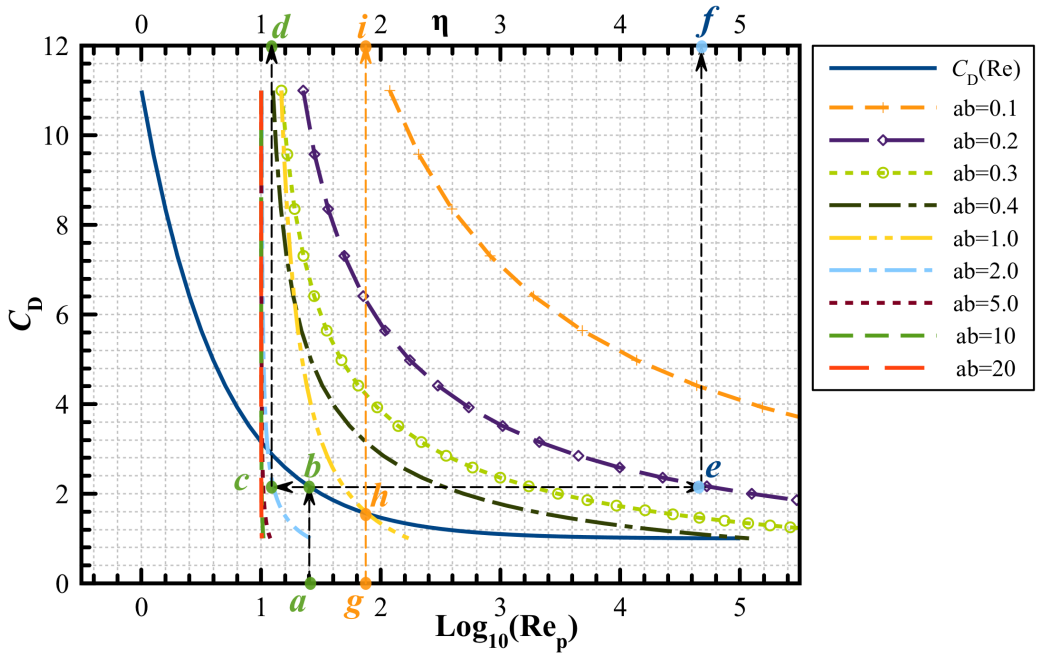

Figure 4.2: The drag coefficient C_D plotted with respect to Re (bottom x-axis) and η (top x-axis) so as to find the optimal geometrical ratios for the bioswale design.

equating Eqs. (4.23) and (4.42) to have

$$\eta = \sqrt{\left(\frac{\pi/\phi\beta}{1+10.0\mathrm{Re}_p^{-2/3}}\right)^2 - 1} = \sqrt{\left(\frac{2/ab}{1+10.0\mathrm{Re}_p^{-2/3}}\right)^2 - 1} \tag{4.49}$$

and asymptotically

$$\eta \simeq \frac{2/ab}{1+10.0\mathrm{Re}_p^{-2/3}} = \frac{2}{ab}\frac{\mathrm{Re}_p^{2/3}}{\mathrm{Re}_p^{2/3}+10.0} \tag{4.50}$$

or

$$L = \frac{11}{Nd}\frac{1}{1+10.0\mathrm{Re}_p^{-2/3}} \tag{4.51}$$

which indicates that a BVL length should be designed longer for low plant density N, smaller stem diameter d, and high runoff Reynolds number, Re_p. Then, Eq. (4.50) can be approximated for small and large Re_p such as

$$\eta \simeq \mathrm{Re}_p^{2/3}\,(5ab)^{-1} \quad \text{for} \quad \mathrm{Re}_p^{2/3} \ll 10.0 \tag{4.52}$$

$$\simeq 2\,(ab)^{-1} \quad \text{for} \quad \mathrm{Re}_p^{2/3} \gg 10.0 \tag{4.53}$$

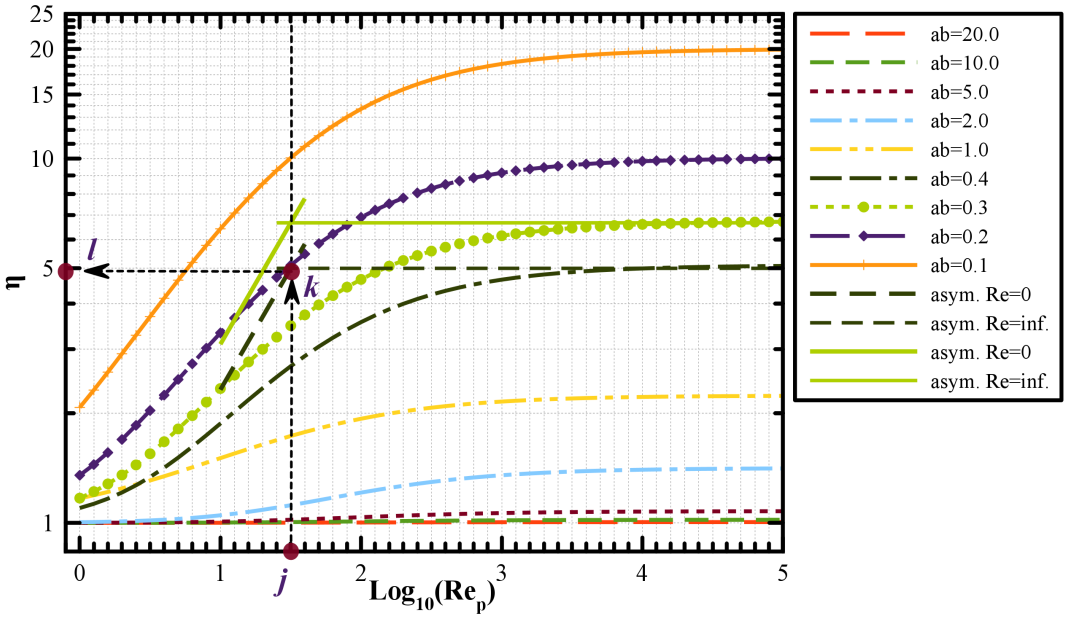

Figure 4.3: η plotted with respect Re to determine optimized length ratio of a bioswale valid for $0.1 \leq ab \leq 20$ and $10^0 \leq Re \leq 10^5$. Asymptotic lines drawn at zero and infinite Re are based on Eqs. (4.52) and (4.53), respectively.

The plateau values shown in Fig. 4.3 matches the limiting value of $\eta = 2/ab$ for high $\mathrm{Re_p}$. For $\mathrm{Re_p^{2/3}} \ll 10.0$, the log η vs. log Re_p plot has a slope of 2/3. The boundary between the two limiting cases can be obtained by equating the two limiting η of Eq. (4.52), which gives the critical Reynolds number

$$\mathrm{Re_{p,cr}} = 10^{1.5} = 31.623 \tag{4.54}$$

which is the exemplary case discussed above. Interestingly, this critical Reynolds number is universal and independent of ab. If the Reynolds number is higher than $\mathrm{Re_{p,cr}}$, then one can simply use $\eta = 2/ab$ without losing design accuracy. Fig. 4.3 also shows the universal $\mathrm{Re_{p,cr}}$ values by drawing asymptotic lines at zero and infinite $\mathrm{Re_p}$ for exemplary cases of $ab = 0.3$ and 0.4. The vertical line passing through position k re-emphasize the critical $\mathrm{Re_p}$=31.623, above which the variation of η with respect to $\mathrm{Re_p}$ becomes insensitive.

4.4.4 Verification and Comparison

Fig. 4.4 shows a plot of Ishikawa et al.'s experimental data onto η vs. Re_p graph [1]. Ishikawa et al. used a straight channel of fixed dimensions of 15 m × 0.3 m (or equivalently $\eta = 15\mathrm{m}/(5.5 \times 0.15\mathrm{m}) = 18.18$) to determine the effect of plant density on the drag force exerted on to the plants. We used their data set for two cases of the plant diameter $d = 6.4$ and 4.0 mm. In each case, they studied the drag coefficient for four plant densities, three bed slopes, and three discharge velocities.

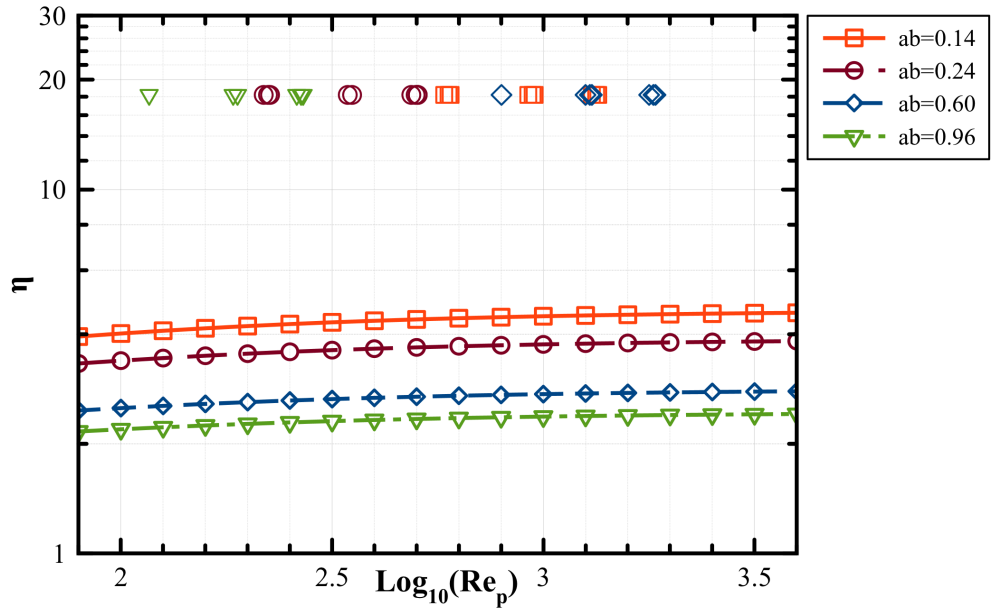

Figure 4.4: Comparison of experimental data from Ishikawa's study [1] ($\eta = 18.18$) with the plot η vs. $\mathrm{Re_p}$.

Ishikawa et al.'s data, as summarized in Fig. 4.4, show a fixed η because a finite BVL size was used in Ishikawa et al.'s study [1]. Scattered data points grouped for a specific ab value indicates monotonously decreasing relationship between ab and Re_p. It is worth noting that variation of η is not sensitive to Re_p for each ab value. As predicted, η ranges approximately from 1.5 to 4.5 for ab values of Ishikawa's cases, and ratio $\eta_{\mathrm{ex}}/\eta_{\mathrm{thr}}$ ranges roughly from 4 to 12, where η_{ex} and η_{thr} are experimental and theoretical η, respectively. This η range ensures that the inertial force is dominant only near the inlet canopy region.

As our predicted value of η indicates the proper BVL length at which the pressure and viscous forces are in balance with each other, the dimensionless length range from η to 2η can be interpreted as a BVL zone so that the inertial force becomes less significant than the viscous force. Moreover, in the range of the dimensionless length greater than 2η, the viscous force becomes dominant so that the BVL provides an effective hydraulic resistance to decelerate the entered runoff flow at the inlet of the canopy zone. We suggest a safety factor of 3–5 to be multiplied to the theoretical η obtained using the graphical method to ensure that the BVL zone effectively provides hydraulic resistance to decelerate the incoming runoff flows.

4.5 Concluding Remarks

Flow resistance and channel-conveyance capacity are basic design parameters required in the

hydraulic design of a vegetated bioswale layer. Current design for bioswales include five methods such as Darcy's law, rational method, Manning's equation, curve number method, and first-flush sizing method. To support the widespread adoption of bioswales, there is a need for improved techniques regarding the predictive capability of hydraulic drag within and above the BVL so as to optimize design methods. This study provides an original contribution to the literature involving the coupling of structural and hydraulic aspects of bioswale systems.

After the in-depth review of canopy-flow theories, we employed Rominger and Nepf [217]'s and Baptist [220]'s work to directly link plant Reynolds number and length scales of the bioswale systems by mathematically eliminating C_{D}. We then predicted a theoretical minimum length so as to balance the pressure and viscous forces near the outlet of the bioswale. These formulas can be unified in a general form of an emergent case that links the plant Reynolds number and $\eta\,(= L/2.75B)$ as a structural design parameter. We suggest a proper length of a vegetated bioswale to be calculated as at least 3–5 times the theoretically predicted η using the graphical method developed in this study. Engineers can draw upon this method as a tool that can provide them with guidance regarding the predictive capability in the proper BVL length so as to enhance bioswale operation and maintenance.

CHAPTER 5
CONCLUSIONS

Within the scope of research for this dissertation, a comprehensive theoretical framework, modeling techniques, and a numerical algorithm have been presented regarding the design of bioswale systems. A series of studies on these topics are specifically examined beginning with Chapter 2, which discusses a theoretical model of quantifying bioswale unit processes. The framework is formed by combining current and modified theories regarding a water and wastewater treatment plant (WWWTP). Findings from this study demonstrate that the structural aspects of a bioswale are perceived as a combined WWWTP. The model effectively describes a bioswale and governing equations for each respective bioswale unit operation. The theoretical analysis is restricted to physical, chemical, and fluidic processes, excluding the biological. In addition, the computational fluid dynamics (CFD) technique was evaluated for its strengths and attributes as a tool in the preliminary design stages as considered for improved bioswale design. CFD simulations offer a rigorous, microscopic approach to represent the coupled transport phenomena within a bioswale. The framework of this study "Understanding bioswale as a small water and wastewater treatment plant: a theoretical review" exists as the foundation from which the CFD modeling study proceeds in the Chapter 3.

For the focus of Chapter 3, a CFD simulation is applied toward the modeling of coupled transport within a bioswale system using OpenFOAM version 4.1 (`www.openfoam.org`). The 2D model presented within Chapter 3 is focused on specific bioswale configurations for polluting and flushing cases using a new solver, `interPhaseDiffusionFoam` (`https://github.com/enphysoft/interPhaseDiffusionFoam`), developed throughout this doctoral work. The polluting scenario indicates storm runoff containing a pollutant concentration entering into an ideally fresh bioswale, without having water content and accumulated pollutant mass. The flushing is an opposite case, in which the bioswale is pre-contaminated with a specific concentration (assumed to be known) and the entering runoff flow have a negligible pollutant concentration. Results from the polluting case showed that for the early-stage infiltration of stormwater, a threshold value of the runoff velocity exists above which the infiltrated water is uniformly distributed. Below this threshold value of the runoff velocity, a slow runoff velocity yields a wavy profile of the down-coming waterfront, which gradually disappears as the running-off velocity increases. This flow behavior is partially attributed to the 2D nature of the simulations. For a fast runoff above a bioswale of high hydraulic conductivity, the soil zone induces asymmetric water-distribution patterns along the respective runoff direction. Also, the bioswale configuration plays a role in the unique behavior of air dynamics inside the bioswale. When the drain pipe does not have holes (or holes are clogged), the pressure of preexisting air within the sub-soil zone increases due to the infiltrating water downward, and, therefore, vertical void columns form for air-flow channeling to the top ground level. In the flushing

case, zinc, a representative non-volatile pollutant, was studied to simulate pollutant concentration build-up within a bioswale from a previous storm event using `interPhaseDiffusionFoam` solver. This new solver incorporates an algorithmic approximation based on the physical interpretation of a phase boundary. In addition, it allows for a closer mimicking of the pollutant diffusion within the two-phase flow as compared to the conventional volume of fluid (VOF) method, which deals with only the phase-averaged quantities to approximate free boundaries. The results from the flushing scenario substantiates that the bioswale can gradually discharge pre-accumulated pollutants. This study offers some insights into how the flushing effect could be used as a maintenance strategy for the gradual or intermittent release of contaminants below a specific concentration during dry periods (between storm events).

Chapter 4 reviews canopy-flow theories currently available, given contemporary research, that are applicable for the initial design of bioswale systems. The findings from this meta-analysis led to the development of a numerical algorithm that directly linked plant Reynolds number and the bioswale vegetation layer (BVL) length-scale, η, by mathematically eliminating the drag coefficient, C_{D}, for an emergent case. As a practical design tool, a graphical method was developed to directly calculate the proper BVL length using an estimated Reynolds number when the pressure and viscous forces are balanced. The results are verified and compared to values in the existing literature in which a safety factor of 3–5 is to be multiplied by the theoretical η. The safety factor ensures that the BVL zone effectively provides hydraulic resistance to decelerate the incoming runoff flows.

The present study addresses pervasive issues within the stormwater management of runoff and non-point source pollution. Taken together, the findings, as presented within this dissertation, extend our respective knowledge as design engineers concerned with improving predictive theoretical and computational approaches for characterizing engineered bioswale systems.

APPENDIX A
APPENDIX

A.1 Brief review of the VOF algorithm with mass transfer

Basic Formalism

The mass conservation for the local concentration $C_k(\boldsymbol{r}, t)$ in a phase k [1 for liquid (water) and 2 for gas (air)] is

$$\frac{\partial C_k}{\partial t} + \nabla \cdot (\boldsymbol{U}_k C_k) = -\nabla \cdot \boldsymbol{J}_k \tag{A.1}$$

where U_k and J_k are the local fluid velocity and diffusive flux of pollutants, respectively. The diffusive fluxJ_k is assumed to follow Fick's law of diffusion:

$$\boldsymbol{J}_k = -D_k \nabla C_k \tag{A.2}$$

where D_k is a diffusivity constant.If a cell volume of a computational grid contains both the liquid and gas phases, Eqs. (A.1) and (A.2) are to be averaged within the cell volume. The following equation shows that a fraction of phase k is defined as a ratio of the volume and the total cell volume,

$$\alpha_k = \frac{V_k}{V_c} \tag{A.3}$$

An average quantity of an arbitrary physical variable q in the cell volume is

$$q = \frac{1}{V_c} \int_{V_c} q \mathrm{d}V = \sum_k \alpha_k \bar{q}_k = \alpha_1 \bar{q}_1 + \alpha_2 \bar{q}_2 \tag{A.4}$$

where

$$\bar{q}_k = \frac{1}{V_k} \int_{V_k} q \mathrm{d}V \tag{A.5}$$

is an average of q only in phase k. If Eq. (A.1) is averaged along the overall cell volume. Thus, we have the following expression

$$\frac{\partial \alpha_k \overline{C_k}}{\partial t} + \nabla \cdot \left(\alpha_k \overline{\boldsymbol{U}_k C_k}\right) = -\nabla \cdot \alpha_k \overline{\boldsymbol{J}_k} \tag{A.6}$$

Now we make a sum of each side of Eq. (A.6) with respect to k, which leads to

$$\frac{\partial C}{\partial t} + \nabla \cdot \boldsymbol{U} C = -\nabla \cdot \boldsymbol{J} \tag{A.7}$$

where

$$C = \alpha_1 \overline{C_1} + \alpha_2 \overline{C_2} \tag{A.8}$$

$$\boldsymbol{U}C \simeq \overline{\boldsymbol{U}C} = \alpha_1 \overline{\boldsymbol{U}_1 C_1} + \alpha_2 \overline{\boldsymbol{U}_2 C_2} \tag{A.9}$$

Similarly, the average flux is defined as $\boldsymbol{J} = \sum_{k=1}^{2} \alpha_k \overline{\boldsymbol{J}_k}$, but if this definition is applied, $\boldsymbol{J}$ cannot be represented using the cell-volume averaged quantities. An approximation using the averaged diffusivity is applied to both the liquid and gas as follows:

$$\boldsymbol{J} \simeq -D \left[\alpha_1 \nabla C_1 + \alpha_2 \nabla C_2\right] \tag{A.10}$$

where the mean diffusivity is calculated as a phase-average

$$D = \alpha_1 D_1 + \alpha_2 D_2 \tag{A.11}$$

For simplicity, we omit the subscript 1 for α and replace α_2 by $1 - \alpha$. At the phase boundary, the pollutant partition between the two phases can be approximated using Henry's law (i.e., $C_2 = HC_1$), where H is a dimensionless Henry's constant. The mean flux $\boldsymbol{J}$ is represented to

$$\boldsymbol{J} = -D \left[\nabla C - \Phi \nabla \alpha\right] \tag{A.12}$$

using a mathematical identity $\alpha_1 \nabla C_1 = \nabla \left[\alpha_1 C_1\right] - C_1 \nabla \alpha$, The final governing equation using the volume average is Eq. (8) in chapter 3, having the effective convective transport controlled by the average phase velocity U.

Additional treatment

Unless solutes are volatile, mass transport between the liquid-gas interface is negligible. In this case, parameters should be appropriately selected to entirely prevent the interfacial diffusive-transport. The diffusivity within a gas phase is approximately $10^3 - 10^4$ times higher than that within a liquid phase. In this case, Eq. (A.11) may not be a proper choice to maintain solute molecules in the liquid phase, minimizing the mass transfer to the gas phase.

If the gas phase concentration C_2 is initially zero and there is no mass transfer from the liquid phase, then C_2 should be maintained as zero. The volume of fluid method linked to the current diffusion algorithm does not guarantee the mass diffusion limited to the liquid phase. To mathematically implement this real phenomena to out CFD simulations, we used an arbitrarily forceful condition:

$$\frac{D_2}{D_1} \approx \frac{C_2}{C_1} = H \ll 1 \tag{A.13}$$

which is similar to original Henry's law. Then, for small values of H, we calculated

$$D = D_1 \left(\alpha + (1-\alpha)\, H\right) \rightarrow \alpha D_1 \quad \text{for small } H \tag{A.14}$$

and more importantly

$$D\Phi = D_1 \left(1 - H\right) C \rightarrow D_1 C \quad \text{for small } H \tag{A.15}$$

Therefore, we have

$$\begin{aligned} \frac{\partial C}{\partial t} + \nabla \cdot \boldsymbol{U} C &= \nabla \left(D_1 \alpha \nabla C\right) - \nabla \left(D_1 C \nabla \alpha\right) \\ &= D_1 \nabla \left(\alpha \nabla C - C \nabla \alpha\right) \end{aligned} \tag{A.16}$$

where $D_1 \nabla(\alpha \nabla C)$ indicates the diffusive flux with a diffusivity D_1weighted by the liquid fraction α, and $-D_1 C \nabla \alpha$ implies back transport of α from the gas phase to the liquid phase. This diffusion coefficient of α is conceptually determined as $C D_1$. This solver is named interPhaseDiffusionFoam and available online [226].

NOMENCLATURE

α_0	empirical coefficient in Eq. (4.19)
α_1	empirical coefficient in Eq. (4.19)
δ_e	length scale of the vertical flow penetration
κ	Von Karman's constant
λ	fraction of the bed area occupied by cylindrical stems
ν	kinematic viscosity
ω_{rms}	vertical turbulent intensity at the interface
ϕ	solid volume fraction
ρ	density of water
τ	stress
$\langle \bar{d} \rangle$	characterstic plant width
$\hat{h}_w$	scaled length of water depth
$\hat{l}$	wetted stem height per water height
$\hat{s}$	scaled length of average vegetation height
$\langle \overline{f_D} \rangle$	average drag in the direction of the average flow per unit length of stem
$\langle \overline{u} \rangle$	fluid velocity averaged over the void space between stems
$\overline{u}$	depth-averaged flow velocity
a	projected plant area per volume, Nd_s
A_c	front cross-sectional area
B	width of a vegetation layer
b	half width of a vegetation layer
C_b	Chézy coefficient of the bed
C_b'	drag force for both submerged and emergent vegetation conditions using Baptist [207]

C_D drag coefficient

C_f bed friction coefficient

d_s stem diameter

f stress ratio

F_{D} average drag force

f_b friction factor

F_i drag force exerted on the fluid in the x- and y- directions for $(i = x, y)$

g gravitational acceleration

H vertical length scale of the canpoy

h_{onset} water height of resistance onset

h_v physical vegetation height

h_w dynamic water height

L length of a vegetation layer

l wetted vegetation height

N number of plants per unit plant area

R flow resistance

r hydraulic radius

S channel slope

s spacing between stems

u fluid velocity in the x-direction

u_* frictional velocity

U_∞ uniform flow

u_{rms} vertical turbulent intensity in the streamwise direction

U_h slip velocity on the top of the obstruction layer

V mean flow velocity averaged over the void space

v	fluid velocity in the y-direction
V_c	maximum velocity within the vegetation layer
V_l	approaching velocity
Re_p	plant Reynolds number
BTH	Barfield, Tollner and Hayes
B	Baptist
Ch	Cheng
SS	Stone and Shen
$_b$	bed
$_v$	vegetation
$_w$	water

BIBLIOGRAPHY

[1] Y. Ishikawa, K. Mizuhara, S. Ashida, Effect of density of tress on drag exerted on trees in river channels, Journal of Forest Research 5 (2000) 271–279.

[2] Prince George's County Maryland, Bioretention Manual, Tech. rep., Environmental Services Division, Department of Environmental Resources (2007).

[3] T. D. Fletcher, W. Shuster, W. F. Hunt, R. Ashley, D. Butler, S. Arthur, S. Trowsdale, S. Barraud, A. Semadeni-Davies, J.-L. Bertrand-Krajewski, P. S. Mikkelsen, G. Rivard, M. Uhl, D. Dagenais, M. Viklander, SUDS, LID, BMPs, WSUD and more - The evolution and application of terminology surrounding urban drainage, Urban Water Journal 12 (2014) 525–542.

[4] California Stormwater Quality Association, Stormwater best management practice handbook: New development and redevelopment, Tech. rep. (2003).

[5] Hawaii Department of Transportation, Plans for Kaneohe watershed stromwater best management practices on Oahu, Tech. rep. (2014).

[6] M. Shafique, R. Kim, Green stormwater infrastructure with low impact development concept: a review of current research, Desalination and Water Treatment 83 (2017) 16–29.

[7] A. Roy-poirier, P. Champagne, A. M. Asce, Y. Filion, Review of bioretention system research and design: Past, present, and future, Journal of Environmental Engineering 136 (2010) 878–889.

[8] New Mexico State Highway and Transportation Department, Drainage manual volume 1, hydrology, Tech. rep. (1995).

[9] City and County of Honolulu, Storm water BMP design guide for new and redevelopment, Tech. rep., Honolulu, Hawaii (2017).

[10] Utah Department of Transportation, Stormwater quality design manual, Tech. rep. (2018).

[11] Washington State Department of Ecology Water Quality, Stormwater management manual for Western Washington, Tech. rep. (2012).

[12] State of Orgeon Department of Environmental Quality, BIOFILTERS (Bioswales, Vegetative Buffers, and Constructed Wetlands) for storm water discharge pollution removal, Tech. rep., Department of Environmental Quality (2003).

[13] Idaho Department of Environmental Quality, Catalog of stormwater best management practices for Idaho cities and counties, Tech. rep. (2005).

[14] National Oceanic and Atmospheric Administration, Low impact development a practitioner's guide, Tech. rep., Hawaii Costal Zone Management Horsley Witten Group, NOAA (2006).

[15] Las Vegas Stormwater Quality Management Committee, Las Vegas valley construction site best management practices guidance manual, Tech. rep. (2009).

[16] Alaska Department of Environmental Conservation, Alaska storm water guide, Tech. rep. (2011).

[17] J. P. Heaney, J. J. Sansalone, A vision for urban stormwater management in 2050, in: W. M. Grayman, D. P. Loucks, L. Saito (Eds.), Toward a Sustainable Water Future, American Society of Civil Engineers, Reston, Virginia, 2010, Ch. 17, pp. 157–165.

[18] J. Zhang, G. Ma, R. Ming, X. Cui, L. Li, H. Xu, Numerical study on seepage flow in pervious concrete based on 3D CT imaging, Construction and Building Materials 161 (2018) 468–478.

[19] B. Andersson, R. Andersson, L. Hakansson, M. Mortensen, R. Sudiyo, B. van Wachem, Computational fluid dynamics for engineers, Cambridge University Press, Ney York, 2012.

[20] T. Tsuchida, J. Irvine, S. Tang, J. Nishikawa, L. Lum, A. Kim, Sewer chamber design under critical conditions using computational fluid dynamics (CFD), Desalination and Water Treatment 108 (2018) 1–14.

[21] H. Yan, G. Lipeme Kouyi, C. Gonzalez-Merchan, C. Becouze-Lareure, C. Sebastian, S. Barraud, J. L. Bertrand-Krajewski, Computational fluid dynamics modelling of flow and particulate contaminants sedimentation in an urban stormwater detention and settling basin, Environmental Science and Pollution Research 21 (2014) 5347–5356.

[22] C. A. Zimmer, I. W. Heathcote, H. R. Whiteley, H. Schroeter, Low-Impact-Development practices for stormwater: Implications for urban hydrology, Canadian Water Resources Journal 32 (2007) 193–212.

[23] S. D. Lloyd, T. H. F. Wong, B. Porter, The planning and construction of an urban stormwater management scheme, Water Science and Technology 45 (2002) 1–10.

[24] N. Bastien, S. Arthur, S. Wallis, M. Scholz, The best management of SuDS treatment trains: A holistic approach, Water Science and Technology 61 (2010) 263–272.

[25] N. R. P. Bastien, S. Arthur, S. G. Wallis, M. Scholz, Runoff infiltration, a desktop case study, Water Science and Technology 63 (2011) 2300–2308.

[26] X. Zhang, X. Guo, M. Hu, Hydrological effect of typical low impact development approaches in a residential district, Natural Hazards 80 (2016) 389–400.

[27] C. Pyke, M. P. Warren, T. Johnson, J. Lagro, J. Scharfenberg, P. Groth, R. Freed, W. Schroeer, E. Main, Landscape and urban planning assessment of low impact development for managing stormwater with changing precipitation due to climate change, Landscape and Urban Planning 103 (2011) 166–173.

[28] Z. Zahmatkesh, S. Burian, M. Karamouz, H. Tavakol-Davani, E. Goharian, Low-impact development practices to mitigate climate change effects on urban stormwater runoff: case study of New York City, Journal of Irrigation and Drainage Engineering 141 (2015) 1–13.

[29] V. Pappalardo, D. L. Rosa, A. Campisano, P. L. Greca, The potential of green infrastructure application in urban runo ff control for land use planning: A preliminary evaluation from a southern Italy case study, Ecosystem Services 26 (2017) 345–354.

[30] H. Jia, Y. Lu, S. L. Yu, Y. Chen, Planning of LID-BMPs for urban runoff control: The case of Beijing Olympic Village, Separation and Purification Technology 84 (2012) 112–119.

[31] J. Gao, R. Wang, J. Huang, M. Liu, Application of BMP to urban runoff control using SUSTAIN model: Case study in an industrial area, Ecological Modelling 318 (2015) 177–183.

[32] L. M. Ahiablame, B. A. Engel, I. Chaubey, Effectiveness of low impact development practices: Literature review and suggestions for future research, Water, Air, and Soil Pollution 223 (2012) 4253–4273.

[33] A. Roy-Poirier, Y. Filion, P. Champagne, An event-based hydrologic simulation model for bioretention systems, Water Science and Technology 72 (2015) 1524–1533.

[34] C. Yu, J. Duan, Simulation of surface runoff using hydrodynamic model, Journal Hydrologoical Engineering 22 (2017) 1–12.

[35] J. Yazdi, S. A. A. S. Neyshabouri, Identifying low impact development strategies for flood mitigation using a fuzzy-probabilistic approach, Environmental Modelling & Software 60 (2014) 31–44.

[36] A. B. Barton, J. R. Argue, Integrated urban water management for residential areas: A reuse model, Water Science and Technology 60 (2009) 813–823.

[37] L. Ahiablame, R. Shakya, Modeling flood reduction effects of low impact development at a watershed scale, Journal of Environmental Management 171 (2016) 81–91.

[38] J. Gwang, A. Selvakumar, K. Alvi, J. Riverson, J. X. Zhen, L. Shoemaker, F.-h. Lai, A watershed-scale design optimization model for stormwater best management practices, Environmental Modelling and Software 37 (2012) 6–18.

[39] T. Afrin, A. A. Khan, N. B. Kaye, F. Y. Testik, Numerical model for the hydrualic performance of perforated pipe underdrains surrounded by loose aggregate, Journal Hydraulic Engineering 04016018 (2016) 1–10.

[40] OpenFoam, Open FOAM the open source CFD toolbox programmer's guide, Tech. rep. (2017).

[41] R. Gjesing, J. Hattel, U. Fritsching, Coupled atomization and spray modelling in the spray forming process using Open FOAM, Engineering Applications of Computational Fluid Mechanics 3 (2009) 471–486.

[42] H. Jasak, OpenFOAM: Open source CFD in research and industry, International Journal of Naval Architecture and Ocean Engineering 1 (2009) 89–94.

[43] National Research Council, A report of the National Research Council: Urban stormwater management in the United States, Tech. rep. (2008).

[44] The National Academies, Urban stormwater management in the United States, The National Academis Press, Washington D.C., 2009.

[45] United States Environmental Protection Agency, Storm water technology fact sheet - wet detention ponds, Tech. Rep. EPA 832-F-99-048 (1999).

[46] Prince George's County, Stormwater management design manual, Tech. rep., Department of Permitting, Inspections and Enforcement (2014).

[47] C.-h. Hsieh, A. P. Davis, B. A. Needelman, Bioretention column studies of phosphorus removal from urban stormwater runoff, Water Environment Research 79 (2007) 177–184.

[48] P. Hamel, T. D. Fletcher, The impact of stormwater source-control strategies on the (low) flow regime of urban catchments, Water Science and Technology 69 (2014) 739–745.

[49] R. A. Brown, R. W. Skaggs, W. F. Hunt, Calibration and validation of DRAINMOD to model bioretention hydrology, Journal of Hydrology 486 (2013) 430–442.

[50] A. Palla, I. Gnecco, Hydrologic modeling of Low Impact Development systems at the urban catchment scale, Journal of Hydrology 528 (2015) 361–368.

[51] P. Xu, F. Gao, J. He, X. Ren, W. Xi, Modelling and optimization of land use/land cover change in a developing urban catchment, Water Science and Technology 75 (2017) 2527–2537.

[52] A. A. Bloorchian, L. Ahiablame, A. Osouli, J. Zhou, Modeling BMP and vegetative cover performance for highway stormwater runoff reduction, Procedia Engineering 145 (2016) 274–280.

[53] J. Zimmermann, C. Dierkes, P. Göbel, C. Klinger, H. Stubbe, W. G. Coldewey, Metal concentrations in soil and seepage water due to infiltration of roof runoff by long term numerical modelling, Water Science and Technology 51 (2005) 11–19.

[54] J. M. Hathaway, W. F. Hunt, R. M. Guest, D. T. McCarthy, Residual indicator bacteria in autosampler tubing: A field and laboratory assessment, Water Science and Technology 69 (2014) 1120–1126.

[55] I. M. Brodie, SSUIS - A research model for predicting suspended solids loads in stormwater runoff from urban impervious surfaces, Water Science and Technology 65 (2012) 2140–2147.

[56] J. M. Hathaway, R. A. Brown, J. S. Fu, W. F. Hunt, Bioretention function under climate change scenarios in North Carolina, USA, Journal of Hydrology 519 (2014) 503–511.

[57] V. Stovin, S. Poë, C. Berretta, A modelling study of long term green roof retention performance, Journal of Environmental Management 131 (2013) 206–215.

[58] Y. Li, R. W. Babcock, Green roof hydrologic performance and modeling: A review, Water Science and Technology 69 (2014) 727–738.

[59] T. Afrin, Numerical investigation of porous and non- porous pipe with free overfall, Ph.D. thesis, Clemson University (2016).

[60] C.-h. Hsieh, A. P. Davis, Evaluation and optimization of bioretention media for treatment of urban storm water runoff, Journal of Environmental Engineering 131 (2005) 1521–1531.

[61] F. E. Botros, Y. S. Onsoy, T. R. Ginn, T. Harter, Richards Equation-Based Modeling to Estimate Flow and Nitrate Transport in a Deep Alluvial Vadose Zone, Vadose Zone Journal 11 (2012) 1–15.

[62] W. H. Green, G. A. Ampt, Studies on soil physics, Part 1, the flow of air and water through soils, Journal of Agricultural Science 4 (1911) 1–26.

[63] R. G. Mein, C. L. Larson, Modeling the infiltration component of the rainfall-runoff process, Tech. rep., Water Resources Research Center, University of Minnesota (1971).

[64] R. G. Mein, C. L. Larson, Modeling infiltration during a steady rain, Water Resources Research 9 (1973) 384–394.

[65] J. Y. Parlange, I. Lisle, R. D. Braddock, R. E. Smith, The three-parameter infiltration equation, Soil Science 133 (1982) 337–341.

[66] W. F. Noh, P. Woodward, SLIC (Simple Line Interface Calculation), in: Proceedings of the Fifth International Conference on Numerical Methods in Fluid Dynamics June 28 – July 2,

1976 Twente University, Enschede, Springer Berlin Heidelberg, Berlin, Heidelberg, 1976, pp. 330–340.

[67] C. W. Hirt, B. D. Nichols, Volume of fluid (VOF) methods for the dynamics of free boundaries, Journal of Computational Physics 39 (1981) 201–225.

[68] M. García-Serrana, J. S. Gulliver, J. L. Nieber, Non-uniform overland flow-infiltration model for roadside swales, Journal of Hydrology 552 (2017) 586–599.

[69] C. McShane, Transforming the use of urban space: A Look at the Revolution in Street Pavements, 1880-1924, Journal of Urban History 5 (1979) 279–307.

[70] United States Environmental Protection Agency, National management measures to control nonpoint source pollution from urban areas, Tech. rep., Office of Water (2005).

[71] United States Environmental Protection Agency, Urban runoff: Low Impact Development, Tech. rep. (2017).

[72] United States Environmental Protection Agency, National water quality inventory: Report to Congress, Tech. rep., Office of Water (2017).

[73] A. Vargas-Luna, A. Crosato, W. S. Uijttewaal, Effects of vegetation on flow and sediment transport: Comparative analyses and validation of predicting models, Earth Surface Processes and Landforms 40 (2015) 157–176.

[74] J. Zhang, Y. Zhong, W. Huai, Transverse distribution of streamwise velocity in open-channel flow with artificial emergent vegetation, Ecological Engineering 110 (2018) 78–86.

[75] K. Shiono, D. W. Knight, Turbulent open-channel flows with variable depth across the channel, Journal of Fluid Mechanics 222 (1991) 617–646.

[76] C. Liu, X. Luo, X. Liu, K. Yang, Modeling depth-averaged velocity and bed shear stress in compound channels with emergent and submerged vegetation, Advances in Water Resources 60 (2013) 148–159.

[77] H. S. Kim, M. Nabi, I. Kimura, Y. Shimizu, Computational modeling of flow and morphodynamics through rigid-emergent vegetation, Advances in Water Resources 84 (2015) 64–86.

[78] M. Nabi, H. J. De Vriend, E. Mosselman, C. J. Sloff, Y. Shimizu, Detailed simulation of morphodynamics: 1. Hydrodynamic model, Water Resources Research 48 (2012) 1–19.

[79] J. Smagorinsky, General circulation experiments with the primitive equations, Monthly Weather Review 91 (1963) 99–164.

[80] M. Gao, W. Huai, Y. Xiao, Z. Yang, B. Ji, Large eddy simulation of a vertical buoyant jet in a vegetated channel, International Journal of Heat and Fluid Flow 70 (2018) 114–124.

[81] J. Lu, H. C. Dai, Three dimensional numerical modeling of flows and scalar transport in a vegetated channel, Journal of Hydro-Environment Research 16 (2017) 27–33.

[82] W. J. Wang, W. X. Huai, S. Thompson, W. Q. Peng, G. G. Katul, Drag coefficient estimation using flume experiments in shallow non-uniform water flow within emergent vegetation during rainfall, Ecological Indicators 92 (2017) 367–378.

[83] M. Moradi Larmaei, T. F. Mahdi, Depth-averaged turbulent heat and fluid flow in a vegetated porous medium, International Journal of Heat and Mass Transfer 55 (2012) 848–863.

[84] N. Siriwardene, A. Deletic, T. D. Fletcher, Clogging of stormwater gravel infiltration systems and filters: Insights from a laboratory study, Water Research 41 (2007) 1433–1440.

[85] S. Achleitner, C. Engelhard, U. Stegner, W. Rauch, Local infiltration devices at parking sites - Experimental assessment of temporal changes in hydraulic and contaminant removal capacity, Water Science and Technology 55 (2007) 193–200.

[86] Montgomery County Maryland Department of Environmental, How to maintain your rain garden, bioswale, and micro-bioretention practice, Tech. rep., Stormwater Faciility Maintenance Program (2013).

[87] G.-T. Blecken, W. F. Hunt, A. M. Al-Rubaei, M. Viklander, W. G. Lord, Stormwater control measure (SCM) maintenance considerations to ensure designed functionality, Urban Water Journal 14 (2017) 278–290.

[88] Washington State Department of Transportation, Vegetative filter strips tutorial, Tech. rep. (2008).

[89] Iowa Department of Natural Resources, Iowa stormwater management manual, Tech. rep. (2013).

[90] E. M. LaBolle, G. E. Fogg, A. F. Tompson, Random-walk simulation of transport in heterogeneous porous media: Local mass-conservation problem and implementation methods, Water Resources Research 32 (1996) 583–593.

[91] M. Bergman, M. R. Hedegaard, M. F. Petersen, P. Binning, O. Mark, P. S. Mikkelsen, Evaluation of two stormwater infiltration trenches in central Copenhagen after 15 years of operation, Water Science and Technology 63 (2011) 2279–2286.

[92] E. Warnaars, A. V. Larsen, P. Jacobsen, P. S. Mikkelsen, Hydrolgoical behavior of stormwater infiltration trenches in a central urban area during 2 3/4 years of operation, Water Science and Technology 39 (1999) 217–224.

[93] A. V. Mikkelsen, P. S., Warnaars, E. Larsen, Nedsivning af regnvand fra en boligkarré på Nørrebro, Tech. rep., University of Denmark (1999).

[94] S. Le Coustumer, T. D. Fletcher, A. Deletic, S. Barraud, P. Poelsma, The influence of design parameters on clogging of stormwater biofilters: A large-scale column study, Water Research 46 (2012) 6743–6752.

[95] United States Environmental Protection Agency, Storm water management model user's manual version 5.1, Tech. rep. (2015).

[96] M. A. Kachchu Mohamed, T. Lucke, F. Boogaard, Preliminary investigation into the pollution reduction performance of swales used in a stormwater treatment train, Water Science and Technology 69 (2014) 1014–1020.

[97] X. Sun, A. P. Davis, Heavy metal fates in laboratory bioretention systems, Chemosphere 66 (2007) 1601–1609.

[98] M. Razzaghmanesh, M. Borst, Investigation clogging dynamic of permeable pavement systems using embedded sensors, Journal of Hydrology 557 (2018) 887–896.

[99] C. Ulrich, S. S. Hubbard, J. Florsheim, D. Rosenberry, S. Borglin, M. Trotta, D. Seymour, Riverbed clogging associated with a California riverbank filtration system: An assessment of mechanisms and monitoring approaches, Journal of Hydrology 529 (2015) 1740–1753.

[100] T. Grischek, R. Bartak, Riverbed clogging and sustainability of riverbank filtration, Water 8 (2016) 1–12.

[101] L. Locatelli, O. Mark, P. S. Mikkelsen, K. Arnbjerg-Nielsen, T. Wong, P. J. Binning, Determining the extent of groundwater interference on the performance of infiltration trenches, Journal of Hydrology 529 (2015) 1360–1372.

[102] K.-M. Yao, M. T. Habibian, C. R. O'Melia, Water and waste water filtration: Concepts and applications, Environmental Science and Technology 5 (1971) 1105–1112.

[103] R. Rajagopalan, C. Tien, Trajectory analysis of deep-bed filtration with the sphere-in-cell porous media model, American Institue of Chemical Engineers Journal 22 (1976) 523–533.

[104] N. Tufenkji, M. Elimelech, Correlation equation for predicting single-collector efficiency in physicochemical filtration in saturated porous media, Environmental Science and Technology 38 (2004) 529–536.

[105] K. E. Nelson, T. R. Ginn, Colloid filtration theory and the Happel sphere-in-cell model revisited with direct numerical simulation of colloids, Langmuir 21 (2005) 2173–2184.

[106] J. Happel, Viscous flow in multiparticle systems: slow motion of fluids relative to beds of spherical particles, American Institue of Chemical Engineers Journal 4 (1958) 197–201.

[107] A. S. Kim, Cylindrical cell model for direct contact membrane distillation (DCMD) of densely packed hollow fibers, Journal of Membrane Science 455 (2014) 168–186.

[108] A. S. Kim, A. E. Contreras, Q. Li, R. Yuan, Fundamental mechanisms of three-component combined fouling with experimental verification, Langmuir 25 (2009) 7815–7827.

[109] A. S. Kim, H. Chen, R. Yuan, EPS biofouling in membrane filtration: An analytic modeling study, Journal of Colloid and Interface Science 303 (2006) 243–249.

[110] A. S. Kim, R. Yuan, Cake resistance of aggregates formed in the diffusion-limited-cluster-aggregation (DLCA) regime, Journal of Membrane Science 286 (2006) 260–268.

[111] J. J. Lenhart, J. E. Saiers, Transport of silica colloids through unsaturated porous media: Experimental results and model comparisons, Environmental Science and Technology 36 (2002) 769–777.

[112] W. Zhang, V. L. Morales, M. E. Cakmak, A. E. Salvucci, L. D. Geohring, A. G. Hay, J.-Y. Parlange, T. S. Steenhuis, Colloid transport and retention in unsaturated porous media: Effect of colloid input concentration, Environmental Science and Technology 44 (2010) 4965–4972.

[113] T. Knappenberger, M. Flury, E. D. Mattson, J. B. Harsh, Does water content or flow rate control colloid transport in unsaturated porous media?, Environmental Science and Technology 48 (2014) 3791–3799.

[114] S. Xu, J. Qi, X. Chen, V. Lazouskaya, J. Zhuang, Y. Jin, Coupled effect of extended DLVO and capillary interactions on the retention and transport of colloids through unsaturated porous media, Science of the Total Environment 573 (2016) 564–572.

[115] J. W. Delleur, New results and research needs on sediment movement in urban drainage, Journal of Water Resources Planning and Management 127 (2001) 186–193.

[116] Q. Xiao, E. G. McPherson, Performance of engineered soil and trees in a parking lot bioswale, Urban Water Journal 8 (2011) 241–253.

[117] J. F. Good, A. D. O'Sullivan, D. Wicke, T. A. Cochrane, Contaminant removal and hydraulic conductivity of laboratory rain garden systems for stormwater treatment, Water Science and Technology 65 (2012) 2154–2161.

[118] S. K. Mohanty, R. Valenca, A. W. Berger, I. K. M. Yu, X. Xiong, T. M. Saunders, D. C. W. Tsang, Plenty of room for carbon on the ground: Potential applications of biochar for stormwater treatment, Science of the Total Environment 625 (2018) 1644–1658.

[119] P. Shrestha, S. E. Hurley, B. C. Wemple, Effects of different soil media, vegetation, and hydrologic treatments on nutrient and sediment removal in roadside bioretention systems, Ecological Engineering 112 (2018) 116–131.

[120] I. Langmuir, The adsorption of gases on plane surfaces of glass, mica and platinum, Journal of the American Chemical Society 40 (1918) 1361–1403.

[121] H. Freundlich, Über die Adsorption in Lösungen, Zeitschrift für Physikalische Chemie 57 (1906) 385–470.

[122] S. M. Charlesworth, E. Nnadi, O. Oyelola, J. Bennett, F. Warwick, R. Jackson, D. Lawson, Laboratory based experiments to assess the use of green and food based compost to improve water quality in a sustainable drainage (SUDS) device such as a swale, Science of the Total Environment 424 (2012) 337–343.

[123] S. A. Trowsdale, R. Simcock, Urban stormwater treatment using bioretention, Journal of Hydrology 397 (2011) 167–174.

[124] A. P. Davis, W. F. Hunt, R. G. Traver, M. Clar, Bioretention technology: Overview of current practice and future needs, Journal of Environmental Engineering 135 (2009) 109–117.

[125] W. F. Hunt, B. Lord, B. Loh, A. Sia, Plant selection for bioretention systems and stormwater treatment practices, Springer, New York, 2015.

[126] M. E. Dietz, J. C. Clausen, A field evaluation of rain garden flow and pollutant treatment, Water, Air, and Soil Pollution 167 (2005) 123–138.

[127] G. Mazer, D. Booth, K. Ewing, Limitations to vegetation establishment and growth in biofiltration swales, Ecological Engineering 17 (2001) 429–443.

[128] Honolulu Board of Water Supply, Oahu water management plan framework and scope of work for Waianae, Koolauloa and Koolaupoko watershed management plans, Tech. rep. (2004).

[129] D. A. Chin, An overview of urban stormwater management practices in Miami-Dade County, Florida, Tech. rep., South Florida Water Management District (2004).

[130] NDS Inc, NDS Principles of exterior drainage: short course, Tech. rep. (2007).

[131] Virginia Department of Environmental Quality, Virgina DEQ stormwater design specification infiltration practices, Tech. rep. (2013).

[132] M. Kayhanian, P. T. Weiss, J. S. Gulliver, L. Khazanovich, The applicaiton of permeable pavement with emphasis on successful design, water quality benefits, and identification of knowledge and data gap, Tech. rep., National Center for Sustainable Transportation (2015).

[133] F. Jaber, D. Woodson, C. LaChance, Y. Charriss, Stormwater management: Rain gardens, Tech. rep., AgriLife Communication, The Texas A&M System (2012).

[134] North American Pipe Corporation, ASTM F758 PVC highway underdrain pipe North American Pipe Corporation's solvent weld, Tech. rep. (2017).

[135] H. N. Jenks, An investigation of perforated-pipe filter underdrains, Experiment Station Record 44 (1921) 162–166.

[136] United States Army Corps of Engineers, Investigation of filter requirements for underdrains, Tech. rep., Corps of Engineers U.S. Army, U.S. Waterways Experiment Station (1941).

[137] G. Roinas, C. Mant, J. B. Williams, Fate of hydrocarbon pollutants in source and non-source control sustainable drainage systems, Water Science and Technology 69 (2014) 703–709.

[138] J. Li, C. Jiang, T. Lei, Y. Li, Experimental study and simulation of water quality purification of urban surface runoff using non-vegetated bioswales, Ecological Engineering 95 (2016) 706–713.

[139] H. Li, K. Li, X. Zhang, Performance evaluation of grassed swales for stormwater pollution control, Procedia Engineering 154 (2016) 898–910.

[140] Ü. Mander, J. Tournebize, K. Tonderski, J. T. Verhoeven, W. J. Mitsch, Planning and establishment principles for constructed wetlands and riparian buffer zones in agricultural catchments, Ecological Engineering 103 (2017) 296–300.

[141] R. A. Purvis, R. J. Winston, W. F. Hunt, B. Lipscomb, K. Narayanaswamy, A. McDaniel, M. S. Lauffer, S. Libes, Evaluating the water quality benefits of a bioswale in Brunswick County, North Carolina (NC), USA, Water 10 (2018) 1–16.

[142] P. Gobel, C. Dierkes, W. G. Coldewey, Storm water runoff concentration matrix for urban areas, Journal of Contaminant Hydrology 91 (2007) 26–42.

[143] National Oceanic and Atmospheric Administration, Low impact development a practitioner's guide, Tech. rep., Hawaii Costal Zone Management Horsley Witten Group, NOAA (2006).

[144] C. Li, T. D. Fletcher, H. P. Duncan, M. J. Burns, Can stormwater control measures restore altered urban flow regimes at the catchment scale?, Journal of Hydrology 549 (2017) 631–653.

[145] H. E. Golden, N. Hoghooghi, Green infrastructure and its catchment-scale effects: an emerging science, Wiley Interdisciplinary Reviews: Water 5 (2018) 1–14.

[146] R. A. McManamay, S. Surendran Nair, C. R. DeRolph, B. L. Ruddell, A. M. Morton, R. N. Stewart, M. J. Troia, L. Tran, H. Kim, B. L. Bhaduri, US cities can manage national hydrology and biodiversity using local infrastructure policy, Proceedings of the National Academy of Sciences 114 (2017) 9581–9586.

[147] C. Bren d'Amour, F. Reitsma, G. Baiocchi, S. Barthel, B. Güneralp, K.-H. Erb, H. Haberl, F. Creutzig, K. C. Seto, Future urban land expansion and implications for global croplands, Proceedings of the National Academy of Sciences 114 (2016) 8939–8944.

[148] Z. Zhang, N. E. Zimmermann, A. Stenke, X. Li, E. L. Hodson, G. Zhu, C. Huang, B. Poulter, Emerging role of wetland methane emissions in driving 21st century climate change, Proceedings of the National Academy of Sciences 114 (2017) 9647–9652.

[149] J. Franczyk, H. Chang, Heej, The effects of climate change and urbanization on the runoff of the Rock Creek basin the Portland metropolitan area, Oregon, USA, Hydrological Processes 23 (2009) 805–815.

[150] J. Xie, H. Chen, Z. Liao, X. Gu, D. Zhu, An integrated assessment of urban flooding mitigation strategies for robust decision making, Environmental Modelling & Software 95 (2017) 143–155.

[151] United States Environmental Protection Agency, Developing your stormwater pollution prevention plan a guide for construction sites, Tech. rep., Office of Water (2007).

[152] M. A. Benedict, E. T. McMahon, Green infrastructure: Smart conservation for the 21st century, Tech. rep., Sprawl Watch Clearinghouse Monograph Series (2000).

[153] G. D. Geldof, Coping with uncertainties in integrated urban water management, Water Science and Technology 36 (1997) 265–269.

[154] V. G. Mitchell, Applying integrated urban water management concepts: A review of Australian experience, Environmental Management 37 (2006) 589–605.

[155] D. Barlow, B. George, J. R. Nolfi, A research report on developing a community level natural resource inventory system, Tech. rep., Center for Studies in Food Self-Sufficiency, Vermont Institute of Community Involvement (1977).

[156] L. S. Coffman, Low-impact development design: A new paradigm for stormwater management mimicking and restoring the natural hydrologic regime an alternative stormwater, Tech. rep., EPA 841-B-00-003 (2000).

[157] United States Environmental Protection Agency, Low impact development (LID) a literature review, Tech. rep., Office of Water (2000).

[158] N.-B. Chang, Hydrological connections between low-impact development, watershed best management practices, and sustainable development, Journal of Hydrologic Engineering 15 (2010) 384–385.

[159] M. Ignatieva, C. Meurk, G. Stewart, Low impact urban design and development (LIUDD): matching urban design and urban ecology, Landscape Review 12 (2008) 61–73.

[160] C. Pratt, A review of source control of urban stormwater runoff, Journal of Charted Institution of Water and Environmental Management 9 (1995) 132–139.

[161] P. Hamel, E. Daly, T. D. Fletcher, Source-control stormwater management for mitigating the impacts of urbanisation on baseflow: A review, Journal of Hydrology 485 (2013) 201–211.

[162] A. R. Cizek, W. F. Hunt, Defining predevelopment hydrology to mimic predevelopment water quality in stormwater control measures (SCMs), Ecological Engineering 57 (2013) 40–45.

[163] D. Butler, J. Parkinson, Towards sustainable urban drainage, Water Science and Technology 35 (1997) 53–63.

[164] CIRIA, Sustainable urban drainage systems best practice manual for England, Scotland, Wales and Northern Ireland, Tech. rep., CIRIA (2001).

[165] Victorian Stormwater Committee, Urban stormwater best practice environmental management guidelines, CSIRO Publishing, Victoria, Australia, 1999.

[166] S. D. Lloyd, T. H. F. Wong, C. Chesterfield, Water sensitive urban design-A stormwater management perspective, Tech. rep., Monash University (2002).

[167] P. J. Morison, R. R. Brown, C. Cocklin, Transitioning to a waterways city: Municipal context, capacity and commitment, Water Science and Technology 62 (2010) 162–171.

[168] J. Abbott, P. Davies, P. Simkins, C. Morgan, D. Levin, P. Robinson, Creating water sensitive places - scoping the potential for water sensitve urban design in the UK, CIRIA, London, UK, 2013.

[169] T. D. Fletcher, H. Andrieu, P. Hamel, Understanding, management and modelling of urban hydrology and its consequences for receiving waters: A state of the art, Advances in Water Resources 51 (2013) 261–279.

[170] K. Eckart, Z. McPhee, T. Bolisetti, Performance and implementation of low impact development a review, Science of the Total Environment 607-608 (2017) 413–432.

[171] H. Rujner, G. Leonhardt, J. Marsalek, M. Viklander, High-resolution modelling of the grass swale response to runoff inflows with Mike SHE, Journal of Hydrology 562 (2018) 411–422.

[172] Arizona Department of Transportation, Erosion and pollution control manual for highway design and construction, Tech. rep. (2012).

[173] Prince George's County Deptartment of Environmental Protection, Design manual for use of bioretention in stormwater management, Tech. rep. (1993).

[174] Public Works Department of Austin Texas, Design guidelines for water quality control basins, Tech. rep. (1996).

[175] P. Higuera, J. L. Lara, I. J. Losada, Three-dimensional interaction of waves and porous coastal structures using OpenFOAM Part I: Formulation and validation, Coastal Engineering 83 (2014) 243–258.

[176] J. U. Brackbill, D. B. Kothe, C. Zemach, A continuum method for modeling surface tension, Journal of Computational Physics 100 (1992) 335–354. ,

[177] A. Bejan, Convection heat transfer, 4th Edition, Johhn Wiley & Sons, Inc., Hoboken New Jersey, 2013.

[178] Y. Haroun, D. Legendre, L. Raynal, Volume of fluid method for interfacial reactive mass transfer: Application to stable liquid film, Chemical Engineering Science 65 (2010) 2896–2909.

[179] J. Schöberl, C++11 Implementation of Finite Elements in NGSolve, Tech. rep., Institute for Analysis and Scientific Computing, Vienna University of Technology (2014).

[180] H. S. Harned, R. M. Hudson, The diffusion coefficient of Zinc Sulfate in dilute aqueous solution at 25Â°, Journal of the American Chemical Society 73 (1951) 3781–3783.

[181] S. F. Patil, A. V. Borhade, M. Nath, Diffusivity of some zinc and cobalt salts in water, Journal of Chemical and Engineering Data 38 (1993) 574–576.

[182] R. Post, A. N. Beeby, Microbial biomass in suburban roadside soils: Estimates based on extracted microbial C and ATP 25 (1993) 199–204.

[183] R. Garcia, E. Millan, Assessment of Cd, Pb, and Zn contamination in roadside soilds and grasses from Gipuzkoa (Spain), Chemosphere 37 (1998) 1615–1625.

[184] P. K. Lee, J. C. Touray, Characteristics of a polluted artificial soil located along a motorway and effects of acidification on the leaching behavior of heavy metals (Pb, Zn, Cd), Water Research 32 (1998) 3425–3435.

[185] A. C. Norrström, G. Jacks, Concentration and fractionation of heavy metals in roadside soils receiving de-icing salts, The Science of the Total Environment 218 (1998) 161–174.

[186] C. Pagotto, N. Remy, M. Legret, P. Le Cloirec, Heavy metal pollution of road dust and roadside soil near a major rural highway, Environmental Technology 22 (2001) 1–6.

[187] P. Murphy, N. B. Kaye, A. A. Khan, Hydraulic performance of aggregate beds with perforated pipe underdrains flowing full, Journal of Irrigation and Drainage Engineering 140 (2014) 1–7.

[188] M. E. Dietz, Low impact development practices: A review of current research and recommendations for future directions, Water, Air, and Soil Pollution 186 (2007) 351–363.

[189] M. E. Dietz, J. C. Clausen, Stormwater runoff and export changes with development in a traditional and low impact subdivision, Journal of Environmental Management 87 (2008) 560–566.

[190] Q. Xiao, E. McPherson, Q. Zhang, X. Ge, R. Dahlgren, Performance of two bioswales on urban runoff management, Infrastructures 2 (2017) 1–14.

[191] M. Bäckström, Sediment transport in grassed swales during simulated runoff events, Water Science and Technology 45 (2002) 41–49.

[192] M. Bäckström, Grassed swales for stormwater pollution control during rain and snowmelt, Water Science and Technology 48 (2003) 123–132.

[193] J. Li, Y. Li, J. Zhang, Y. Li, Bioswale column experiments and simulation of pollutant removal from urban road stormwater runoff, Desalination and Water Treatment 57 (2016) 24894–24912.

[194] S. Petryk, Drag on cylinders in open channel flow, Ph.D. thesis, Colorado State University (1969).

[195] J. J. Finnigan, P. J. Mulhearn, A simple mathematical model of airflow in waving plant canopies, Boundary-Layer Meteorology 14 (1978) 415–431.

[196] J. J. Finnigan, Turbulent transport in flexible plant canopies, The Forest-Atmosphere Interaction (1985) 443–480

[197] J. J. Finnigan, Y. Brunet, Turbulent airflow in forests on flat and hilly terrain, in: Wind and trees, Cambridge University Press, New York, 1995, pp. 3–40.

[198] B. M. Stone, H. T. Shen, Hydraulic resistance of flow in channels with cylindrical roughness, Journal of Hydraulic Engineering 128 (2002) 500–506.

[199] Y. Tanino, H. M. Nepf, Laboratory investigation of mean drag in a random array of rigid, emergent cylinders, Journal of Hydraulic Engineering 134 (2008) 34–41.

[200] M. Fathi-Maghadam, N. Kouwen, Nonrigid, nonsubmerged, vegetative roughness on floodplains, Journal of Hydraulic Engineering 8 (1997) 51–57.

[201] J. Finnigan, Turbulence in plant canopies, Annual Rview Fluid Mechanics 32 (2000) 519–571.

[202] A. Espinosa-Gayosso, M. Ghisalberti, G. N. Ivey, N. L. Jones, Particle capture and low-Reynolds-number flow around a circular cylinder, Journal of Fluid Mechanics 710 (2012) 362–378.

[203] A. Espinosa-Gayosso, M. Ghisalberti, G. N. Ivey, N. L. Jones, Particle capture by a circular cylinder in the vortex-shedding regime, Journal of Fluid Mechanics 733 (2013) 171–188.

[204] A. Espinosa-Gayosso, M. Ghisalberti, G. N. Ivey, N. L. Jones, Density-ratio effects on the capture of suspended particles in aquatic systems, Journal of Fluid Mechanics 783 (2015) 191–210.

[205] A. T. King, R. O. Tinoco, E. A. Cowen, A k-ϵ turbulence model based on the scales of vertical shear and stem wakes valid for emergent and submerged vegetated flows, Journal of Fluid Mechanics 701 (2012) 1–39.

[206] M. Jamali, X. Zhang, H. M. Nepf, Exchange flow between a canopy and open water, Journal of Fluid Mechanics 611 (2008) 237–254.

[207] X. Zhang, H. M. Nepf, Thermally driven exchange flow between open water and an aquatic canopy, Journal of Fluid Mechanics 632 (2009) 227–243.

[208] F. Huthoff, Modeling hydraulic resistance of floodplain vegetation, Ph.D. thesis, Universiteit Twente, Enschede, the Netherlands (2007).

[209] W. Yang, S. U. Choi, A two-layer approach for depth-limited open-channel flows with submerged vegetation, Journal of Hydraulic Research 48 (2010) 466–475.

[210] N. S. Cheng, Representative roughness height of submerged vegetation, Water Resources Research 47 (2011) 1–18.

[211] Y. Ishikawa, T. Sakamoto, K. Mizuhara, Effect of density of riparian vegetation on effective tractive force, Journal of Forest Research 8 (2003) 235–246.

[212] S. Petryk, G. Bosmajian, Analysis of flow through vegetation, Journal of Hydraulics Division 101 (1975) 871–884.

[213] R. Raupach, Drag and drag partition on rough surfaces, Boundary-Layer Meteorology 60 (1992) 375–395.

[214] C. S. James, A. L. Birkhead, A. A. Jordanova, J. J. O'Sullivan, Flow resistance of emergent vegetation, Journal of Hydraulic Research 42 (2004) 390–398.

[215] R. G. Sharpe, C. S. James, Deposition of sediment from suspension in emergent vegetation, Water SA 32 (2006) 211–218.

[216] U. C. Kothyari, H. Hashimoto, K. Hayashi, Effect of tall vegetation on sediment transport by channel flows, Journal of Hydraulic Research 47 (2009) 700–710.

[217] J. T. Rominger, H. M. Nepf, Flow adjustment and interior flow associated with a rectangular porous obstruction, Journal of Fluid Mechanics 680 (2011) 636–659.

[218] B. Barfield, E. Tollner, J. Hayes, Filtration of sediment by simulated vegetation I. Steady-state flow with homogenous sediment, Transactions of the American Society of Agricultural Engineers 22 (1979) 1063–1067.

[219] C. Herschel, On the origin of the Chezy formula, Journal of the Association of Engineering Societies 18 (1859) 363–370.

[220] M. J. Baptist, Modelling floodplain biogeomorphology, Ph.D. thesis, Delft University of Technology (2005).

[221] F. M. White, Viscous fluid flow, 2nd Edition, McGraw-Hill, New York, 1991.

[222] M. Ghisalberti, Obstructed shear flows: Similarities across systems and scales, Journal of Fluid Mechanics 641 (2009) 51–61.

[223] S. Ergun, Fluid flow through packed columns, Chemical Engineering Science 48 (1952) 89–94.

[224] D. L. Koch, A. J. C. Ladd, Moderate Reynods number flows through periodic and random arrays of aligned cylinders, Journal of Fluid Mechanics 349 (1997) 31–66.

[225] S. E. Belcher, N. Jerram, J. C. R. Hunt, Adjustment of a turbulent boundary layer to a canopy of roughness elements, Journal of Fluid Mechanics 488 (2003) 369–398.

[226] Albert S. Kim, Joshua Lelemia Irvine, interPhaseDiffusionFoam, (https://github.com/enphysoft/interPhaseDiffusionFoam) (2018).